الجمهورية الجزائرية الديمقراطية الشعبية

REPUBLIQUE ALGERIENNE DEMOCRATIQUE ET POPULAIRE

وزارة التعليم العالي والبحث العلمي

MINISTERE DE L'ENSEIGNEMENT SUPERIEUR ET DE LA RECHERCHE SCIENTIFIQUE

جامعة فرحات عباس سطيف 1

UNIVERSITE FERHAT ABBAS SETIF-1

FACULTE DE TECHNOLOGIE

THESE

Présentée au Département d'Electronique

Pour l'Obtention du Diplôme de

DOCTORAT EN SCIENCES

Filière : Electronique　　　　　　　　**Option : Electronique**

Par

Mr. BELAOUT Abdesslam

THEME

Application des Techniques d'Intelligence Artificielle dans les Systèmes Photovoltaïques en vue de Diagnostic des Défauts

Soutenue le : 16 / 10 /2018 devant le jury composé de :

Zegadi Ameur	Professeur	Univ. Sétif-1	Président
KRIM Fateh	Professeur	Univ. Sétif-1	Directeur de thèse
Mellit Adel	Professeur	Univ. Jijel	Co-directeur de thèse
Talha Abdelaziz	Professeur	Univ. USTHB	Examinateur
Chemali Hamimi	Professeur	Univ. Sétif-1	Examinateur
Mustapha Hatti	M. R. A	UDES. Tipaza	Examinateur

Application of Artificial Intelligence Techniques for Faults Diagnosis in Photovoltaic Systems

by

BELAOUT Abdesslam

A thesis

Presented to the University of Sétif-1

In fulfillment of the

Thesis requirement for the degree of

Doctor in Sciences

In

Electronics

To my mother

To my father

To my wife, to my children Firas and Hind

To my sisters and brothers

To the memory of my brothers Hafidh and Fateh, and my uncle Mounir

Acknowledgement

Abstract:

This thesis deals with application of artificial intelligence techniques for the diagnosis, detection and classification of defects in photovoltaic systems. These latter like all electrical and electronic systems, can break down and degrade during the operating period. This requires a diagnostic whose main objective is to provide an automatic tool that can early detect defects to protect the persons and installations, and in addition can classify these defects. At the end of 2016, 303 GW of photovoltaic energy was installed around the world. About 75 GW installed only in the year of 2016, and this comes from the fact that new solutions have encouraged government to rely more and more on this kind of energy. For the development of fault classification algorithms in photovoltaic systems, at the beginning, a database is collected using real time emulator. Then, classifiers based on artificial intelligence were built, such as the fuzzy classifier, neuronal and the neuro-fuzzy classifier. Finally, the diagnostic task was sophisticated with the introduction of a new classifier "multi-class neuro-fuzzy classifier (MC-NFC)". This latter has been implemented on a DSPACE platform "DS1104" to demonstrate its ability to detect and classify faults in real time.

Keywords: Artificial Intelligence; neuro-fuzzy classifier; diagnostic; faults classification; photovoltaic systems; real time simulation.

Table of Contents iv

Chapter 4: Construction and Reduction of Classifier's Features (Inputs)

Chapter 5: Fault Classification Using Artificial Intelligence Algorithms

List of Figures

List of Tables

List of Acronyms

AC	Alternative Current
AF	Arc Fault
AFCI	Arc Fault Circuit Interrupter
AFD	Arc Fault Detector
AI	Artificial Intelligence
AIT	Artificial Intelligence Techniques
ANFIS	Adaptive Neuro-Fuzzy Inference System
ANN	Artificial Neural Network
BkD	Blocking Diode
BpD	Bypass Diode
DC	Direct Current
DF	Diode Fault
ECM	Earth Capacitance Measurement
ENN	Extension Neural Network
EWMA	Exponentially Weighted Moving Average
F	Fault
FC	Fault Classification
FC	Fuzzy Classifier
FD	Fault Detection
FDC	Fault Detection and Classification
FDM	Fault Detection Method
FF	Fill factor
FFT	Fast Fourier Transformer
Fi	Fault number i
FIS	Fuzzy Inference System
FPGA	Field-Programmable Gate Array
GBSS	Graph-Based Semi-Supervised
GCPV	grid-connected PV
GCPVS	grid-connected PV system
GF	Ground Fault
GFDI	Ground Fault Detection Interrupter
HS	Hot Spot

IEC	International Electrotechnical Commission
ISR	Increased Series Resistance
I-V	Current-Voltage
I-VCA	I-V Characteristics Analysis
JB	Junction Box
JSC	Joint Research Centre
LL	Line-to-Line
LLF	Line-to-Line Fault
LM	Levenberg-Marquardt
MC-NFC	Multiclass Neuro-Fuzzy Classifier
MDL	Multi Level Decomposition
MF	Membership Function
ML	Machine Learning
MLP	Multilayer Perceptron
MPPT	Maximum Power Point Tracking
MPRE	Mean percent relative error
MS	Monitoring System
MSC	Multi-resolution Signal Decomposition
NEC	National Electrical Code
NFC	Neuro-Fuzzy classifier
NO	Normal Operation
OC	Over Current
OCPD	Over Current Protection Devices
PCS	Power Conditioning System
PID	Potential-Induced Degradation
PLA	Power Losses Analysis
PR	Power Ratio
PV	photovoltaic
PVA	photovoltaic array
PVE	PV Emulator
PVM	Photovoltaic Module
PVMF	PVM Fault
PVP	PV Plant
PVS	PV System
PWM	Pulse Width Modulation

R^2	Correlation coefficients
RBF	Radial Basis Function
RMSE	Root Mean Square Error
SC	Short Circuit
S_i	Feature number i
SSE	Sum squared error
SSPA	Statistical and Signal Processing Approaches
SS-PVA	Small-Scale PV Array
SS-PVP	Small-Scale PV Plant
SS-PVS	Small-Scale PV system
STD	Standard deviation
T-S	Takagi-Sugeno
TDR	Time-Domain Reflectometery
VCM	Voltage and Current Measurement
VCM	Voltage and Current Measurement
V_{oc}	Open –Circuit Voltage
VR	Voltage Ratio
V_{th}	Threshold Voltage
WSN	Wireless Sensor Network
WT	Wavelet Transform

List of Symbols

K	Degree Kelvin
a	Bishop tuning parameter
A	diode ideality factor
a-Si	amorphous –Silicon
$^{\circ}C$	Degree Celsius
D	Duty Cycle
G	Irradiance
GW	Giga Watt
I	Current
I sc	Short-Circuit Current
I0	dark saturation current
Im	Maximum Current
Iph	photo-current
k	Boltzmann constant
KVA	Kilo Volt Ampere
KW	Kilo Watt
kWp	Kilo Watt Peak
m	Bishop tuning parameter
MW	Mega Watt
Pm	Maximum Power
q	electron charge
RS	Series Resistance
Rsh	shunt resistance
T	Temperature
Tstc (K)	temperature in STC
V	Voltage
Vbr	Breakdown Voltage
Vm	Maximum Voltage
Voc	Open-Circuit Voltage
$Vrms$	Root Mean Square of Voltage
VT	thermal junction voltage

CHAPTER 1

Introduction

1.1. Background and Motivation

Photovoltaic systems' reliability is defined in terms of maximizing the electricity production, and minimizing the factors that cause the power losses of the photovoltaic array (PVA), which is related to the implemented strategies for Maximum Power Point Tracking (MPPT) algorithms [1.1-1.3] and protection devices avoiding both energy and material losses [1.4]. At the end of 2016, 303 GW of photovoltaic energy was installed around the world. About 75 GW installed only in the year of 2016 [1.5], and this is comes from the fact that new solutions have encouraged government to rely more and more on this kind of energy. PVS like all electrical and electronic systems can break down and degrade during the operating period. This requires a diagnostic whose main objective is to provide an automatic tool that can early detect defects to protect peoples and installations, and in addition classifying these defects.

To stop unexpected events in solar photovoltaic (PV) systems, fault detection and protection are essential. Solar PV systems are subject to various faults along the PV arrays, power conditioning units, battery banc, cabling, and utility interconnections [1.1, 1.2]. It is difficult to shut down PV array completely during faults, since they are energized by sunlight. In a large PV array, it may become difficult to properly detect or identify a fault, which can remain hidden in the PV system until the whole system breaks down. In addition, conventional series-parallel PV configurations increase voltage and current ratings, leading to higher risk of large fault currents or dc arcs.

Due to faults occurring within PV arrays, several fires have been reported in PV systems [1.6-1.9]. Figure 1.1 shows a fire case in a 383 *kW* PV array in Bakersfield, California in 2009 [1.6, 1.7]. Another fire is illustrated in Figure 1.2, which occurred in a 1 *MW* PV power plant in Mount Holly, North Carolina, in 2011 [1.9]. In these cases, the fault remained undetected in the PV installation until the catastrophic fire is initiated. These fire cases not only show the failing in conventional fault detection and protection designs in PV arrays, but also disclose the urgent need of a better way to stop such issues.

Figure 1.1: Fire hazards in a 1,208kW PV array, in Mount Holly, North Carolina, in 2011 [1.9].

Due to the large usage of real time simulators in PV systems, there has been a possibility of PVA faults creation, repeating and changing easily. As a result, excessive PV data can be collected (both for faulty and healthy PVA). For example, as shown in Figure 1.3 a typical grid-connected PV system, various PV data can be collected. These PV data are mainly used to train and test classifiers and thus evaluate the PV system performance and calculate the energy losses. Hence, it is possible to develop more responsive fault-detection classifiers that can make better use of these readily available PV data.

Figure 1.2: Fire hazards in a 383kW PV array, in Bakersfield, California, in 2009 [1.6].

The existing fault detection and classification algorithms are built using fixed classifier's inputs and fault scenarios that do not cover all possible real cases. Constructed features (classifier's inputs) are applied without prior information on their effect on the classifier performance. Moreover, what it is known certainly, is that the constructed features have not the same effect on the classifier decision (output), some of them have the same effect, and some others have no effect on the classifier output at all. These reasons conduct us to reduce the classifiers' inputs space. This leads, to avoid redundant information, in the case where some collinear features exist, and also eliminating features that have no effect on output of the decision function. Thus, optimized architectures are designed.

1.2. Problem statement

Figure 1.3 shows a typical grid-connected PV system including a PV array, a PV inverter, protection devices (OCPD, GFDI). Many fault types could occur within PV arrays, such as increased series resistance, ground faults, open-circuit faults, and bypass diode fault. Conventional fault detection and protection methods usually use OCPD (e.g., fuses) and GFDI with PV components [1.10] to protect PV components from large fault current.

However, certain faults in PV arrays may not be cleared by OCPD or GFDI due to non-linear output characteristics of PV arrays, PV current-limiting nature, high fault impedances, low irradiance conditions, PV grounding schemes, or MPPT of PV inverters [1.11]. These drawbacks fetch what is known under the name of "blind spots" in the readily protection solutions, leading to more power losses in PV system, accelerates system aging. DC arcs and similar fire hazards are reported in [1.9, 1.11].

- Fault #1: Partial Shading (*F1*).
- Fault #2: Increased Series Resistance (*F2*).
- Fault #3: Bypass Diode Short Circuited (*F3*).
- Fault #4: Bypass Diode Impedance (*F4*).
- Fault #5: PV module short-circuited (*F5*).
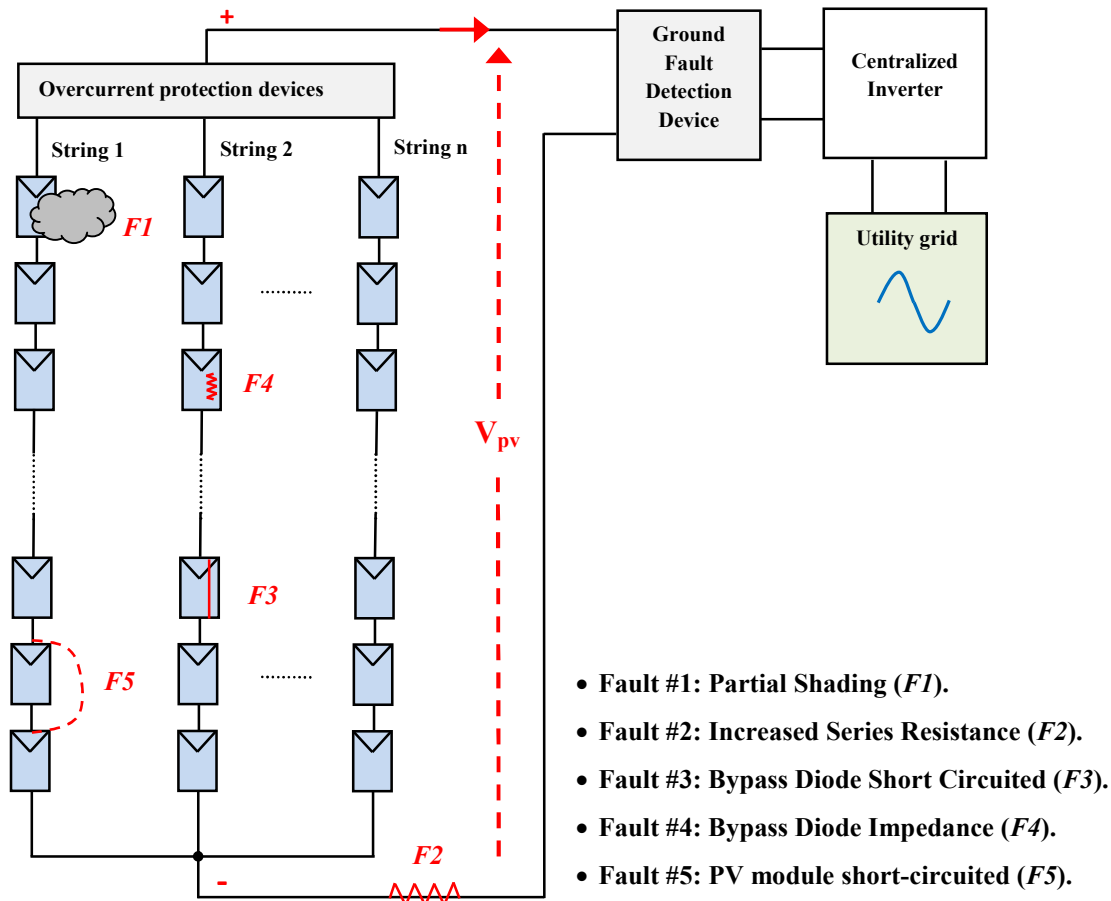
Figure 1.3: Schematic diagram of a grid-connected PV system, together with different types of faults in the PV array.

1.3. Thisis Organization

Motivated by the previously discussed research problems, this thesis aims to analyze and elucidate the restrictions of existing methods and to recommend new fault detection and classification method. Thus, fault detection gap in solar PV arrays are limited. Specifically, the thesis is organized as follows:

The state of the art is presented in Chapter 2. Chapter 3 explains how to collect data from PVA emulator for detection and classification algorithms development purpose. Chapter 4 focuses on classifier inputs (features) reduction techniques. Chapter 5 develops the multiclass neuro-fuzzy classifiers that detect and also classify faults in PVA. In Chapter 6, a brief summary of the research results is presented and future research works are addressed.

***In chapter 2*:** State of the Art of fault detection and classification methods in Photovoltaic Array will be presented.

➢ Faults that can occur in PVA will be presented.

➢ The existing fault detection and classification methodologies will be presented.

***In chapter 3*:** A Real Time Emulator will be development and Data sets for classifiers training and testing will be collected.

A real time emulator for PVA is developed for data collection. Thus, detection and classification algorithms development.

➢ The model of PVA is implemented in a DS1104 platform, where is able to create faults and record data for faulty and healthy cases.

➢ Control algorithms for MPPT are tested successfully with changing irradiance and then with changing temperature. Diagnosis algorithms was also tested and implemented.

➢ An interface human/machine was created in ControlDesk software of ds1104 platform for facility of manipulation.

➢ A sufficient number of data was recorded in Matlab workspace for further processing. In fact, a total of 2860 couples of current-voltage characteristics combined with its corresponding values of irradiance and temperature.

***In chapter 4*:** classifier's features will be constructed and reduced.

➢ Features are constructed using mathematics formulas, new features are introduced.

➢ A Matlab program is developed in order to reduce the classifier input dimensionality. Features are selected for each classifier.

A standard algorithm was implemented in Matlab to choose the best set of features for each classifier.

In chapter 5: Fault Classification Using Artificial Intelligence Algorithms

➢ The limitations of existing methods for PV fault detection and classification are explained.

➢ The building blocks for Multiclass Neuro-Fuzzy Classifier (MC-NFC) classifier are presented (fuzzy classifier and neural network classifier).

➢ A Multi-Class Neuro-Fuzzy Classifier is developed for fault detection and classification in PVA. The developed classifier is compared to the artificial neural network (ANN) classifier.

➢ The proposed classifier is implemented and tested with experimental PVA data.

In chapter 6: Conclusions and Future Research

➢ The conclusions and future research are presented.

1.4 Contributions

This thesis shows some key research contributions and scientific improvements over the existing solutions.

1- First, new features have been introduced into the classifier input. Namely, I-V curve area and slopes at different points of the I-V curve.

2- A new way for classifier inputs' is presented, starting by using many features and then reducing their number by using features dimensionality reduction techniques. This alternative solution saves a lot of time for classifiers development.

3- Third, in the proposed method some patterns of faults are used, but it can detect all possible real patterns for the concerned fault.

4- Finally, a MC-NFC is developed to discriminate between five different types of faults in a PVA.

REFERENCES

[1.1] Mellit, A., Rezzouk, H., Messai, A., & Medjahed, B. (2011). FPGA-based real time implementation of MPPT-controller for photovoltaic systems. *Renewable Energy*, 36(5), 1652-1661.

[1.2] Mellit, A., & Kalogirou, S. A. (2014). MPPT-based artificial intelligence techniques for photovoltaic systems and its implementation into field programmable gate array chips: Review of current status and future perspectives. *Energy*, 70, 1-21.

[1.3] Dhimish, M., Holmes, V., & Dales, M. (2017). Parallel fault detection algorithm for grid-connected photovoltaic plants. *Renewable Energy*, 113, 94-111.

[1.4] Article 690 - Solar Photovoltaic Systems, NFPA70, National Electrical Code, 2016.

[1.5] IEA, Snapshot of global photovoltaic markets, IEA PVPS T1-31:2017.

[1.6] Brooks, B. (2011). The Bakersfield fire-A lesson in ground-fault protection. *SolarPro Mag* , 62-70.

[1.7] Jackson, P. (2009). Target roof PV fire of 4-5-09, 9100 rosedalehwy Bakersfield, California, City of Bakersfield, CA Development Services. *Building Department Memorandum*, 4-29.

[1.8] Ladd, C., Taylor, J., Whitley, J. R., Cowperthwaite, C., & Leegard, R. (2011). Improving the safety and reliability of commercial solar electric systems. *Southern Energy Menagment*.

[1.9] NC PV DG program SEPA presentation. *Duke Energy*, (2011): 1-14.

[1.10] Yuventi, J. (2014). DC electric arc-flash hazard-risk evaluations for photovoltaic systems. *IEEE Transactions on Power Delivery*, 29(1), 161-167.

[1.11] Spooner, E. D., & Wilmot, N. (2008). Safety issues, arcing and fusing in PV arrays.

CHAPTER 2

State of the Art

2.1 Introduction

Photovoltaic Arrays are subject to many failures, mainly due to the external operating conditions. Faults in photovoltaic system (PVS) are caused by: shading effects, module soiling, inverter failure, and mismatch due to variation in manufacturing or aging of PV modules (PVM). The main catastrophic failures in PV arrays (PVA) are: the line-to-line fault (LLF), ground fault (GF) and arc fault (AF) [2.1].

Fault detection and classification (FDC) for PVA, is an essential task to protect this latter from damage and fire risks [2.2, 2.3]. The main task of fault detection (FD), in PVA, consists of comparing the difference between the measured and calculated parameters with reference values, in order to verify the occurrence of any fault, while the fault classification (FC) identifies the type of faults [2.4]. Fault localization remains a big challenge, particularly in large scale PV plants [2.5]. A review on the application of non-electrical methods (e.g. infrared, thermal imagining) for FDC of PVA is presented in [2.6, 2.7]. The most common techniques on image analysis can detect and localize faults, but they have been applied and verified only for SS-PVP. A brief review on fault detection and monitoring systems was published recently in [2.8], in which the authors addressed the major PVS failures.

This chapter presents the state of the art of fault detection and classification (FDC) techniques for PVA. Different fault types are reported in this chapter.

2.2. Types of faults in PVA

Any fault occurring in PVA causes efficiency reduction, output power reduction, and safety hazards. Different types of fault in PVM are detailed in [2.9]. These include discoloration, cracking, antireflection coating damage, bubbles, soiling, busbar oxidation and corrosion, back sheet adhesion loss, etc. Some failure modes detection methods are presented in [2.10]. The faults consist of: bypass and blocking diodes faults, faults in a junction box, hotspot, faults in a PVM, PVA, arc, line-to-line faults and ground fault.

2.2.1 Bypass Diode fault and Blocking Diode fault (DF)

The electrical faults associated to these diodes are: short circuited diode, open circuited diode and impedance. The common reason of these faults may occur when shading in PV module/array for a long period of time [2.11, 2.12] is occurred. Bypass diode (BpD) is a key element for safe system operation [2.13]. However, blocking diode (BkD) in series with PVM will stop Over Current Protection Devices (OCPD) to operate correctly [2.14]. The reverse current under LLF will be cut off by BkD and the system fails.

(a)   (b)
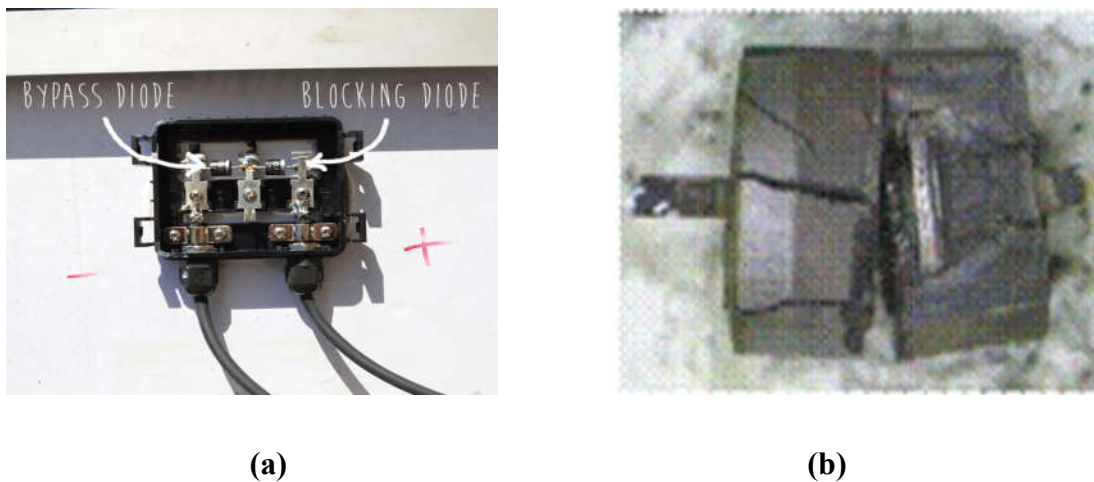
Figure 2.1: (a) good bypass diode and blocking diode, **(b)** damaged diode.

2.2.2 Junction box fault (JBF)

Corrosion occurred in junction box (JB) may lead to a quick increase in contact resistance [2.15]. An electric arc between the contact leads to wearing out and melting of the JB. This would finally damage the modules and the whole array, causing the PVS owner further damages due to loss of energy production.

(a)   **(b)**

Figure 2.2: (a) good junction box; **(b)** damaged junction box.

2.2.3 PV module fault (PVMF)

The faults on the PVM can occur when the array is isolated from the ground, due to corrosion, delamination of the PVM, leakage currents within a module and manufacturing defects which may lead to shunted module and short circuit within a module [2.16]. Generally, faults in PVM may cause electrical shock hazard and fire risk.

2.2.4 Hot spot (HS) fault

Hot Spot (HS) can be caused when some cells in a PV string/array have different I-V curves [2.17], i.e., there are variations in I-V characteristics of PVMs, high resistance or cold solder points due to manufacturing processes [2.17]. In addition, such characteristic may be affected by soiling and dust accumulation [2.18], degradation of the cells, incomplete edge isolation [2.19] by transparent module materials or by the manufacture's tolerance and the non-uniform insolation. The partial shadow effect can be considered as a particular case of the mismatch fault. The HS phenomenon can result when the bypass diode of the shaded cells is damaged/disconnected, thus its current decreases and its voltage becomes negative, so the shaded cells consumes power from other non-shaded cells instead of generating it [2.20], and if this phenomenon persists the affected solar cells will be damaged [2.21]. Some methods for detecting HS are reported in [2.22], but many techniques for quick detection of HS in a PVM are based on infrared measurements.

(a)

(b)

(c)

(d)
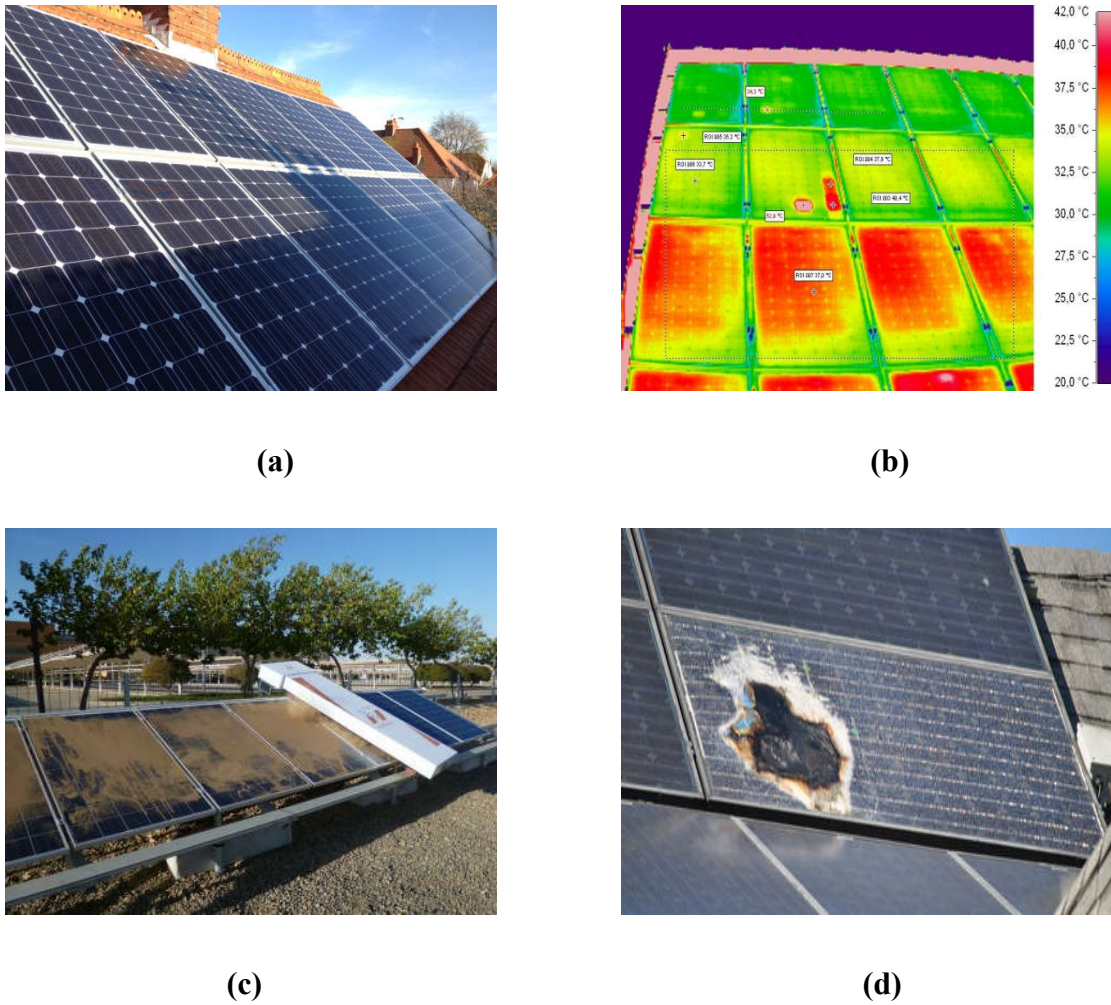
Figure 2.3: Hot Spot fault: causes (a) Shading, (b) Hot Spot phenomena in PVM, (c) Soiling and dust accumulation, (d) Hot Spot damage in PVM

2.2.5 Arc faults (AF)

An Arc Fault (AF) is the unintended flow of current through air or another dielectric. AFs are generally divided into two categories [2.23]:

➢ Series AF: arc from discontinuity in electrical conductor
➢ Parallel AF: electrical discharge between conductors with different potentials.

An AF Detector (AFD) should be included in each system. There are two approaches to detect an AF; the first one is based on the measured value of the DC current in a conductor, it consists of adding small impedance in series with the circuit and measures the resultant voltage. While, the second is based on the measured value of the AC current in a conductor, this approach is relatively easy, due to the oscillatory nature of an AC current; a transformer

may be used as the sensing element. More details about both approaches can be found in [2.24]. Parallel and series AF must be de-energized to protect PVS from fires [2.23]. With reference to NEC 2011, Article 690.11 [2.24] a PV system higher than 80 V penetrating a local or a utility network is suggested to integrate an AF circuit interrupter (AFCI) device as a protection measure.

2.2.6 Line-to-Line fault (LLF)

A line to line fault (LLF) is an unintended low-resistance connection between two points of different potential in an electrical network or system. In PVS, a LLF is usually defined as a short-circuit fault among PVM or array cables with different potential [2.25]. LLF in PVA may be caused by: insulation failure of cables, incidental short circuit between current carrying conductors, low insulation between string connectors in DC string box and mechanical damage. To protect the PVA from LL incidents, many companies have developed protecting devices.

2.2.7 Ground fault (GF)

A ground fault (GF) in PVA can be considered as an unintended electrical short circuit connecting ground and one or more normally designated current-carrying conductors [2.26]. GF in PVA often represent people's safety issues because they may generate DC arcs at the fault point on the GF path. If the fault is not removed properly, the DC arcs could maintain and cause a fire hazard [2.14, 2.26]. Identifying ground faults is a significant problem in ungrounded PVS because such earth faults do not provide sufficient fault currents for their detection and location during system operation [2.27]. GF is the most common fault in PVS and may be caused by the following reasons [2.26]: secondary short circuit between normal conductor and ground, insulation failure of cables, and GF within PVM.

Figures 2.4 and figure 2.5 are taken from [2.28]; in figure 2.4 the fault remains undetected, unless the fault shown in figure 2.5 is detected and cleared.
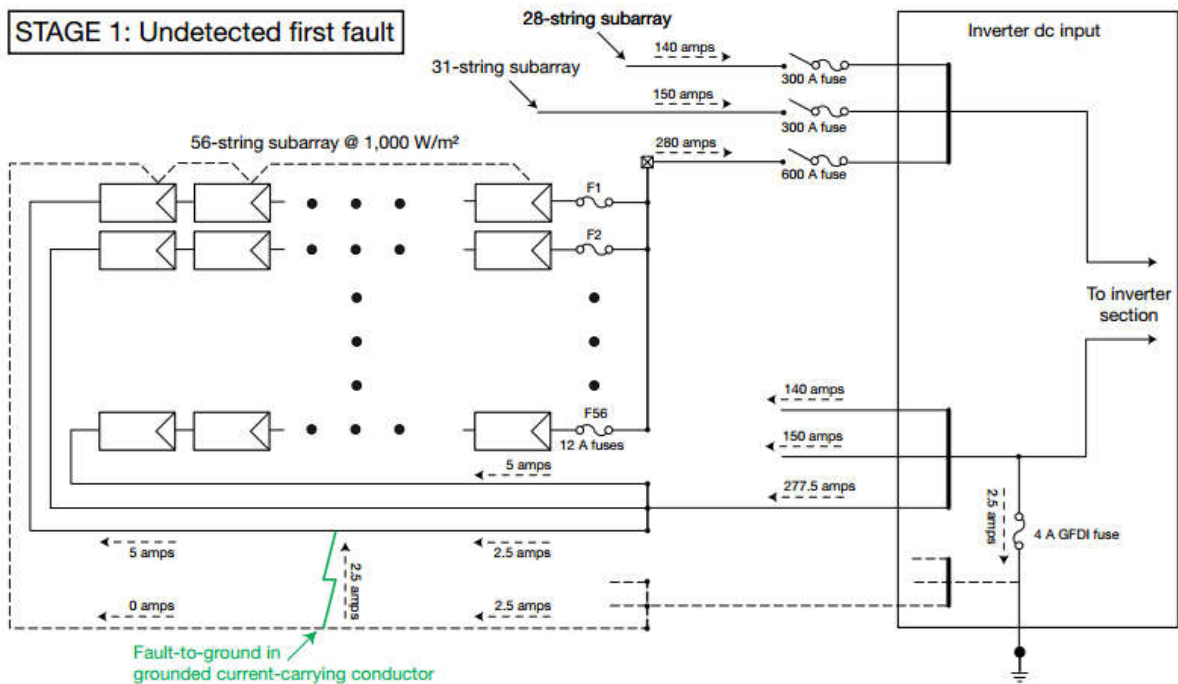
Figure 2.4: The first undetected ground fault between a grounded current-carrying conductor (i.e., the negative conductor) and the equipment-grounding conductor.
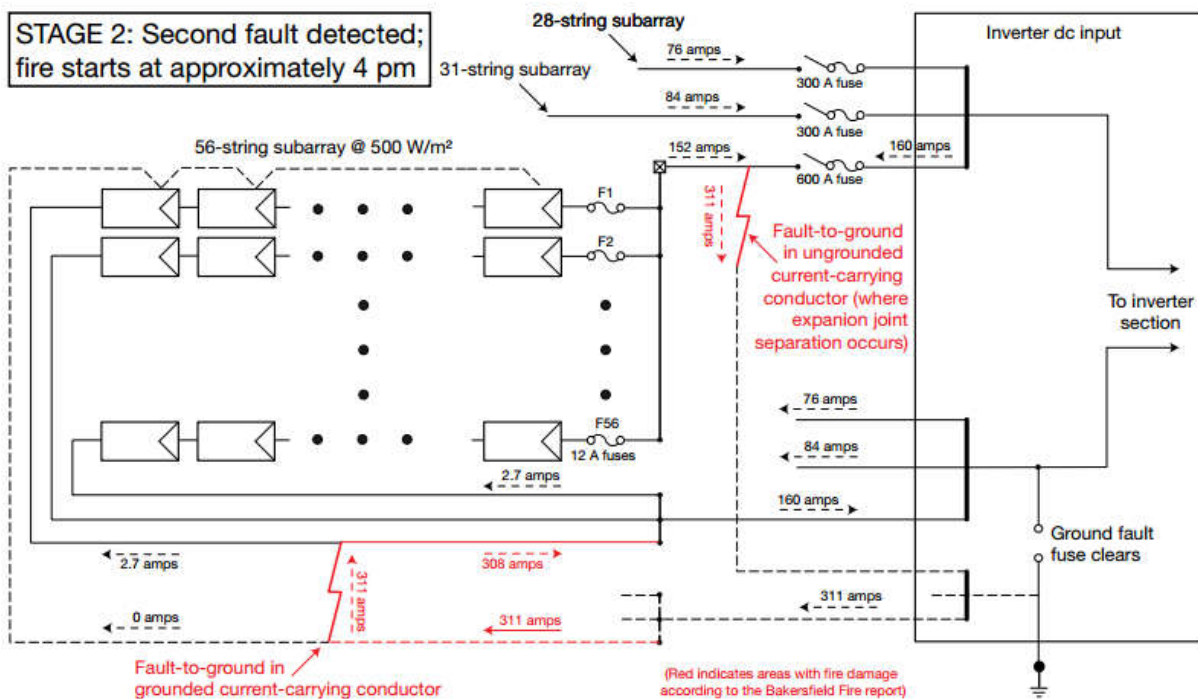
Figure 2.5: The second ground fault between an ungrounded current-carrying conductor (i.e., the positive conductor) and the equipment-grounding conductor.

2.3 Existing Fault detection and classification methods

Many systems have been recently proposed intending to perform a real-time monitoring of PV array (PVA); in this context all methods should respond to the standard IEC 61724 requirements [2.29], and the guidelines of the European Joint Research Centre (JSC) in Ispra, Italy [2.30, 2.31].

Several FDC methods have been proposed in literature, the main features that can characterize such methods are: detecting the defect quickly, the input data required (climatic and electrical data), and selectivity (i.e., ability to distinguish between different faults). They can be classified into two main groups:

➢ Visual & thermal methods [2.7], which can be used for detecting discoloration, browning, surface soiling, hot spot, breaking, and delamination, and;
➢ Electrical methods that can be used for detecting and diagnosing faulty PVM, strings and arrays including arc fault, grounding fault, diodes fault, etc.

Most electrical-based FDC methods rely on some type of PVA model to detect various types of faults.

Electrical methods can be classified into five groups [2.32]:

➢ statistical and signal processing approaches (SSPA);
➢ I-V characteristics analysis (I-VCA);
➢ power losses analysis (PLA);
➢ voltage and current measurement (VCM);
➢ Artificial intelligence techniques (AIT).

Some FDC methods based on electrical techniques are recently reported in [2.33].

In this chapter, we did not present Visual & thermal based methods, the readers can be reported to [2.7] for more information.

2. 3.1 Methods based on statistical signal and processing approaches (SSPA)

Signal processing methods are mainly based on the analysis of the signals. In [2.34], time-domain reflectometery (TDR) technique is used to find the position of the failed PVM in a PVA. The authors underlined that the method can be employed for fault detection and localization, however the method is dependent on the installation conditions such as modules mounting, wiring, or PVA components materials.

An electrical method [2.35] is based on the Earth Capacitance Measurement (ECM) and TDR to detect which PVM in a string is disconnected. According to the authors, the ECM can be used to detect the disconnection positions between the PVM in the string without the effects of the irradiance change, and the TDR could detect the position of the degradation, such as the increase in the Rs between the PVs. The work done by Takashim et al. [2.35] showed that the ECM method could be applied not only to a PV string consisting of crystalline Si PVM, but also to a string consisting of amorphous –Silicon (a-Si) PVM. The TDR technique [2.36] was used to detect breaks of the circuit, insulation defects, wiring anomalies in strings including open circuit and inversed polarity. A 1 MW PV plant (PVP) was tested for a couple of days. The method is basically based on the analysis of the waveform of the output voltage.

An AF circuit protection technique is proposed in [2.37]. This technique can be used to detect and interrupt arcing faults resulting from a failure in the intended continuity of a conductor, connection, module, or other system components in the direct current PV source and output circuits. In [2.38], the authors developed a fault detection method (FDM) for a grid-connected PV system (GCPVS) using wavelet transform (WT). The advantage of the method is the simple calculation and precise diagnostic capabilities of the fault diagnosis. A monitoring system (MS) which provides real-time measurements of each PVM's voltage and current is considered in [2.39]. The presented method employs a classical approach to outlier detection, employing more recent work in robust statistics to overcome the problem of multiple clustered anomalous observations. It has been examined only for two types of faults, AF and GF [2.39]. As reported in [2.40], it is possible to detect AF using Fast Fourier Transform (FFT), but it is not as significant as using WT, particularly when it comes to the problem for a threshold setting for AF determination. The proposed method is validated experimentally with good results.

Recently, a statistical method named exponentially weighted moving average (EWMA) chart is developed in [2.41], the method is used to investigate the following faults: short-circuit, open circuit and shading in PVS. The method has been tested for a GCPV system and the results are very promising.

2. 3.2 Methods based on the I-V characteristic analysis (I-VCA)

Fault diagnosis of PVA based on the I-V characteristic is firstly introduced in [2.16], in which a procedure for the detection of PVA faults is proposed. It consists of comparing the actual to expected electrical parameters from I-V characteristics. Faulty disconnection in PVA is investigated. Experimental testing has demonstrated the ability of the method to detect some PVA faults. The analysis of the shape of the I-V characteristic of PVA cannot always detect faults. For this reason, Miwa et al. [2.42] have proposed a method based on the analysis of the (dI/dV)-V characteristic in order to evaluate automatically the output drop of PVS caused by different loss factors. It was demonstrated that an appearance of a peak of the (-dI/dV)-V characteristic is effective to diagnose the power output drop of a PVS.

Five common types of faults (mismatch, DF, connectivity, PVMF and GF) in PVA were investigated in [2.43]. A Matlab/Simulink based model is developed for this study. Simulation results show that the designed model can simulate the different faults investigated. Daliento et al. [2.44] developed a novel method to detect failures based on simple electrical measurements. The authors analyzed the first and the second derivation of I-V curve in order to detect possible faults in R_S and BpD. The method is simulated and validated experimentally, although the applicability of the method is limited.

2. 3.3 Methods based on the power losses analysis (PLA)

An automatic supervision and FD procedure, based on the PLA is proposed in [2.45], which permits to identify three groups of faults and a false alarm: faulty modules in a string, faulty string, and a group of different faults such as partial shadow, ageing, and MPPT error. The automatic supervision method is based on the analysis of the power losses present in the DC side of the PVA and capture losses. Two kinds of capture losses have been introduced: thermal capture losses and miscellaneous capture losses. A procedure for fault diagnosis in PVS with distributed MPPT at module level, power optimizers DC-DC or micro-inverters DC-AC, is proposed in [2.46]. It has been shown that the designed procedure can diagnose a large scope of failures including: fixed object shading, possible HSs, small localized dirt,

module degradation, generalized dirt and cable losses. The method was experimentally verified.

Shimakage et al. [2.47] developed a fault detection system by comparing the present and past conditions in a faulty PVA, and the proposed method was evaluated at specific fault conditions based on the assumption that some modules are bypassed by the behavior of a BpD because of a module fault or a partial shadow on modules in a string. Multiple faults can be detected in the algorithm proposed in [2.48], in which they have used two indicators PR and VR in order to determine the fault type, time and the location where this fault occurred in the PV system. The method is based on a statistical analysis of data and theoretical thresholds. The method is not able to detect any fault occurred in AC side of the system.

2. 3.4 Method based on voltage and current measurements (VCM)

In [2.49] the authors developed a graph-based semi-supervised learning model for fault detection and classification in PVA. A graph-based semi-supervised learning has been proposed for possible detection of hidden faults in PVA. Experiments demonstrated that the proposed method can correctly detect and classify specific normal conditions, LLFs, and overcurrent (OC) faults in real-working conditions.

In [2.50] the authors define new current and voltage indicators (named: NRc and NRv) as well as the thresholds for both parameters to identify PV string and inverter failures. Investigated faults are: faulty string (one string in open circuit) and bypassed module (one PVM bypassed in one string). With respect to the authors, the proposed method is simple but effective while considering the minimum number of sensors and minimizes the monitoring and supervision system, which can be included in the inverter. Moreover, the supervision of the PVS could be carried out in real time by the inverter itself.

A hardware realization based on Arduino device has been realized for mismatch identification of solar cells [2.51]. Three parameters have been measured: voltage, temperature and resistance of the module. The method can detect easily the mismatch fault. A method for detecting the number of open and short circuit faults, and discriminate between them and partial shading condition is proposed in [2.52]. The method is based on the measurement of the operating voltage of PV string and ambient temperature. A case study for a PVA formed by 8×3 PVM was also presented and results showed that the algorithm is able to identify the actual fault of the system with high probability.

2. 3.5 Methods based on artificial intelligence techniques (AIT)

In the last decade artificial intelligence techniques (AIT) have proven their capability for modeling, control, prediction and forecasting in PVS [2.53].

A matter element model is combined with an ANN to build an intelligent fault diagnosis system as shown in [2.54]. According to the authors, the proposed fault diagnosis method was adopted to identify the faulty types of a 3.15 kW PVS. The simulation results indicate that the proposed fault diagnosis method can detect the fault types of PVS rapidly and accurately with lower time and memory consumption.

In [2.55] the authors presented a method on ANN-based Genetic Algorithm (GA) to diagnose and repair the PVS dynamically. They have shown that, the proposed method proved how good it is for the practical applications. The designed approach can be used for detecting the following faults: short-circuit (SC), open-circuit (OC) and degradation in PVM faults.

A fault diagnosis meter based on a ZigBee Wireless Sensor Network (WSN) for PV power generation systems is proposed in [2.56]. An Extension Neural Network (ENN) fault diagnosis method is used to identify whether the PV power generation system is operating normally or a fault has occurred. The method includes as inputs the solar irradiation and module temperature of the PVM and then using this information together with the characteristics captured from the PV power generation system, provide fault diagnosis, including P_m, I_m, V_m and V_{oc} of the PVA during operation.

A novel fault diagnostic technique for PVA based on ANN was proposed recently in [2.32, 2.57]. The analysis is performed using two different Algorithms:

➢ Algorithm 1, implements a signal threshold approach and isolates the faults that have a different combination of attributes;
➢ Algorithm 2, consists of an ANN based approach and detects the faults that are characterized by the same combination of attributes.

It has been demonstrated that the designed technique is able to detect and identify accurately the investigated fault categories in the PV string, using only the parameters of the I-V characteristic as well as the irradiance level and cell temperature.

A fault detection method for photovoltaic module under partially shaded conditions is introduced in [2.58]. It uses an ANN in order to estimate the output photovoltaic current and voltage under variable working conditions. The results confirm the ability of the technique to correctly localize and identify the different types of faults. The designed diagnostic method is cheap because it requires as input only the following parameters: solar irradiance, PV module's temperature, and PV array's current and voltage [2.58]. In [2.59] the authors developed a fuzzy logic technique for fault detection in a PVA. The designed algorithm is able to discriminate between the most frequently occurring PVM module faults, such as increased series losses, BpD and BkD with good accuracy (90–98%).

A method to detect line-to-line and line-to-ground fault, mainly based on the application of a multi-resolution signal decomposition (MSD) technique on fuzzy inference system is developed in [2.60]. Results show that the method is able to detect faults in a PV array, and it was demonstrated experimentally for a Small-Scale PV Array (SS-PVA). In [2.27] a fault detection method based on WT and ANN is developed for an ungrounded PV system. The designed method is able to detect and localize GF and LL faults in a PVA. Finally, the effectiveness of the designed fault locator is tested with a variety of system parameters. The results demonstrate that the proposed approach has accurate and robust performance even with noisy measurements and changes in operating conditions. A method based on the theoretical I-V curves analysis and FL classification system for fault detection in DC-side of a 1.1 kWp grid-connected PV system (GCPVS) is developed in [2.61, 2.62]. The investigated fault is partial shading effect in PV modules. The classification rate is more than 98%. Recently, the authors in [2.63] developed a novel fault diagnosis approach to detect and classify the following faults: degradation, open circuit, short circuit and partial shading effect on a PVA. The approach is based on the use of I-V curves and the emerging kernel based extreme learning machine. With reference to the authors, both the simulation and experimental results show that the designed approach can achieve high accuracy.

2.4 Existing Fault Protection Solutions

Once the fault is detected, a fault signal can activate interruption devices to clear the fault, in order to protect PV components from damage. The fundamental objective of system protection is to provide isolation of fault in the power system rapidly, so that the damage to the rest of the PV system is minimized [2.64].

In PV applications, the fault area in the solar PV arrays should be isolated so that the impact to the rest of the PV system is minimized. Passive methods use ground fault detection interrupters (GFDI), overcurrent protection devices (OCPD) or blocking diodes [2.65, 2.66]. On the other hand, active methods use more complex sensing circuitry to detect the fault, and rely on circuit breakers, contactors, or semiconductors switches to de-energize and isolate the affected PV components [2.67, 2.68].

Passive protection devices have obvious limitations. Furthermore, blocking diodes are not a substitute of OCPD and they can prevent OCPD from normal operation [2.65]. To improve fault protection, active fault protection devices have been developed and shown the advantages over passive ones. But, they greatly dependent on the fault detection methods (i.e., decision-making algorithms). Therefore, there is still a great need of fault detection methods that can provide responsive and reliable tripping signal to active protection devices.

For a thorough presentation of the existing methods for fault detection and classification the reader can be reported to [2.33, 2.69 and 2.70].

2.5 Conclusion

In this chapter, we present the state of the art of existing fault detection, classification, location and protection solutions for solar photovoltaic (PV) arrays (dc side). Required by the National Electrical Code (NEC), ground-fault detection interrupters (GFDI) and overcurrent protection devices (OCPD) are widely used for fault protection in PV installations. However, their weakness and limitations have been discovered, which may lead to the fire hazards.

To address this issue, a new method has been proposed using artificial intelligence techniques. Therefore, there is an urgent need of better fault detection methods to prevent PV systems from fault hazards.

REFERENCES

[2.1]. Alam, M. K., Khan, F., Johnson, J., & Flicker, J. (2015). A comprehensive review of catastrophic faults in PV arrays: types, detection, and mitigation techniques. *IEEE Journal of Photovoltaics*, 5(3), 982-997.

[2.2]. Falvo, M. C., & Capparella, S. (2015). Safety issues in PV systems: Design choices for a secure fault detection and for preventing fire risk. *Case Studies in Fire Safety*, 3, 1-16.

[2.3]. Krueger, J., & Smith, D. (2003). A practical approach to fire hazard analysis for offshore structures. *Journal of hazardous materials*, 104(1-3), 107-122.

[2.4]. Al-Sheikh, H., & Moubayed, N. (2012). Fault detection and diagnosis of renewable energy systems: An overview. *In Renewable Energies for Developing Countries (REDEC), 2012 International Conference on*, 1-7.

[2.5]. Hasenfus, G. D. (2012). U.S. Patent No. 8,294,451. *Washington, DC: U.S. Patent and Trademark Office*.

[2.6]. Tsanakas, J. A., Vannier, G., Plissonnier, A., Ha, D. L., & Barruel, F. (2015). Fault diagnosis and classification of large-scale photovoltaic plants through aerial orthophoto thermal mapping. *In Proceedings of the 31st European Photovoltaic Solar Energy Conference and Exhibition 2015*, 1783-1788.

[2.7]. Tsanakas, J. A., Ha, L. D., & Al Shakarchi, F. (2017). Advanced inspection of photovoltaic installations by aerial triangulation and terrestrial georeferencing of thermal/visual imagery. *Renewable Energy*, 102, 224-233.

[2.8]. Triki-Lahiani, A., Abdelghani, A. B. B., & Slama-Belkhodja, I. (2017). Fault detection and monitoring systems for photovoltaic installations: A review. *Renewable and Sustainable Energy Reviews*.

[2.9]. Colli, A. (2015). Failure mode and effect analysis for photovoltaic systems. *Renewable and Sustainable Energy Reviews*, 50, 804-809.

[2.10]. Cristaldi, L., Faifer, M., Lazzaroni, M., Khalil, M. M. A. F., Catelani, M., & Ciani, L. (2015). Diagnostic architecture: A procedure based on the analysis of the failure causes applied to photovoltaic plants. *Measurement*, 67, 99-107.

[2.11]. Winter, C. J., Sizmann, R. L., & Vant-Hull, L. L. (Eds.). (2012). Solar power plants: fundamentals, technology, systems, economics. *Springer Science & Business Media*.

[2.12]. Rezgui, W., Mouss, N. K., Mouss, L. H., Mouss, M. D., Amirat, Y., & Benbouzid, M. (2014). Faults modeling of the impedance and reversed polarity types within the PV generator operation. *In 2014 IEEE EFEA*, 1-6.

[2.13]. Kato, K. (2012). PV module failures observed in the field-solder bond and bypass diode failures. *27th EUPVSEC*.

[2.14]. Zhao, Y., Lehman, B., de Palma, J. F., Mosesian, J., & Lyons, R. (2011). Challenges to overcurrent protection devices under line-line faults in solar photovoltaic arrays. *In Energy Conversion Congress and Exposition (ECCE), 2011 IEEE (pp. 20-27). IEEE.*

[2.15]. Jakobi WN K-M, Paterna M, Ansorge F, Baar C. K. (2014). Ring Faults of Contacts in PV Module Junction Boxes due to Fretting Corrosion. *In: Proceedings of the 29th European Photovoltaic Solar Energy Conference and Exhibition*, 2505 –2510.

[2.16]. Stellbogen, D. (1993). Use of PV circuit simulation for fault detection in PV array fields. *In Photovoltaic Specialists Conference, 1993, Conference Record of the Twenty Third IEEE* , 1302-1307.

[2.17]. Massi Pavan, A., Mellit, A., De Pieri, D., & Lughi, V. (2014). A study on the mismatch effect due to the use of different photovoltaic modules classes in large-scale solar parks. *Progress in photovoltaics: research and applications*, 22(3), 332-345.

[2.18]. Pavan, A. M., Mellit, A., & De Pieri, D. (2011). The effect of soiling on energy production for large-scale photovoltaic plants. *Solar energy*, 85(5), 1128-1136.

[2.19]. Ndiaye, A., Charki, A., Kobi, A., Kébé, C. M., Ndiaye, P. A., & Sambou, V. (2013). Degradations of silicon photovoltaic modules: A literature review. *Solar Energy*, 96, 140-151.

[2.20]. Hu, Y., Cao, W., Ma, J., Finney, S. J., & Li, D. (2014). Identifying PV module mismatch faults by a thermography-based temperature distribution analysis. *IEEE Transactions on Device and Materials Reliability*, 14(4), 951-960.

[2.21]. Yang, H., Xu, W., Wang, H., & Narayanan, M. (2010). Investigation of reverse current for crystalline silicon solar cells—New concept for a test standard about the reverse current. *In Photovoltaic Specialists Conference (PVSC), 2010 35th IEEE*, 002806-002810.

[2.22]. Simon, M., Meyer, EL. (2010). Detection and analysis of hot-spot formation in solar cells". *Sol Energy Mater Sol Cells,* 94:106–113.

[2.23]. Johnson, J., Montoya, M., McCalmont, S., Katzir, G., Fuks, F., Earle, J., & Granata, J. (2012). Differentiating series and parallel photovoltaic arc-faults. *In Photovoltaic Specialists Conference (PVSC), 2012 38th IEEE*, 000720-000726.

[2.24]. McCalmonit, S. (2013). Low cost arc fault detection and protection for PV systems. *Contract*, 303, 275-3000.

[2.25]. Zhao, Y., Ball, R., Mosesian, J., de Palma, J. F., & Lehman, B. (2015). Graph-based semi-supervised learning for fault detection and classification in solar photovoltaic arrays. *IEEE Transactions on Power Electronics*, 30(5), 2848-2858.

[2.26]. PVPN1: "Ground-Fault Analysis and Protection in PV Arrays Tech topics: Photovoltaic protection"; 2011.

[2.27]. Karmacharya, I. M., & Gokaraju, R. (2017). Fault location in ungrounded photovoltaic system using wavelets and ANN. *IEEE Transactions on Power Delivery*.

[2.28]. Brooks, B. (2011). The bakersfield fire-a lesson in ground-fault protection. *SolarPro Magazine*, 62-70.

[2.29]. IEC61724 S. (1998). Photovoltaic System Performance Monitoring – Guidelines for Measurement, Data Exchange and Analysis. *IEC*.

[2.30]. Blaesser GM. D. (1993). Guidelines for the Assessment of Photovoltaic Plants, Document A, Photovoltaic System Monitoring. *Commission of the European Communities, JRC, Ispra, Italy, EUR 16338 EN.*

[2.31]. Blaesser GMD. (1993). Guidelines for the assessment of photovoltaic plants, document B, Analysis and presentation of monitoring data. *Commission of the European Communities, JRC, Ispra, Italy, EUR 16339 EN*.

[2.32]. Chine, W., & Mellit, A. (2017). ANN-based fault diagnosis technique for photovoltaic stings. *In Electrical Engineering-Boumerdes (ICEE-B), 2017 5th International Conference on*, 1-4.

[2.33]. Daliento, S., Chouder, A., Guerriero, P., Pavan, A. M., Mellit, A., Moeini, R., & Tricoli, P. (2017). Monitoring, diagnosis, and power forecasting for photovoltaic fields: a review. *International Journal of Photoenergy*, 2017.

[2.34]. Takashima, T., Yamaguchi, J., Otani, K., Kato, K., & Ishida, M. (2006, May). Experimental studies of failure detection methods in PV module strings. *In Photovoltaic Energy Conversion, Conference Record of the 2006 IEEE 4th World Conference on*, 2, 2227-2230.

[2.35]. Takashima, T., Yamaguchi, J., & Ishida, M. (2008). Disconnection detection using earth capacitance measurement in photovoltaic module string. *Progress in Photovoltaics: Research and Applications*, 16(8), 669-677.

[2.36]. Schirone, L., Califano, F. P., Moschella, U., & Rocca, U. (1994). Fault finding in a 1 MW photovoltaic plant by reflectometry. *In Photovoltaic Energy Conversion, 1994., Conference Record of the Twenty Fourth. IEEE Photovoltaic Specialists Conference-1994, 1994 IEEE First World Conference on*, 1, 846-849.

[2.37]. Dini, D. A., Brazis, P. W., & Yen, K. H. (2011). Development of arc-fault circuit-interrupter requirements for photovoltaic systems. *In Photovoltaic Specialists Conference (PVSC), 2011 37th IEEE*, 001790-001794.

[2.38]. Kim, I. S. (2011). Fault detection algorithm of the photovoltaic system using wavelet transform. *In Power Electronics (IICPE), 2010 India International Conference on*, 1-6.

[2.39]. Braun, H., Buddha, S. T., Krishnan, V., Spanias, A., Tepedelenlioglu, C., Yeider, T., & Takehara, T. (2012). Signal processing for fault detection in photovoltaic arrays. *In Acoustics, Speech and Signal Processing (ICASSP), 2012 IEEE International Conference on*, 1681-1684.

[2.40]. Wang, Z., & Balog, R. S. (2013, June). Arc fault and flash detection in DC photovoltaic arrays using wavelets. *In Photovoltaic Specialists Conference (PVSC), 2013 IEEE 39ᵗʰ*, 1619-1624.

[2.41]. Garoudja, E., Harrou, F., Sun, Y., Kara, K., Chouder, A., & Silvestre, S. (2017). Statistical fault detection in photovoltaic systems. *Solar Energy*, 150, 485-499.

[2.42]. Miwa, M., Yamanaka, S., Kawamura, H., & Ohno, H. (2006). Diagnosis of a power output lowering of PV array with a (-dI/dV)-V characteristic. *In Photovoltaic Energy Conversion, Conference Record of the 2006 IEEE 4th World Conference on*, 2, 2442-2445.

[2.43]. Fezzani, A., Mahammed, I. H., Drid, S., & Chrifi-alaoui, L. (2015). Modeling and Analysis of the Photovoltaic array Faults. *In Control, Engineering & Information Technology (CEIT), 2015 3rd International Conference on*, 1-9.

[2.44]. Daliento, S., Di Napoli, F., Guerriero, P., & d'Alessandro, V. (2016). A modified bypass circuit for improved hot spot reliability of solar panels subject to partial shading. *Solar Energy*, 134, 211-218.

[2.45]. Chouder, A., & Silvestre, S. (2010). Automatic supervision and fault detection of PV systems based on power losses analysis. *Energy conversion and Management*, 51(10), 1929-1937.

[2.46]. Solórzano, J., & Egido, M. A. (2013). Automatic fault diagnosis in PV systems with distributed MPPT. *Energy conversion and management*, 76, 925-934.

[2.47]. Shimakage, T., Nishioka, K., Yamane, H., Nagura, M., & Kudo, M. (2011). Development of fault detection system in PV system. *In Telecommunications Energy Conference (INTELEC), 2011 IEEE 33rd International*, 1-5.

[2.48]. Dhimish, M., & Holmes, V. (2016). Fault detection algorithm for grid-connected photovoltaic plants. *Solar Energy*, 137, 236-245.

[2.49]. Zhao, Y., Ball, R., Mosesian, J., de Palma, J. F., & Lehman, B. (2015). Graph-based semi-supervised learning for fault detection and classification in solar photovoltaic arrays. *IEEE Transactions on Power Electronics*, 30(5), 2848-2858.

[2.50]. Silvestre, S., da Silva, M. A., Chouder, A., Guasch, D., & Karatepe, E. (2014). New procedure for fault detection in grid connected PV systems based on the evaluation of current and voltage indicators. *Energy Conversion and Management*, 86, 241-249.

[2.51]. Mahendran, M., Anandharaj, V., Vijayavel, K., & Winston, D. P. (2015). Permanent mismatch fault identification of photovoltaic cells using arduino. *ICTACT Journal on Microelectronics*, 1(02).

[2.52]. Gokmen, N., Karatepe, E., Silvestre, S., Celik, B., & Ortega, P. (2013). An efficient fault diagnosis method for PV systems based on operating voltage-window. *Energy conversion and management*, 73, 350-360.

[2.53]. Mellit, A., & Kalogirou, S. A. (2008). Artificial intelligence techniques for photovoltaic applications: A review. *Progress in energy and combustion science*, 34(5), 574-632.

[2.54]. Chao, K. H., Chen, C. T., Wang, M. H., & Wu, C. F. (2010, June). A novel fault diagnosis method based-on modified neural networks for photovoltaic systems. *In International Conference in Swarm Intelligence. Springer, Berlin, Heidelberg*, 531-539.

[2.55]. Mohamed, A. H., & Nassar, A. M. (2015). New algorithm for fault diagnosis of photovoltaic energy systems. *International Journal of Computer Applications*, 114(9).

[2.56]. Chao, K. H., Chen, P. Y., Wang, M. H., & Chen, C. T. (2014). An intelligent fault detection method of a photovoltaic module array using wireless sensor networks. *International Journal of Distributed Sensor Networks*, 10(5), 540147.

[2.57]. Chine, W., Mellit, A., Lughi, V., Malek, A., Sulligoi, G., & Pavan, A. M. (2016). A novel fault diagnosis technique for photovoltaic systems based on artificial neural networks. *Renewable Energy*, 90, 501-512.

[2.58]. Mekki, H., Mellit, A., & Salhi, H. (2016). Artificial neural network-based modelling and fault detection of partial shaded photovoltaic modules. *Simulation Modelling Practice and Theory*, 67, 1-13.

[2.59]. Belaout, A., Krim, F., & Mellit, A. (2016). Neuro-fuzzy classifier for fault detection and classification in photovoltaic module. *In Modelling, Identification and Control (ICMIC), 2016 8th International Conference on*, 144-149.

[2.60]. Yi, Z., & Etemadi, A. H. (2017). Fault detection for photovoltaic systems based on multi-resolution signal decomposition and fuzzy inference systems. *IEEE Transactions on Smart Grid*, 8(3), 1274-1283.

[2.61]. Dhimish, M., Holmes, V., Mehrdadi, B., & Dales, M. (2017). Diagnostic method for photovoltaic systems based on six layer detection algorithm. *Electric Power Systems Research*, 151, 26-39.

[2.62]. Dhimish, M., Holmes, V., Mehrdadi, B., Dales, M., & Mather, P. (2017). Photovoltaic fault detection algorithm based on theoretical curves modelling and fuzzy classification system. *Energy*, 140, 276-290.

[2.63]. Chen, Z., Wu, L., Cheng, S., Lin, P., Wu, Y., & Lin, W. (2017). Intelligent fault diagnosis of photovoltaic arrays based on optimized kernel extreme learning machine and IV characteristics. *Applied Energy*, 204, 912-931.

[2.64]. Blackburn, J. L., & Domin, T. J. (2006). Protective relaying: principles and applications. *CRC press*.

[2.65]. Zhao, Y., De Palma, J. F., Mosesian, J., Lyons, R., & Lehman, B. (2013). Line–line fault analysis and protection challenges in solar photovoltaic arrays. IEEE *transactions on Industrial Electronics*, 60(9), 3784-3795.

[2.66]. NFPA70, "National Electrical Code, "NEC Article 690: Solar Photovoltaic Systems", 2014.

[2.67]. Luebke, C. J., Hastings, J. K., Pahl, B., Zuercher, J. C., & Yanniello, R. (2011). U.S. Patent Application No. 12/582,367.

[2.68]. Pozsgay, A. (2016). U.S. Patent No. 9,306,082. Washington, DC: U.S. Patent and Trademark Office.

[2.69]. Mellit, A., Tina, G. M., & Kalogirou, S. A. (2018). Fault detection and diagnosis methods for photovoltaic systems: A review. *Renewable and Sustainable Energy Reviews*, 91, 1-17.

[2.70]. Pillai, D. S., & Rajasekar, N. (2018). A comprehensive review on protection challenges and fault diagnosis in PV systems. *Renewable and Sustainable Energy Reviews*, 91, 18-40.

CHAPTER 3

Real Time Emulator Development

3.1 Introduction

Data sets have been collected by using a real time emulator [3.1] developed in power electronics and industrial control laboratory (LEPCI) at Sétif-1- University, Algeria (See Figure 3.1 and Figure 3.2). The advantage of using a real time emulator is that we cannot create faults in a real PVA and we cannot also change the operation conditions. Therefore, in the emulator these constraints can be avoided, and it allows also repeating the same results (I-V curves) and introducing more testing conditions that are not feasible on real PV modules (such as PV cell cracking).

3.1.1 Reasons bihind Real Time Solution

One of the major problems encountered to develop control and diagnosis algorithms for PVG is the instantaneous variation of temperature and irradiance in real conditions. So the traditional solution (using real PV modules) is avoided due to the following drawbacks:

➢ Climatic changing (irradiance and temperature) prevent researchers from testing their control and diagnosis algorithms efficiently.

➢ In real PVS, it is difficult to have a desired configuration.

➢ Experimenting with different PV module technologies is not possible with a fixed installation.

➢ It's not easy to have a desired PV plant power.

➢ Time and energy consuming for researchers and development engineers.

The Photovoltaic emulator (PVE) is an efficient alternative to the real PVS, thanks to these advantages:

➢ Setting the exact couple of (temperature, irradiance).

➢ Implementation of any PV module technology, characteristics and parameters.

➢ Choosing any type of configuration, series, parallel, series-parallel modules to get the desired output current, voltage and power.

➢ Adjusting the PV plant power to our needs.

➢ Saving time and energy for researchers and engineers developing control and diagnosis algorithms.

➢ Saving space, money and material used to make installations.

One of the main disadvantages of the PVE is that the maximum power of the programmable DC/AC power source cannot be exceeded.

3.1.2 Review of Real Time Emulators

Some PVE based on five parameters PV cell model are presented in [3.2-3.7] and they did not consider any type of faults in their discussion. In [3.2] a novel real time PVE based on Field-Programmable Gate Array (FPGA) was developed, a buck DC/DC power converter is controlled by a FPGAs based unit. In [3.3] a PVE is presented. A switch of buck DC/DC converter is controlled via PWM block receiving a reference signal coming from an external controller to avoid computation time delay, a two-stage LC output Filter is used to make the resonance frequency higher. In [3.4] a PVE is developed using as the basic power unit a flyback converter which is controlled by a reference signal coming from a 'low end' dsPIC microcontroller. In [3.5], a numerical solution approach was developed to start with a well-suited initial value improve computational time cost. In [3.6] authors have developed portable solar PV module emulator using a buck converter. In [3.7] authors have implemented a PVE model in DS1104 platform to generate a reference signal feeding a programmable DC power supply.

Only partial shading was considered in [3.8-3.14], and a five parameters PV cell model also used in this case. In [3.8] a partial shading effect was simulated using multi-small-scale PV module simulators units. In [3.9] a laboratory emulator of a PV module is presented, and controllable insolation was realized by keeping good dynamic performance. In [3.10] to construct solar PV panel emulation model, a behavioral model is implemented by integrating PV cell degradation and partial shading effect. In [3.11] a tool for researchers and engineers to test control algorithms is presented. The authors developed wind and solar power emulators. The programmable DC power supply is used to simulate solar panel I-V characteristics. A DC motor is used to emulate the three blade wind turbine. In [3.12] a simple hardware based PVE for power electronics testing was presented, the particular behavior due to the partial shading is pointed out. In [3.13] the proposed PVE is based on DC/DC step down converter topology. A pole placement technique is used. In [3.14] a PVE was developed for testing grid-connected inverters. A PI controller produces a reference signal to DC/DC converter via PWM bloc.
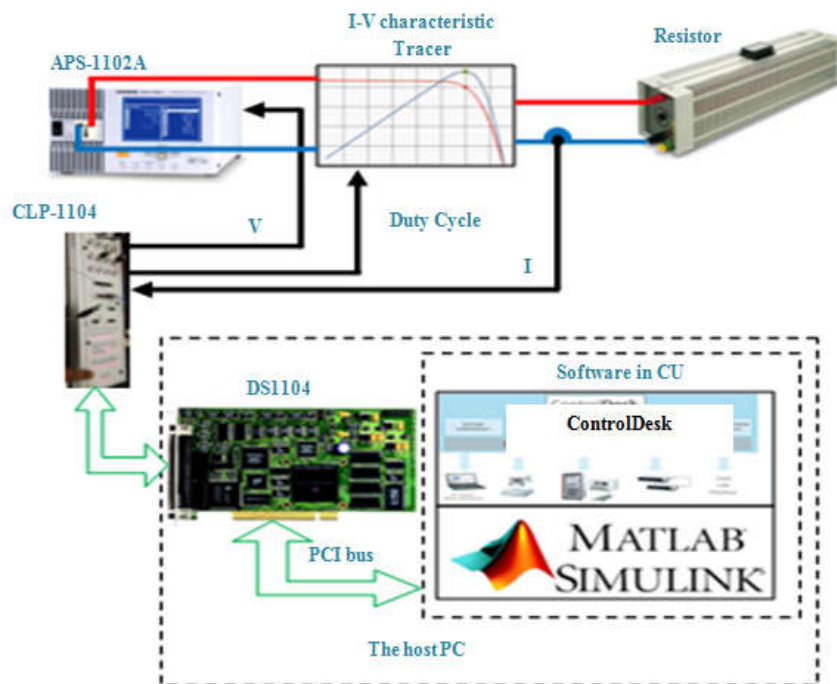
Figure 3.1: Schematic of the photovoltaic emulator with an APS61102A Programmable Power Source.

In the above mentioned methods the PV cell model used for PVE model building was the one diode model. In [3.15] the author takes into account the effect of the avalanche effect of the faulty PV cell by using the Bishop model. The major PVA faults were also considered in

this thesis. A controllable DC power supply was fed by a control signal coming from   DS-1104 platform.

The real time emulator can switch between two modes: control and diagnosis modes. In the first one, the emulator uses only a five parameters PV cell model. And, in the second one, the model used for the emulator is the Bishop model. The advantages of using two models, is that in the first mode we do not need to represent the PV cell in the negative side (non faulty PV cell). As a result, we can minimize the computational time of the implemented model. In the second mode, representing the negative side of the PV cell is mandatory, and a full and accurate model should be used. This emulator constitutes an efficient tool for developing, and testing control and diagnosis algorithms.

3.2 PV Array Implementation in DS1104 Platform

The schematic representation of the developed real time emulator is shown in Figure 3.1. It consists basically of two parts. A software part: Matlab/simulink, and ControlDesk. And a hardware part: the DS1104 platform which is connected to the PC via PCI slot, and to the programmable DC/AC power source via PLC1104 module. Current sensor is used to provide a feedback signal to the implemented PVA model. The control voltage in the external input of the programmable power comes from the controller board. Duty cycle changes regularly from 0 to 1 with a constant slope, then controlling the I-V plotter switch. A resistive load of 5 ohms /8 A is used.

3.2.1 Typical PVA Emulator

The model of PVA was developed under Matlab software, and then implemented into a DS1104 control board. The PVA consists of a connection in series and parallel of several modules and a module is a connection in series of many solar cells (the PV cell model used is a Bishop model [3.16, 3.17 and 3.18]). The computation of its parameters is done by the method described in [3.19]. The electrical characteristics of the PV module that will be used in next sections are given in Table 3.1.

TABLE 3.1: PV module's electrical characteristics and temperature coefficients **(**JW-50P**)**

JW-50P PV module's electrical characteristics	
Number of series cells	36
Open-circuit voltage (Voc)	21.9 V
Voltage at maximum power (Vm)	17.4 V
Short-circuit current (Isc)	3.13 A
Current at maximum power (Im)	2.87 A
Maximum power at. STC (Pm)	50 Wp

Figure 3.2: Photograph of the emulator used for data collection: 1) buck converters, 2) load, 3) programmable power source, 4) scope, 5) ControlDesk, 6) ds1104 platform.

3.2.2 PV Array Parameters

In order to fulfill the main task of this emulator two different PV cell models should be used. The former, is the single diode model that is used for control algorithms test purpose (See Figure 3.3). The later, is the Bishop model that is used for diagnostic algorithms test purpose (See Figure 3.4).
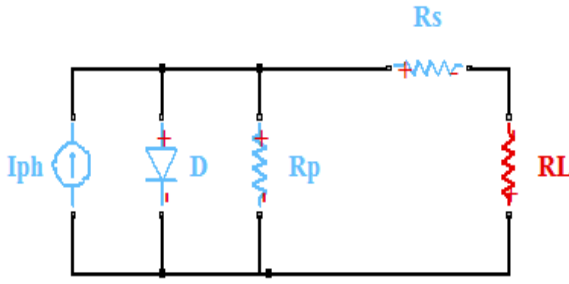
Figure 3.3: single diode model.   **Figure 3.4:** Bishop model.
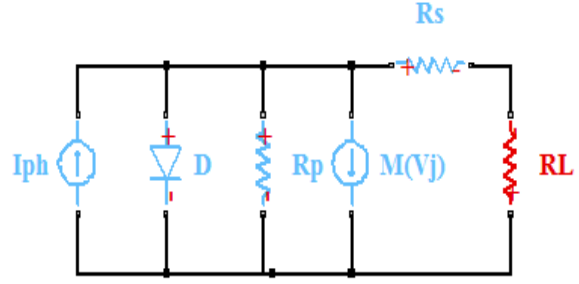
Two variables *I* and *V*, and a vector of five parameters:

$$\theta = \left(I_{ph}, I_0, V_T, R_s, R_{sh} \right) \tag{1}$$

Are used to describe the behavior of the solar PV cell in the single diode model given by the equation:

$$I = I_{ph} - I_0 \left[\exp\left(\frac{V + IR_s}{V_T} \right) - 1 \right] - \frac{V + IR_s}{R_{sh}} \tag{2}$$

$$V_T = \frac{AkT_{stc}}{q} \tag{3}$$

Where:

I_{ph}: is the photo-current in *STC*. I_0: is the dark saturation current in STC. R_s: is the module series resistance. R_{sh}: is the module shunt resistance. And V_T: is the thermal junction voltage. *A* is the diode ideality factor, *k* is the Boltzmann constant; *q* is the electron charge, and T_{stc} (*K*) is a temperature in *STC*.

In the Bishop model [3.17], three parameters are added, breakdown voltage V_{br}, Bishop tuning parameters *m* and *a*, to get a new vector of eight parameters:

$$\Phi = \left(I_{ph}, I_0, V_T, R_s, R_{sh}, V_{br}, a, m \right)$$
(4)

By adding the breakdown voltage term to the second side of the equation (2) we get a new one:

$$I = I_{ph} - I_0 \left[\exp\left(\frac{V + IR_s}{V_T} \right) - 1 \right]$$

$$-\frac{V + IR_s}{R_{sh}}\left[1 + a\left(1 - \frac{V + IR_s}{V_{br}}\right)^{-m}\right] \tag{5}$$

Since the photovoltaic module is a connection in series of PV cells with the same electrical characteristics, the PV module current is the same, and the PV module voltage, is the PV cell voltage multiplied by the number of cells. We can get the desired PVA voltage and current by connecting modules in series and parallel.

3.2.3 Model Implementation in DS1104 Platform

Model implementation in the DS1104 R&D Controller Board starts first by PVA model development in Matlab/Simulink. The electrical parameters of the PV module are adjusted according to the PV module used in experimentation. A simple Build procedure in model windows creates files with different extensions (.SDF, .PPC …etc). These files are then transferred automatically to the controller board. The file with extension (.SDF) appears in ControlDesk, containing all model parameters. Here we can experiment easily (visualizing *I-V* curve, adjusting PV model parameters, weather condition changing, record any parameter or curve…, and many other flexible manipulations.

3.2.4 PV Characteristic Plotter

A DC/DC buck converter allows getting full *I-V* characteristics, by controlling the switch S, (See Figure 3.5).
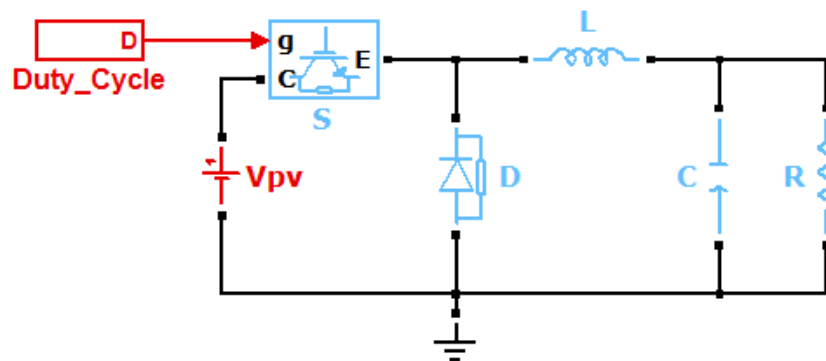
Figure 3.5: DC/DC buck converter used as current-voltage characteristics plotter.

Changing duty cycle *D* (from 0 to 1) leads to change the converter output voltage in the range (0-V_{oc}) volts. Thus, the output current changes from I_{sc} to 0 Amps.

3.2.5 Programmable AC/DC Power Source (APS-1102A)

The programmable power source used in the proposed real time emulator is an *APS-1102A* model. It provides an *AC/DC* electrical power at its output. The rated voltage is 200 *Vrms*, with maximum output capacity of 1*KVA*.

It can be controlled remotely via the External Signal Input connector, and provides the same power as in a real PVA implemented in the platform via the Output outlet.

3.2.6 Fault Diagnosis using I-V Characteristics

I-V characteristics of the faulty and healthy PV array are plotted in Figure 3.6.

First, fault detection should be performed for personnel and material protection purpose. Fault classification will be performed ones the fault is detected by analyzing the maximum PVA current and maximum PVA voltage. These latter are mainly determined by weather conditions (module temperature and irradiance).
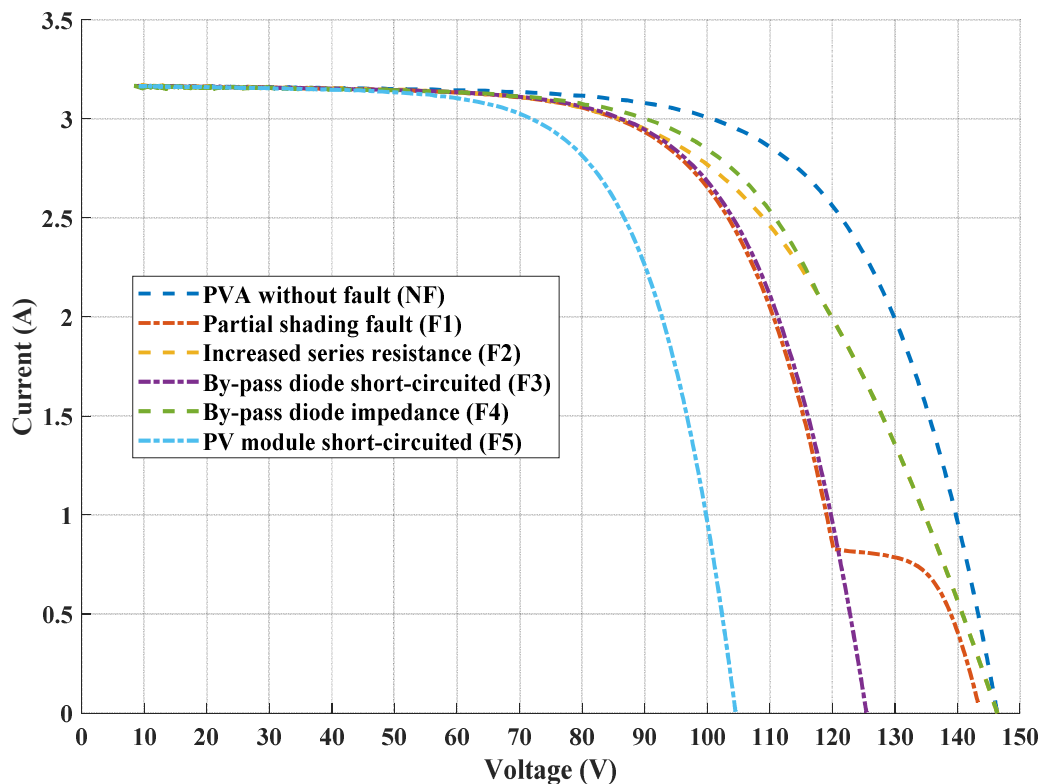
Figure 3.6: *I-V* curves of different PV array faults.

3.3 PVA Emulator Validation

The test and validation of the proposed PV real time emulator has been performed in two stages. The first consists of control algorithms test. And, the second one consists of diagnosis algorithms test. In order to realize this task, a Semikron 3-phase Inverter (*AN-8005*) has been used. This later can be configured to operate as a buck converter to plot the *I-V* characteristic, and as a boost converter to track the maximum power point. The electrical characteristics of the used PV module (*JW-50P*) are given in Table 3.1. Two type of PVA configuration will be used, to show the generalization ability of the proposed emulator.

3.3.1 Control Algorithms Testing

This section shows the test results using an MPPT (Maximum Power Point Tracking) algorithm based on Perturb and Observe (*P&O*) technique developed in **LEPCI** laboratory. The results are shown by changing firstly irradiance, and, then secondly temperature. In this part of study, the PVA is a connection of two PV string in parallel, where the string is a connection of three PV modules in series, and this configuration is named *configuration-1*.

3.3.1.1 MPPT with Changing Irradiance
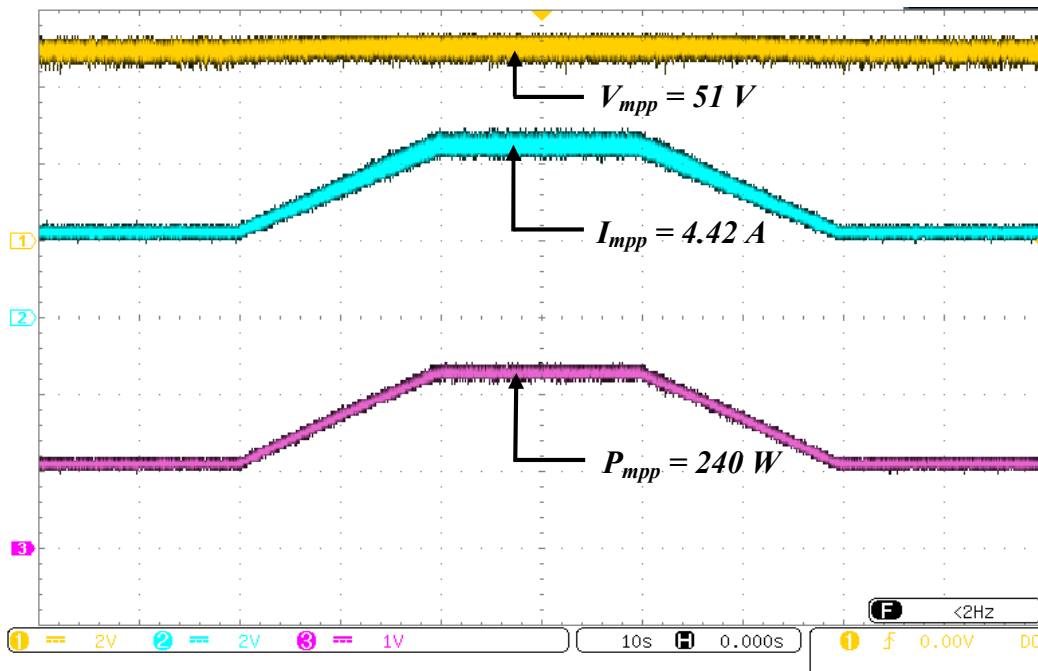
Figure 3.7: Voltage, Current, and Power curves measured by changing irradiance, where *configuration-1* is used.

Figure 3.7 shows voltage, current, and power curves for the maximum power point chosen by MPPT algorithm and by changing irradiance.

The power curves shown in Figure 3.7 were generated at the output of the inverter by the implemented MPPT algorithm, with different irradiance levels. The solar irradiance profile is fixed initially at 400 $W/m2$, and then after 20 *seconds* begins to rise constantly to 800 W/m^2 during an interval of 20 *seconds*, and then stays at this level during the same period of time, and finally returns to 400 W/m^2 in 20 *seconds*, and so on. In all this experiment the temperature is kept constant at 25 $C°$ and no fault is introduced.

3.3.1.2 MPPT with Changing Temperature

This section shows test results when temperature is changing. The temperature profile is a trapezoidal signal starting initially from 5 $C°$, and stays at this value during 20 *seconds*, then keeps rising constantly to 75 $C°$ during 20 *seconds* (by working with an emulator, the temperature changing has been accelerated), and stays at this level for the same period of time, and, then backward to 5 $C°$ in 20 *seconds*, and so on. In all this experiment the irradiance is kept constant at 800 W/m^2 and no fault is introduced.
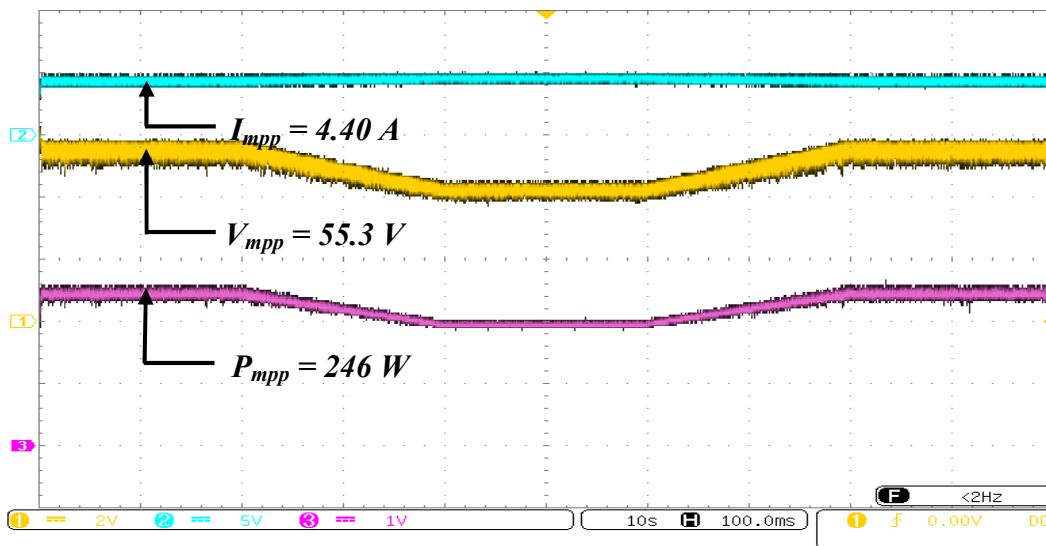
Figure 3.8: Voltage, Current, and Power curves measured by changing temperature, where *configuration-1* is used.

Figure 3.8 shows current, voltage, and power curves at the maximum power point chosen by MPPT algorithm and by changing temperature.

3.3.2 Diagnostic Algorithm Testing

The algorithm used for testing the PVE is given in Figure 3.9. For more details on it refer to [3.20] and [3.22]. In how to build such algorithm (decision making part in the same figure), a neuro-fuzzy classifier is proposed in [3.16]. Here, two single faults are considered; shading fault (*F1*) and increased series resistance (*F2*). In this part of study, the PVA is a connection of six PV modules in series, and this configuration is named *configuration-2*.
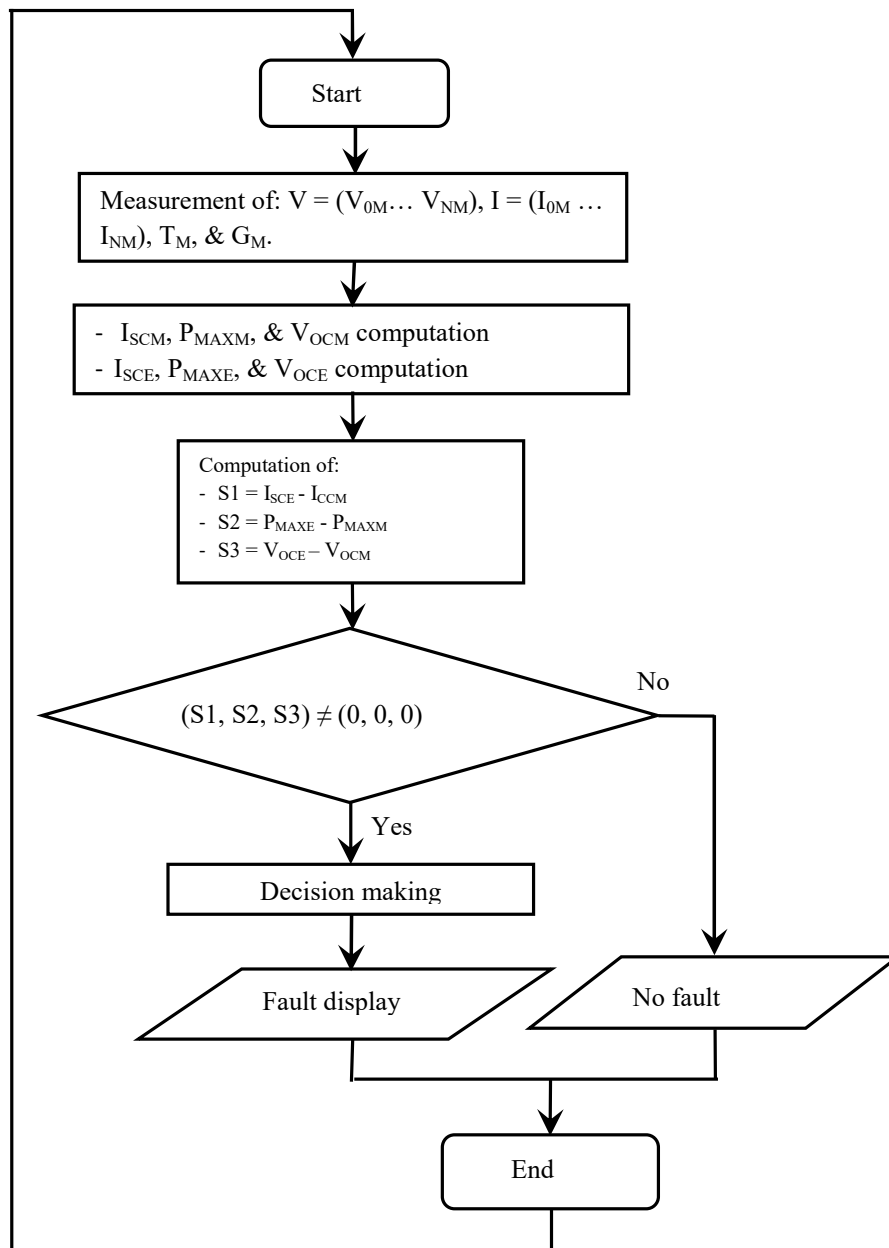
Figure 3.9: Flowchart of the diagnostic algorithm
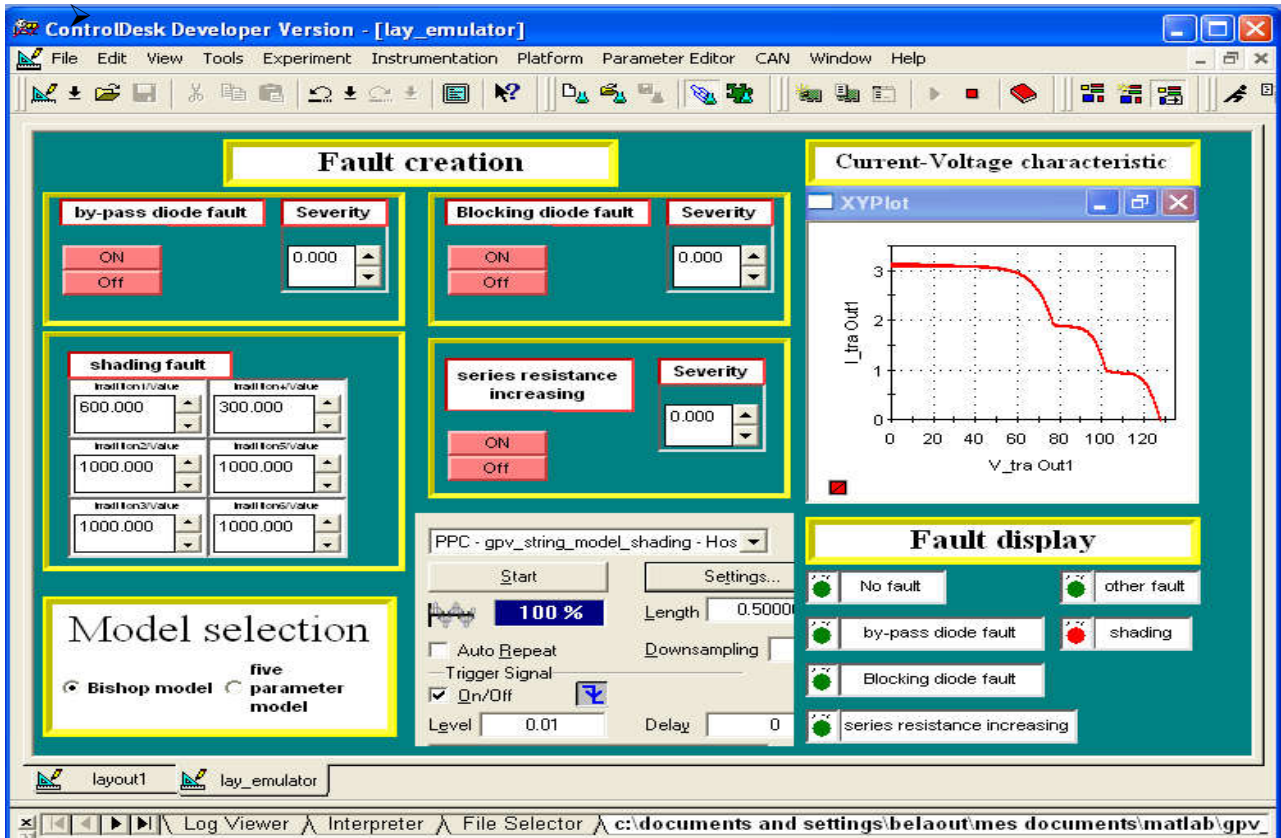
Figure 3.10: ControlDesk interface showing Shading fault condition, where *configuration-2* is used.
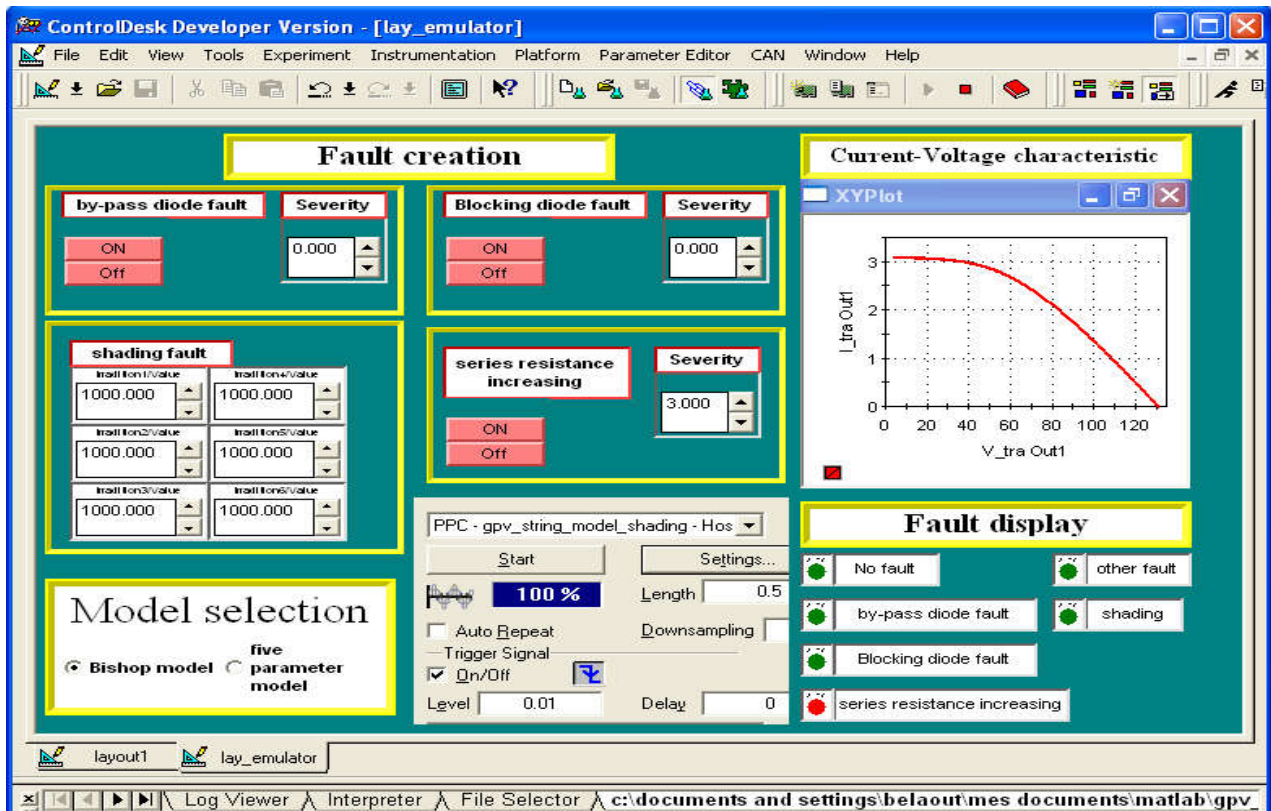
Figure 3.11: ControlDesk interface showing Increased Series Resistance condition, where *configuration-2* is used.

In the algorithm given by Figure 3.9:

➢ *V* and *I* are respectively the measured voltage and measured current vectors, allowing the *I-V* characteristic plotting.

➢ *ISCM, VOCM, PMAXM* are respectively the measured short-circuit current, open-circuit voltage, and maximum power of the PV array.

➢ *ISCE, VOCE, PMAXE* are respectively the expected short-circuit current, open-circuit voltage, and maximum power of the PV array.

The diagnostic algorithm computes three symptoms (S1, S2, and S3) from the measured and the expected quantities. Decision is made by a simple threshold based approach [16, 19-20]. This algorithm is an improved version of the algorithm presented in [21].

In Figure 3.10 and Figure 3.11 the interfaces contain four different parts: fault creation, model selection, current-voltage characteristics, and, finely fault display. The first part is used to create a fault in PVG. The second one is used to select the PV cell model. The third one consists of current-voltage characteristic curve. Finally, the situation of the PVA is shown in the fault display part (healthy or faulty PVA).

In Figure 3.10 a shading fault is introduced. One PV module is shaded at 40 %, and another is shaded at 70%. Here, it can be seen clearly that the fault is detected by the diagnostic algorithm, and in the fault display part the shading LED is red, and the remaining LEDs are green.

In Figure 3.11 series resistance is increased. The series resistance of the whole string is increased by 3 *ohms*. Here, it can be seen clearly that the diagnostic algorithm has detected the fault, and in the fault display part the series resistance increasing LED is red, and the remaining LEDs are green.

In the above tests the irradiance was kept to 1000 W/m^2, and the temperature, 25 $C°$.

A useful remark should be joined to the above results is that this section do not showing the significance of the implemented algorithms, but rather shows the ability of the proposed emulator to handle both test and control algorithms.

3.4 Data Collection for Classifier Building

As mentioned in section 3.2.1, the model of PVA was developed under Matlab software, and then implemented into a *DS1104* control board. The PVA consists of six PV modules connected in series and each module is a connection in series of 36 solar cells (this new configuration is used for data collection that will be used in chapter 4 and 5).

As a real time emulator is used, the data collection period was accelerated by implementing a loop that changes the type of the fault and its severity by considering all possible combinations of solar irradiance and module temperature. The whole dataset was collected within about 6 hours divided into two days. In fact, the whole dataset cannot be stored at ones, because of memory limitation of the existing system.

For the following situations, the I-V curves have been measured by changing solar irradiance and PV module temperature in order to cover all possible real operating conditions, and then the fault is introduced with different discrete values.

3.4.1 PVA without fault (NF)

PVA without fault, normal operation (*NO*): the normal operation condition is in the range of [100 W/m^2, 1000 W/m^2] for the solar irradiance, with step of 100 W/m^2. The module temperature is arranged [0°C, 60°C], with step of 5°C. The same conditions will be applied in the following situations, but degrees of the fault severity will be added.

Figure 3.12: *I-V* curves for normal operation (see figure 1 in the appendix)

3.4.2 Partial shading fault (*F₁*)

Partial shading fault (F_1): Nine different partial shading patterns have been considered. 25%, 50% and 75% of nine PV cell in one PV module, 25%, 50% and 75% of nine PV cell in two PV modules. Finally 25%, 50% and 75% of nine PV cell in three PV modules.

(For all these figures see figure from 2 to 10 in the appendix)

Figure 3.13.a: *I-V* curves for shading *pattern-1* (25% of nine PV cell in one PV module)

Figure 3.13.b: *I-V* curves for shading *pattern-2* (50% of nine PV cell in one PV module)

Figure 3.13.c: *I-V* curves for shading *pattern-3* (75% of nine PV cell in one PV module)

Figure 3.13.d: *I-V* curves for shading *pattern-4* (25% of nine PV cell in two PV modules)

Figure 3.13.e: *I-V* curves for shading *pattern-5* (50% of nine PV cell in two PV modules).

Figure 3.13.f: *I-V* curves for shading *pattern-6* (75% of nine PV cell in two PV modules).

Figure 3.13.g: *I-V* curves for shading *pattern-7* (25% of nine PV cell in three PV modules)

Figure 3.13.h: *I-V* curves for shading *pattern-8* (50% of nine PV cell in three PV modules)

Figure 3.13.i: *I-V* curves for shading *pattern-9* (75% of nine PV cell in three PV modules)

3.4.3 Increased series resistance (F_2)

Increased series resistance (F_2): The Rs of one PV module is increased by 1 Ω, 5 Ω, 10 Ω, 15 Ω and 20 Ω.

(For all these figures see figure from 11 to 15 in the appendix)

Figure 3.14.a: ISR *pattern-1* (the series resistance of one module is increased by 1 Ω).

Figure 3.14.b: ISR *pattern-2* (the series resistance of one module is increased by 5 Ω).

Figure 3.14.c: ISR *pattern-3* (the series resistance of one module is increased by 10 Ω).

Figure 3.14.d: ISR *pattern-4* (the series resistance of one module is increased by 15 Ω).

Figure 3.14.e: ISR *pattern-5* (the series resistance of one module is increased by 20 Ω).

3.4.4 By-pass diode short-circuited (F_3)

By-pass diode short-circuited (F_3): One by-pass diode in the whole PVA short-circuited.

Figure 3.15: By-pass diode short-circuited (1 BPD in the whole PVA short-circuited).

(See figure 16 in the appendix)

3.4.5 By-pass diode impedance (F_4)

By-pass diode impedance (F_4): By-pass diode is assimilated to resistors with different values, 1 Ω, 5 Ω, 10 Ω, 15 Ω and 20 Ω.

(For all these figures see figure from 17 to 21 in the appendix)

Figure 3.16.a: By-pass diode impedance (BPD is assimilated to a resistor of 1 Ω).

Figure 3.16.b: By-pass diode impedance (BPD is assimilated to a resistor of 5 Ω).

Figure 3.16.c: By-pass diode impedance (BPD is assimilated to a resistor of 10 Ω).

Figure 3.16.d: By-pass diode impedance (BPD is assimilated to a resistor of 15 Ω).

Figure 3.16.e: By-pass diode impedance (BPD is assimilated to a resistor of 20 Ω).

3.4.6 PV module short-circuited (F_5)

PV module short-circuited (F_5): The contribution of one PV module in the energy of PVA was eliminated by making it short-circuit.

Figure 3.17: One PV module is short-circuited.

(See figure 22 in the appendix)

By changing the operation conditions (module temperature and solar irradiance), and introducing faults in the plant (single faults), we get more *I-V* characteristics. These characteristics are recorded in workspace of Matlab software. Then, we obtain two matrices (one for the current, and the other one for the voltage). Accordingly, the real time simulation is finished.

Five datasets are considered, each of them corresponds to one type of fault, and the normal operation dataset (See Table 3.2). The whole database was split into two equal sets. The first one contains a training data for model construction, and the second one contains a test data for the accuracy estimation of the classifier.

TABLE 3.2: Datasets for normal and faulty cases of the investigated PVA

# of Dataset	Fault type	# of samples
0	Normal operation (NF)	130
1	Shading (F_1)	1170
2	Increased series resistance (F_2)	650
3	By-pass diode short-circuited (F_3)	130
4	By-pass diode impedance (F_4)	650
5	PV module short-circuited (F_5)	130

From the Table 3.2, it can be seen that 2730 *I-V* curves (faulty PVA), and 130 *I-V* curves (healthy PVA) have been collected and stored into two distinct matrices, the first one is the

current matrix (2860x200), and the second one is the voltage matrix (2860x200). The number 200 comes from the number of points in each I and V vectors.

3.5 Conclusion

In this chapter, a real time PVE has been developed using Programmable Power Source. Test results shows that the developed emulator can handle both control and diagnostic algorithms. The real time interfacing with ControlDesk makes it an easy tool to change PV module parameters, operation point, as well as to introduce faults, change their severity, visualize current-voltage characteristics and fault signalization. Database that will be used in the next chapters for multiclass neuro-fuzzy classifier building is collected.

REFERENCES

[3.1]. Belaout, A., Krim, F., Talbi, B., Feroura, H., Laib, A., Bouyahia, S., & Arabi, A. (2017). Development of real time emulator for control and diagnosis purpose of Photovoltaic Generator. *In Systems and Control (ICSC), 2017 6th International Conference on*, 139-144.

[3.2]. Koutroulis, E., Kalaitzakis, K., & Tzitzilonis, V. (2009). Development of an FPGA-based system for real-time simulation of photovoltaic modules. *Microelectronics journal*, *40*(7), 1094-1102.

[3.3]. Koran, A., Sano, K., Kim, R. Y., & Lai, J. S. (2009). Design of a photovoltaic simulator with a novel reference signal generator and two-stage LC output filter. In *Energy Conversion Congress and Exposition, 2009. ECCE 2009. IEEE*, 319-326.

[3.4]. Wandhare, R. G., & Agarwal, V. (2011). A low cost, light weight and accurate photovoltaic emulator. In *Photovoltaic Specialists Conference (PVSC), 2011 37th IEEE*, 001887-001892.

[3.5]. Can, H., Ickilli, D., & Parlak, K. S. (2012). A new numerical solution approach for the real-time modeling of photovoltaic panels. In *Power and Energy Engineering Conference (APPEEC), 2012 Asia-Pacific*, 1-4.

[3.6]. Erkaya, Y., Moses, P., Flory, I., & Marsillac, S. (2015). Development of a solar photovoltaic module emulator. In *Photovoltaic Specialist Conference (PVSC), 2015 IEEE 42nd*, 1-3.

[3.7]. Ebrahim, A. F., Ahmed, S. M. W., Elmasry, S. E., & Mohammed, O. A. (2015). Implementation of a PV emulator using programmable DC power supply. In *SoutheastCon 2015*, 1-7.

[3.8]. Nagayoshi, H., & Atesh, M. (2005). Partial shading effect emulation using multi small scale module simulator units. In *Photovoltaic Specialists Conference, 2005. Conference Record of the Thirty-first IEEE*, 1710-1713.

[3.9]. Qin, S., Kim, K. A., & Pilawa-Podgurski, R. C. (2013). Laboratory emulation of a photovoltaic module for controllable insolation and realistic dynamic performance. In *Power and Energy Conference at Illinois (PECI), 2013 IEEE*, 23-29.

[3.10]. Xenophontos, A., Rarey, J., Trombetta, A., & Bazzi, A. M. (2014). A flexible low-cost photovoltaic solar panel emulation platform. In *Power and Energy Conference at Illinois (PECI), 2014*, 1-6.

[3.11]. Islam, R. R., Liao, M., Vo, T. H., & Ravishankar, J. (2014). Experimental setup of a microgrid with wind and solar power emulators. In *Electrical Energy Systems (ICEES), 2014 IEEE 2nd International Conference on*, 9-14.

[3.12]. Midtgard, O. M. (2007). A simple photovoltaic simulator for testing of power electronics. In *Power Electronics and Applications, 2007 European Conference on*, 1-10.

[3.13]. Di Piazza, M. C., & Vitale, G. (2010). Photovoltaic field emulation including dynamic and partial shadow conditions. *Applied Energy*, *87*(3), 814-823.

[3.14]. Geury, T., & Gyselinck, J. (2013). Emulation of photovoltaic arrays with shading effect for testing of grid-connected inverters. In *Power Electronics and Applications (EPE), 2013 15th European Conference on*, 1-9.

[3.15]. Bun, L., Raison, B., Rostaing, G., Bacha, S., Rumeau, A., & Labonne, A. (2011). Development of a real time photovoltaic simulator in normal and abnormal operations. In *IECON 2011-37th Annual Conference on IEEE Industrial Electronics Society*, 867-872.

[3.16]. Belaout, A., Krim, F., & Mellit, A. (2016). Neuro-fuzzy classifier for fault detection and classification in photovoltaic module. In *Modelling, Identification and Control (ICMIC), 2016 8th International Conference on*, 144-149.

[3.17]. Bishop, J. W. (1988). Computer simulation of the effects of electrical mismatches in photovoltaic cell interconnection circuits. *Solar cells*, *25*(1), 73-89.

[3.18]. Belaout, A., Krim, F., Arabi, A., & Ayad, M. (2016). Comparaison entre les Modèles à une seule Diode et de Bishop de la Cellule Solaire. *In 1st National Conference on Electronics and Electrical Engineering (NCEEE'2016)*.

[3.19]. Sera, D., Teodorescu, R., & Rodriguez, P. (2007). PV panel model based on datasheet values. In *Industrial Electronics, 2007. ISIE 2007. IEEE International Symposium on*, 2392-2396.

[3.20]. Belaout, A. (2018). Etude et diagnostic des défauts fréquents aux systèmes photovoltaïques (PV) par emploi de la caractéristique courant-tension (*Magister dissertation*).

[3.21]. Belaout, A., Krim, F., & Mellit, A. (2016). Fuzzy Classifier for Fault Detection and Classification in Photovoltaic Module. *In International Conference on Technological Advances in Electrical Engineering*.

[3.22]. Chine, W., Mellit, A., Lughi, V., Malek, A., Sulligoi, G., & Pavan, A. M. (2016). A novel fault diagnosis technique for photovoltaic systems based on artificial neural networks. *Renewable Energy*, *90*, 501-512.

CHAPTER 4

Construction and Reduction of Classifier's Features (Inputs)

4.1 Introduction

Huge data can be collected and processed due to the available technical means nowadays. However, the data is only valuable if it is powerfully processed and useful information is extracted from it. It is now common to find applications that require data with thousands of features (inputs to the classifiers). Problem with processing such datasets is that they require huge amount of resources. To conquer this difficulty, research and scientific communities have introduced effective algorithms called feature reduction techniques. Feature reduction allows only selecting relevant features that we can use instead of using the entire features space.

4.1.1 Reasons behind Features Reduction Techniques

The main objective of feature selection is to select a subset of features from the entire feature space. The selected features could provide the same information provided by the entire feature set. However, different researchers explain feature selection from different points of view. Some of these are:

1) *Faster and more cost-effective models:* Feature selection tends to provide minimum number of features to subsequent processes, so that these processes don't need to process

the entire set of features. The reduced number of features means the minimum execution time for the model.

2) *Avoid overfitting and improve performance:* By selecting the best features that provide most of the information and by removing noisy, redundant and irrelevant features, the accuracy and effectiveness of model can be enhanced. It reduces the number of dimensions and thus improves the performance of the classifier.

3) *Deeply understand the process that generated data:* Feature selection also provides opportunity to understand the relationships between attributes to better understand the principal process. It helps understand the relationship between the features and about the process that generated data.

4.1.2 Review of Feature selection techniques

Feature selection is one of the solutions to the problem of curse of dimensionality. It is the process of selecting a subset of features from original feature space that provides most valuable information [4.1]. The selected features can then be used instead of the original feature space. So, a good feature selection algorithm should choose features that tend to provide complete or most of the information as presented in the entire feature space and omit the irrelevant and redundant features. Dimensionality reduction techniques can be categorized into two groups, "*feature selection*" and "*feature extraction*". Feature extraction techniques [4.2–4.14] project original feature space to a new feature space with lesser number of dimensions. The new feature space is normally constructed by combining the original feature in some way. The problem with these approaches is that the original semantics of data are lost. Feature selection techniques [4.15–4.28] on the other hand tend to select features from the original features to represent the original concept. Based on the nature of available data, feature selection can be categorized either as supervised feature selection or unsupervised feature selection. In supervised feature selection, the class labels are already provided and the feature selection algorithm selects the features on the basis of classification accuracy. In unsupervised feature selection, the class labels are missing and the feature selection algorithms have to select feature subset without label information. On the other hand, when class labels for some instances are given and missing for some, semi-supervised feature selection algorithms are used.

Because of the nature of data used in this study, a supervised feature selection technique will be used.

4.1.3 Research Contribution Obtained in this Chapter

Unlike in [4.29-4.32], where authors start by some features, and in the case where they found it insufficient to discriminate the total chosen faults, they add new ones. Others like in [4.33] used some indicators, and when they found them not meaningful they omit them and seek for new significant parameters. This seems to be done visually by looking to data and using some performance criteria, without using any based-automatic methods for features selection. This chapter presents an inverse method, starting by using many features, and then reducing their number by using variable dimensionality reduction techniques. This alternative solution saves a lot of time for classifiers development.

4.2 Features construction

Feature construction is a process which makes a map from raw data to the classifier input. The aim is to build more efficient features for fault detection and classification task. Voltage and current matrices collected from the PVA, are stored in Matlab workspace for further processing are:

$$V = \begin{bmatrix} V_{11} & \cdots & V_{1n} \\ \vdots & \ddots & \vdots \\ V_{m1} & \cdots & V_{mn} \end{bmatrix} \tag{1}$$

$$I = \begin{bmatrix} I_{11} & \cdots & I_{1n} \\ \vdots & \ddots & \vdots \\ I_{m1} & \cdots & I_{mn} \end{bmatrix} \tag{2}$$

Let us introduce some useful notations for the two matrices. For the i-th I-V characteristic, such as i runs over 1 to m, there are n points (in our thesis, $n = 200$ points) of index j for each characteristic (these notations are common for both voltage and current matrices).

From the raw data (I and V matrices) we extract features S_f ($f=1…12$) for both healthy and faulty PVA using the following formulas:

4.2.1 Feature 1: I-V curve area (S_1).

The area under the I-V curve is calculated by the integral:

$$S_1 = \int_0^{V_{oc}} V(I) dI \tag{3}$$

Since the voltage and current vectors (for *I-V* characteristic) have non-uniform spaced discrete values, one can use the following approximation for numerical implementation of the area of the *i*-th *I-V* curve:

$$S_1 = \int_0^{V_{oc}} V(I) dI \approx \frac{1}{2} \sum_{j=1}^{n} \left(I_{j+1} - I_j \right) \left(f\left(I_{j+1} \right) + f\left(I_j \right) \right) \tag{4}$$

This method is known as the trapezoidal rule.

4.2.2 Feature 2: short-circuit current (*S2*).

This feature can be obtained by the following simple formula:

$$S_2 = I|_{V=0} = I_{sc} \tag{5}$$

From Eq. 5 short-circuit current is the current provided by the PV array where its voltage is equal to zero.

4.2.3 Feature 3: open-circuit voltage (*S3*).

The open-circuit voltage can be calculated as:

$$S_3 = V|_{I=0} = V_{oc} \tag{6}$$

From Eq. 6 open-circuit voltage is the voltage provided by the PV array where its current is equal to zero.

4.2.4 Feature 4: maximum power point (*S4*).

The maximum power of the *I-V* curve is given as:

$$S_4 = \max(V \times I) \tag{7}$$

4.2.5 Feature 5: voltage at the maximum power point (*S_5*).

If the index of the voltage *V* for the *i*-th *I-V* curve at the maximum power point (MPP) is *P*, then:

$$S_5 = V\Big|_{V_{ip}}$$

(8)

4.2.6 Feature 6: current at the maximum power point (S_6).

V_{ip} is defined in Feature 5.

$$S_6 = I\Big|_{V_{ip}}$$

(9)

4.2.7 Feature 7: I-V curve slope at the vicinity of V_{oc} (S_7).

$$S_7 = \frac{dI}{dV}\Big|_{V_{oc}}$$

(10)

4.2.8 Feature 8: I-V curve slope at the midpoint between MPP and open-circuit voltage point (S_8).

We denote by *md1* this first midpoint, so:

$$S_8 = \frac{dI}{dV}\Big|_{md1}$$

(11)

4.2.9 Feature 9: I-V curve slope at the MPP (S_9).

$$S_9 = \frac{dI}{dV}\Big|_{V_{iP}}$$

(12)

4.2.10 Feature 10: I-V curve slope at short-circuit current I_{sc} (S_{10}).

$$S_{10} = \frac{dI}{dV}\Big|_{I_{sc}}$$

(13)

4.2.11 Feature 11: I-V curve slope at the midpoint between short-circuit current point and MPP (S_{11}).

We denote by *md2* the second midpoint, so:

$$S_{11} = \frac{dI}{dV}\Big|_{md2}$$
.

(14)

4.2.12 Feature 12: filling factor *(S12)*.

$$S_{12} = \frac{(S_5 \times S_6)}{S_2 \times S_3}$$

(15)

Features for faulty PVA have been compared to those of normal PVA, and then the results are normalized. In fact, all features for abnormal operation are compared to those for normal operation by using the following formula to get normalized features:

$$\text{feature} = \frac{\text{feature(normal)} - \text{feature(abnormal)}}{\text{feature(normal)}}$$

(16)

The obtained values for all features are normalized by using Eq (16), and the final product is a matrix of dimension (2860x12). This latter will be used in this chapter and the next chapter for MC-NFC model construction.

By changing solar irradiance, and module temperature in the way to sweep all possible combinations of the operating conditions, we get 130 I-V curves (healthy case). The same conditions have been applied for faulty condition, but degrees of fault severity have been involved. For more clearness, we take the case of Increased series resistance (*F2*): repeating 130 possible combination of couple (*G, T*) five times (the number of Increased Series Resistance scenarios), the number of normalized features using eq (16) is 130×5 = 650 samples. Thus, the 130 *I-V* curves for healthy case are used for generating samples by eq (16) for all scenarios of different fault types, the raison why we get only 2730 samples at the end.

Once the classifier built, the unknown samples will be normalized using the same equation (Eq. (16)). Where feature (normal) is computed from the implemented model in ds1104 platform, and feature (abnormal) is computed from the real PVA, according to the flowchart presented in figure 4.1:

If unknown samples are presented to the neuro-fuzzy classifier, the decision at the classifier output will be "other fault", indicating that PVA is subject to another fault type that is not considered in this study.
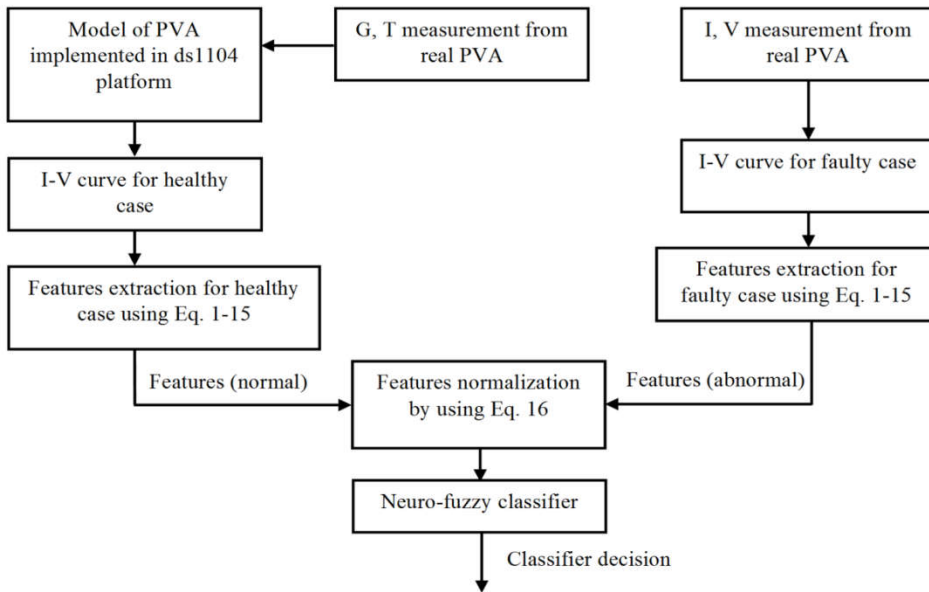
Figure 4.1: Overview of the proposed method for real-time fault detection and classification phase of unknown samples.

If FD = D_1 then partial shading is occurring.
If FD = D_2 then increased series resistance losses.
If FD = D_3 then one by-pass diode is court-circuited.
If FD = D_4 then by-pass diode impedance.
If FD = D_5 then one PV module short-circuited.
If FD = 0 then no fault in PVA.
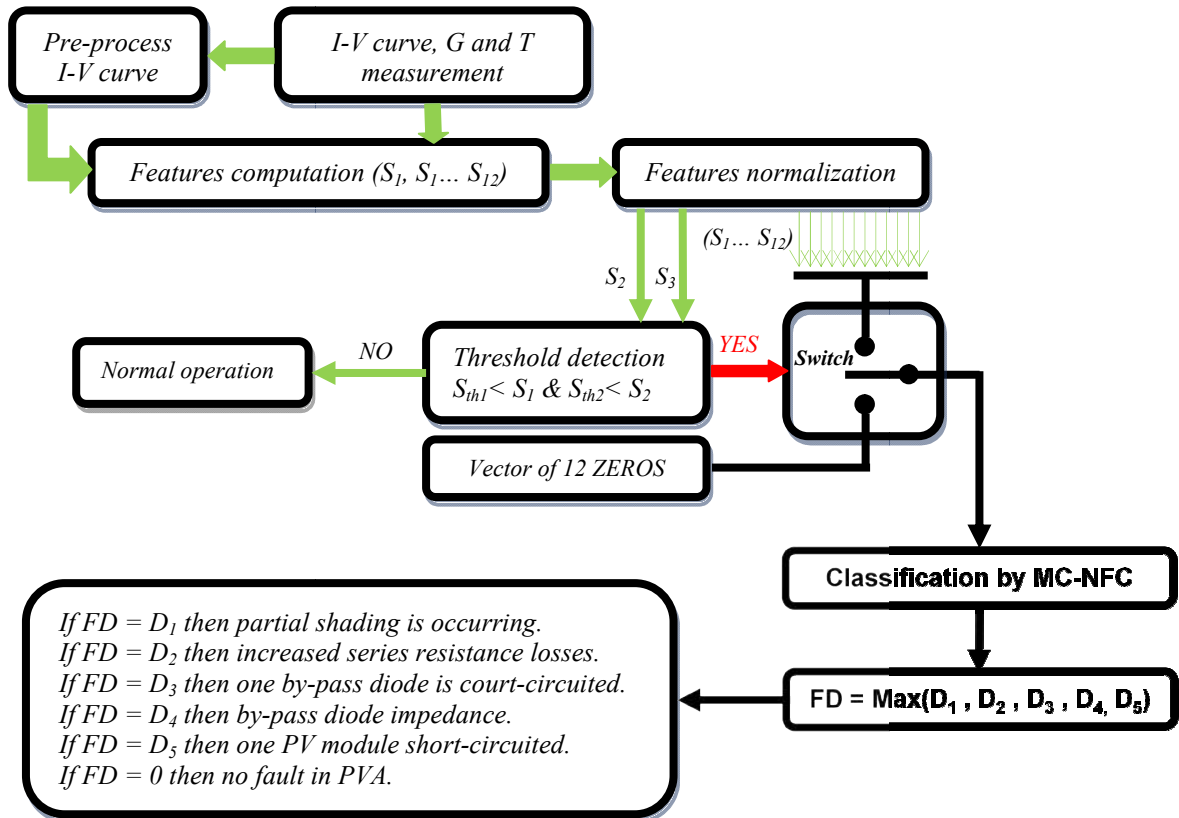
Figure 4.2: The structure of the fault detection and classification algorithm based on classifiers decision outputs fusion.

Figure 4.2 shows the detection and classification algorithm basic tasks. First, *I-V* curve is preprocessed for noise elimination. Second, features extracted from *I-V* curve by Eqs. 4.3-4.15 have been normalized by using Eq. 3.16. Then, switch is positioned on normalized features only if thresholds S_{th2} and S_{th3} are reached, otherwise classifiers will be fed by a zero values for all its inputs components (which means that no fault occurring in the PVA).

Finally classifier output decisions have been compared to decide which one is the biggest for final decision.

3.3 Feature Reduction for MC-NFC Building

The importance of feature dimensionality reduction techniques and the advantage of MC-NFC over traditional ones will be shown. First, in the section 3.3.1, the proposed method for feature dimensionality reduction has been applied to five classifiers: Partial shading fault classifier (F_1 classifier), increased series resistance classifier (F_2 classifier), By-pass diode short-circuited classifier (F_3 classifier), By-pass diode impedance classifier (F_4 classifier), and PV module short-circuited classifier (F_5 classifier). Then, in next chapter, the proposed MC-NFC trained and tested with the reduced entire original feature space, which is defined by a vector of 12 features. Finally, in the same chapter the MC-NFC will be compared to an ANN classifier.

3.3.1 Feature selection for each neuro-fuzzy classifier

First, constructed features have been created without prior information on their effect on the classifier that will be designed. However, what it is known certainly, is that the constructed features will not have the same effect on the classifier decision (output), some of them have the same effect, and some others have no effect on the classifier output at all. These reasons conduct us to reduce the feature space dimensionality. This leads, to avoid redundant information, in the case where some collinear features exist, and also eliminating features that have no effect on output of the decision function.

A standard way to pick a best set of features is via feature space dimensionality reduction techniques. A Matlab program (See Figure 4.3) has been developed in order to reduce the classifier input dimensionality. Let us consider *n* the total number of features, and *k* the number of selected features, and then the number of trained classifier is given by the following formula (known as combination without repetition):

$$P = \binom{n}{k} = \frac{n!}{k!(n-k)!} \qquad (29)$$

The following flowchart explains the algorithm used for inputs (features) classifier reduction.
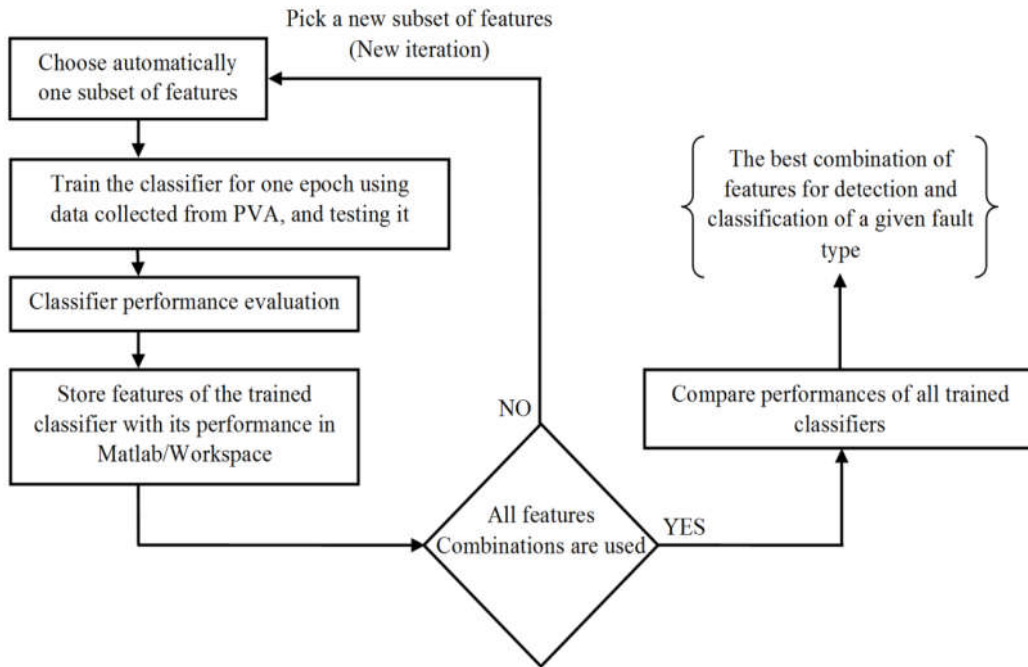
Figure .4.3: Overview of the proposed method used for inputs (features) classifier reduction.

As indicated in Figure 4.3, the algorithm chooses automatically a subset of 12 features (described in section 4.2) and train and test the classifier using these latter. Then, the built model will be stored with its performance for further use. The procedure is repeated until all features combinations are used. At the end, all classifier performances will be compared, and the features will be retained for a given fault type detection and classification.

An ANFIS classifier was built for each combination, and in order to reduce the computation time, the classifier was trained for only one epoch. After that, obtained classifiers must be classified according to their RMSE, and the most relevant combination predicting the output is retained.

As we have five classifiers, the best combination of features is selected for each one of them. In the following, n is always equal to 12 (the total number of features), and k varies from 1 to 12(the number of features selected for each combination).

- *F_1 classifier features reduction*

Table 4.1 demonstrates the result of selecting classifier inputs from one to four, and the best combination of features has been hold. It can be seen clearly that the minimal training (and checking) error are reduced by increasing the number of the selected features. Therefore we will stick to the four-feature classifier for further investigation.

TABLE 4.1: Features (inputs) selection for F_1 classifier

n	12	12	12	12
k	1	2	3	4
RMSE for training	0.6277	0.4183	0.2342	0.1660
RMSE for testing	0.6041	0.4271	0.2046	**0.1740**
Best combination of features	S_3	$S_3\ S_{11}$	$S_4\ S_8\ S_{12}$	**$S_1\ S_3\ S_6\ S_{12}$**

- *F2 classifier features reduction*

Concerning F_2 classifier (See Table 4.2) increasing the number of features from 3 to 4 does not minimize significantly the training (checking error), which indicates clearly that the newly added feature does not improve the classification accuracy much. For better generalization, we always prefer a model with fewer inputs. Therefore we will stick to the three-feature classifier for further investigation.

TABLE 4.2: Features (inputs) selection for F_2 classifier

n	12	12	12	12
k	1	2	3	4
RMSE (Training)	0.7600	0.6298	0.5758	0.5500
RMSE (Testing)	0.7572	0.6319	**0.5539**	0.5200
Best combination of features	S_3	$S_4\ S_{12}$	**$S_4\ S_{11}\ S_{12}$**	$S_2\ S_8\ S_{11}\ S_{12}$

- *F3 classifier features reduction*

For the same raisons as in F_2 classifier, only two features have been selected for F_3 classifier (See Table 4.3).

TABLE 4.3: Features (inputs) selection for *F3* classifier

n	12	12	12	12
k	1	2	3	4
RMSE (Training)	0.1073	0.0626	0.0356	0.0231

RMSE (Testing)	0.0428	**0.0352**	0.0331	0.0400
Best combination of features	S_3	**$S_3\ S_4$**	$S_1\ S_3\ S_{12}$	$S_1\ S_3\ S_8\ S_{12}$

- ***F4 classifier features reduction***

For the same raisons as in F_2 classifier, only two features are selected for F_4 classifier (See Table 4.4).

TABLE 4.4: Features (inputs) selection for F_4 classifier

n	12	12	12	12
k	1	2	3	4
RMSE (Training)	0.7290	0.5940	0.5521	0.5250
RMSE (Testing)	0.7252	**0.5662**	0.5301	0.5100
Best combination of features	S_4	**$S_1\ S_4$**	$S_1\ S_4\ S_8$	$S_1\ S_2\ S_4\ S_{11}$

- ***F5 classifier features reduction***

For the same raisons as in F_2 classifier, only two features are selected for F_5 classifier (See Table 4.5).

TABLE 4.5: Features (inputs) selection for $F5$ classifier

n	12	12	12	12
k	1	2	3	4
RMSE(Training)	0.3428	0.0027	0.0012	0.0005
RMSE(Testing)	0.3420	**0.0014**	0.0011	0.0004
Best combination of features	S_1	**$S_3\ S_4$**	$S_1\ S_3\ S_4$	$S_1\ S_3\ S_4\ S_{12}$

The results from the above Tables (4-1 to 4-5) indicate that the combinations (S_1, S_3, S_6, S_{12}), (S_4, S_{11}, S_{12}), (S_3, S_4), (S_1, S_4) and (S_3, S_4) are the most influential features with respect to the decision function output the *F1* classifier, *F2* classifier, *F3* classifier, *F4* classifier and *F5* classifier, respectively. Consequently, the whole space dimensionality has been reduced from 12 features to only 5 features, namely S_1, S_3, S_4, S_{11} and S_{12}.

3.4 Conclusion

From the experiments presented in this chapter, it can be strongly recommended the use of the space dimensionality reduction techniques for classification of photovoltaic array faults, owing to its capability to speed up the process of classifiers building, not only for the

classifier that will be constructed, but also for any other type of classifier. This provides for the classifiers a clean manner to select their inputs. Furthermore, it provides high classification accuracy and lower features (inputs) space dimensionality.

REFERENCES

[4.1] Jensen, R., & Shen, Q. (2008). Computational intelligence and feature selection: rough and fuzzy approaches (Vol. 8). *John Wiley & Sons*.

[4.2] Neeman, S. (2008). Introduction to wavelets and principal components analysis. *VDM Verlag Dr. Muller Aktiengesellschaft& Co. KG*.

[4.3] Engelen, S., Hubert, M., & Branden, K. V. (2005). A comparison of three procedures for robust PCA in high dimensions. *Austrian Journal of Statistics*, *34*(2), 117-126.

[4.4] Cunningham P. (2008). Dimension reduction. *Machine learning techniques for multimedia. Springer, Berlin/Heidelberg*,: 91–112.

[4.5] Van Der Maaten, L., Postma, E., & Van den Herik, J. (2009). Dimensionality reduction: a comparative. *J Mach Learn Res*, *10*, 66-71.

[4.6] Friedman, J. H., & Stuetzle, W. (1981). Projection pursuit regression. *Journal of the American statistical Association*, *76*(376), 817-823.

[4.7] Borg, I., & Groenen, P. (2003). Modern multidimensional scaling: theory and applications. *Journal of Educational Measurement*, *40*(3), 277-280.

[4.8] Dalgaard, P. (2008). Introductory statistics with R. *Springer Science & Business Media*.

[4.9] Zeng, X., & Luo, S. (2008). Generalized locally linear embedding based on local reconstruction similarity. In *Fifth International Conference on Fuzzy Systems and Knowledge Discovery*, 305-309.

[4.10] Saul, L. K., Weinberger, K. Q., Ham, J. H., Sha, F., & Lee, D. D. (2006). Spectral methods for dimensionality reduction. *Semisupervised learning*, 293-308.

[4.11] Liu, R., Wang, Y., Baba, T., & Masumoto, D. (2008). Semi-supervised learning by locally linear embedding in kernel space. In *Pattern Recognition, 2008. ICPR 2008. 19th International Conference on*, 1-4.

[4.12] Gerber, S., Tasdizen, T., & Whitaker, R. (2007). Robust non-linear dimensionality reduction using successive 1-dimensional Laplacian eigenmaps. In *Proceedings of the 24th international conference on Machine learning*, 281-288.

[4.13] Donoho, D. L., & Grimes, C. (2003). Hessian eigenmaps: Locally linear embedding techniques for high-dimensional data. *Proceedings of the National Academy of Sciences*, *100*(10), 5591-5596.

[4.14] Teng, L., Li, H., Fu, X., Chen, W., & Shen, I. F. (2005). Dimension reduction of microarray data based on local tangent space alignment. In *Cognitive Informatics, 2005.(ICCI 2005). Fourth IEEE Conference on*, 154-159.

[4.15] Raman, B., & Ioerger, T. R. (2002). Instance-based filter for feature selection. *Journal of Machine Learning Research*, *1*(3), 1-23.

[4.16] Yan, G., Liu, L., Du, L., Yang, X., & Ma, Z. (2008). Unsupervised sequential forward dimensionality reduction based on fractal. In *Fuzzy Systems and Knowledge Discovery, 2008. FSKD'08. Fifth International Conference on*, 2, 48-52.

[4.17] Tan, F., Fu, X., Zhang, Y., & Bourgeois, A. G. (2008). A genetic algorithm-based method for feature subset selection. *Soft Computing*, *12*(2), 111-120.

[4.18] Loughrey, J., & Cunningham, P. (2005). Using early-stopping to avoid overfitting in wrapper-based feature selection employing stochastic search. *Trinity College Dublin, Department of Computer Science*.

[4.19] Valko, M., Marques, N. C., & Castellani, M. (2005). Evolutionary feature selection for spiking neural network pattern classifiers. In *Artificial intelligence, 2005. epia 2005. portuguese conference on*, 181-187.

[4.20] Huang, J., Lv, N., & Li, W. (2006). A novel feature selection approach by hybrid genetic algorithm. In *Pacific Rim International Conference on Artificial Intelligence, Springer, Berlin, Heidelberg,* 721-729.

[4.21] Khushaba, R. N., Al-Ani, A., & Al-Jumaily, A. (2008). Differential evolution based feature subset selection. In *Pattern Recognition, 2008. ICPR 2008. 19th International Conference on*, 1-4.

[4.22] Roy, K., & Bhattacharya, P. (2008). Improving features subset selection using genetic algorithms for iris recognition. In *IAPR Workshop on Artificial Neural Networks in Pattern Recognition*, *Springer, Berlin, Heidelberg*, 292-304.

[4.23] Dy, J. G., & Brodley, C. E. (2004). Feature selection for unsupervised learning. *Journal of machine learning research*, *5*, 845-889.

[4.24] He, X., Cai, D., & Niyogi, P. (2006). Laplacian score for feature selection. In *Advances in neural information processing systems*, 507-514.

[4.25] Wolf, L., & Shashua, A. (2005). Feature selection for unsupervised and supervised inference: The emergence of sparsity in a weight-based approach. *Journal of Machine Learning Research*, *6*, 1855-1887.

[4.26] Bryan, K., Cunningham, P., & Bolshakova, N. (2005). Biclustering of expression data using simulated annealing. In *Computer-Based Medical Systems, 2005. Proceedings. 18th IEEE Symposium on*, 383-388.

[4.27] Handl, J., Knowles, J., & Kell, D. B. (2005). Computational cluster validation in post-genomic data analysis. *Bioinformatics*, *21*(15), 3201-3212.

[4.28] Gluck, M. (1985). Information, uncertainty and the utility of categories. In *Proc. of the Seventh Annual Conf. on Cognitive Science Society*.

[4.29] Belaout, A., Krim, F., & Mellit, A. (2016). Neuro-fuzzy classifier for fault detection and classification in photovoltaic module. In *Modelling, Identification and Control (ICMIC), 2016 8th International Conference on*, 144-149.

[4.30] Chine, W., Mellit, A., Lughi, V., Malek, A., Sulligoi, G., & Pavan, A. M. (2016). A novel fault diagnosis technique for photovoltaic systems based on artificial neural networks. *Renewable Energy*, *90*, 501-512.

[4.31] Kim, I. S. (2016). On-line fault detection algorithm of a photovoltaic system using wavelet transform. *Solar Energy*, *126*, 137-145.

[4.32] Spataru, S., Sera, D., Kerekes, T., & Teodorescu, R. (2015). Diagnostic method for photovoltaic systems based on light I–V measurements. *Solar Energy*, *119*, 29-44.

[4.33] Hachana, O., Tina, G. M., & Hemsas, K. E. (2016). PV array fault DiagnosticTechnique for BIPV systems. *Energy and Buildings*, *126*, 263-274.

CHAPTER 5

Fault Classification Using Artificial Intelligence Algorithms

5.1 Introduction

Fault detection is used for protecting the PV installation and the personal from any dangers. Moreover, fault classification is used to identify the fault type, and, then help maintenance team to take a right and quick decision. Based on data collected from the systems, artificial intelligence algorithms are usually used to achieve automatic fault classification. This chapter studies fault classification methods and focuses on multiclass neuro-fuzzy classifier (MC-NFC) for PV fault detection and classifications (FDC).

5.1.1 Existing Detection and Classification Methods and their Limitations

Fault diagnosis techniques (FDT) play an important role to reduce the energy and material losses. Fault diagnosis in DC-side of a PVA can be classified into three categories, according to the used detection and classification methods, the type of fault to be discriminated, and the chosen features feeding the classifier input:

1) Different types of detection and classification methods were proposed in literature. For example, in [5.1] the authors proposed a Neuro-Fuzzy classifier (NFC), by first, constructing an initial Fuzzy Classifier (FC), and then upgrading it with learning algorithms. A database obtained by exhaustive simulation with Matlab/Simulink software. A total of 5790 I-V curves have been stored for features extraction, and further treatment.

A FD technique based on artificial neural network (ANN) technique was proposed in [5.2]. Two different algorithms have been used; the first one is based on threshold detection and isolates six types of fault, while the second one is based on an ANN algorithm. Radial Basis Function (RBF) and Multilayer Perceptron (MLP) architectures have been compared. This later detects and isolates four types of fault [5.2]. In [5.3] a wavelet transform approach has been developed, this method uses also two algorithms, the first one was developed to detect switch open and over harmonic fault using 3-level Multi Level Decomposition (MLD) algorithm, and the second one detects the islanding condition using wavelet coefficients energies. A combination of three FCs, and a sensitivity of the indicators to different type of factors was analyzed in [5.4], such as solar irradiance and PV module temperature conditions. In [5.5] the authors proposed a Graph-Based Semi-Supervised (GBSS) learning algorithm, the model developed has the ability of self-leaning in real-time conditions. Accordingly, it is a low cost model in terms of training. Many other methods can be found in the literature [5.6-5.10].

2) The fault types to be detected and classified are varying from one author to other. For example in [5.1] the authors proposed a method to detect and then classify three types of faults: increased series resistance, by-pass diode fault, and blocking diode fault. Eight PVA fault types have been detected and classified [5.2]: PV cells, PV module, PV string and by-pass diode faults. The switch open fault and any over harmonic, and islanding condition were detected and classified in [5.3]. These faults occur in a Power Conditioning System (PCS), and it manifests as current-distortion at the output of the PCS. In [5.4], partial shading, increased series resistance (ISR) losses and Potential-Induced Degradation (PID) in string PV systems where detected and classified by measurements and extraction of the indicators value of the full PV string I-V characteristic. Ref [5.5] focuses on two groups of frequently occurring faults in PVAs that cannot be cleared by conventional protection schemes: the line-to-line fault and open-circuit fault. The authors in [5.11] have constructed a three state Markov model to represent the state transition relationship of no faults, intermittent faults, and permanent faults for not only PVA, but for all PV components.

3) Selection of classifier input plays an important role to get a high classifier performance for both detection and classification phases. In [5.1] the authors have used two features: Maximum Power Point (MPP), and open-circuit voltage (*Voc*), and when they found it

insufficient to discriminate the considered PV module faults, they add a new ones, namely short-circuit current and filling factor. Five features have been used in [5.2]: a reduction in the short circuit current (C1), A reduction in the open circuit voltage (V1), a reduction or an increase in the output current (C2), a reduction or an increase in the output voltage (V2) and number of peaks in the current-voltage characteristics. The contribution of the previous attributes is analyzed and the most influencing are retained for each type of fault. In [5.3] the employed features are: Multi-level Decomposition (MLD) of the wavelet transform, and wavelet coefficients energies are extracted from the grid current and the grid voltage. In [5.4] the authors used as inputs classifier: the equivalent thermal voltage (Vte), *I-V* curve flexing factor (IVf), Maximum power point factor (MPPf), Equivalent series resistance (Rse) and Fill factor (FF).

In the above three categories, the methods have been used for detection and classification of the PV string/array faults, which are mainly based on I-V curves to extract features and run their algorithms. There are many other methods based on visual inspection, and infrared imaging, in which surface soiling, dust accumulation, and hot spot phenomena in PV modules can be detected and removed [5.12-5.15].

5.1.2 Research Contributions Obtained in this Chapter

An outline of the main contributions of this chapter is as follow:

➢ First, new features have been introduced into the classifier input. Namely, *I-V* curve area and slopes at different points of the *I-V* curve.

➢ Second, in the developed method some patterns of faults are used, but it can detect all possible real patterns for the concerned fault, unlike in [5.16], where they used some discrete real situation and these patterns could not be exist in real conditions.

➢ Finally, a MC-NFC has been developed to discriminate between five different types of faults in a PVA.

5.2 Basics of Artificial Intelligence Based Classifiers

5.2.1 Steps Toward Multiclass Neuro-Fuzzy Classifier Development

For an efficient and organized manner, six basic steps are necessary in the process of classifier development (See Figure .5.1):

1) Implement the PVA model;

2) Datasets collection covering the most possible scenario for each fault, and the normal operation;

3) Features extraction;

4) Threshold adjustment for faults detection;

5) Classifiers training and testing;

6) Classifiers' decisions fusion for final decision.
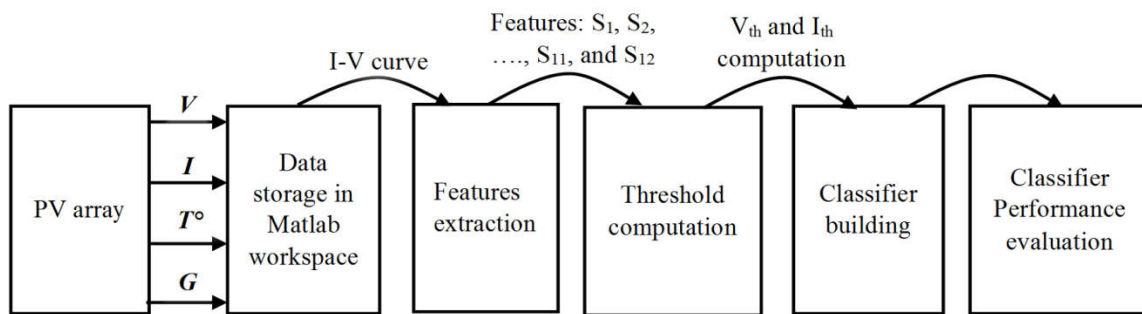
Figure .5.1: Process of classifier building for fault detection and classification in a PVA

5.2.2 Basics of Artificial Intelligence Techniques

Scientists have long dreamed of building machines that think [5.17-5.19]. When programmable computers were first designed, people wondered whether such machines might become smart, more than a hundred years before one was constructed [5.20]. Today, artificial intelligence (AI) is a flourishing area with many realistic applications and dynamic research area. We look to intelligent software to computerize tasks, recognize speech or images, make diagnosis in medicine and faults detection and classification in electrical systems. At the beginning of artificial intelligence, the field rapidly undertaken and solved problems that are seriously difficult for human beings but rather simple for computers [5.21].

Figure .5.2 shows the relation between AI and ML. Accordingly, ML is a branch of AI. A Venn diagram showing how a deep learning is kind of representation learning, which is in

turn a kind of machine learning. Each section of the Venn diagram includes an example of an AI technology [5.21].

The branch of machine learning is a subset of Artificial Intelligence, and it can be divided into three main kinds of learning: supervised learning, unsupervised learning, and reinforcement learning.
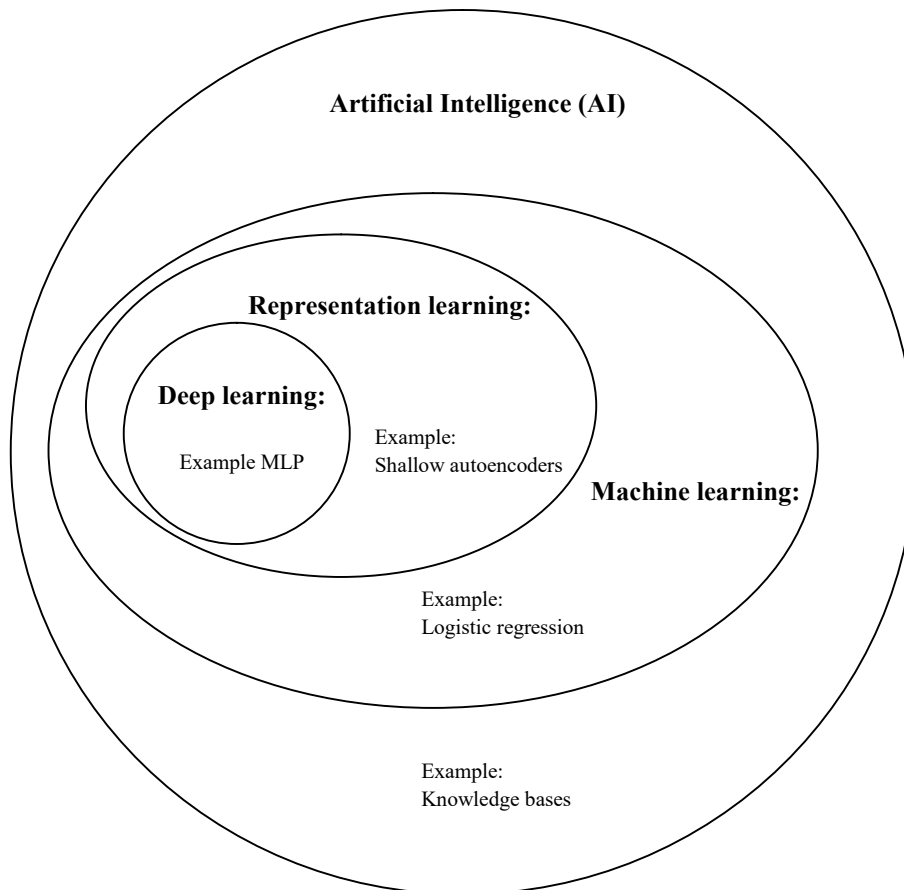

Figure .5.2: simplified flowchart of Artificial Intelligence techniques: Artificial Intelligence (AI), Machine learning (ML), Representation learning and deep learning.
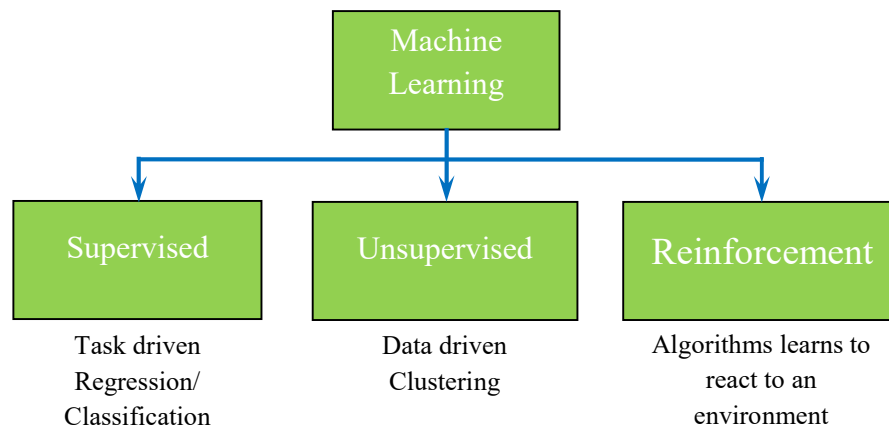

Figure .5.3: Types of machine learning

1. Principals of supervised learning are as follow:
    ➢ The training dataset contains classifier inputs data (features) and the output (the class you want to predict). In this type of learning you have a target, a value or a class to predict, the reason why it named supervised.
    ➢ The model uses the training data to learn a map from input to outputs. The basic idea is that the trained model can be generalized and then used on new data of the same system.

2. In opposition, unsupervised learning does not have output data. Most of the time unsupervised learning algorithms are used to pre-train supervised learning algorithms or to pre-process the data, during the exploratory analysis.

3. Reinforcement learning algorithms try to find the best ways to get the best reward. Given the states of both the environment and the agent, this latter will pick at the action that will capitalize on its reward or will explore a new state. By executing this loop several times, the agent's behavior will be better.

This chapter focuses on supervised learning (See Figure .5.3) since the data and its labels can be obtained easily from the PV system using real time emulator solution.

5.2.3 Artificial Intelligence Techniques in PV Arrays

The schematic of the studied PV system is shown in (Figure 5.4). Typically includes the grid-connected PV system and the detection and classification method.
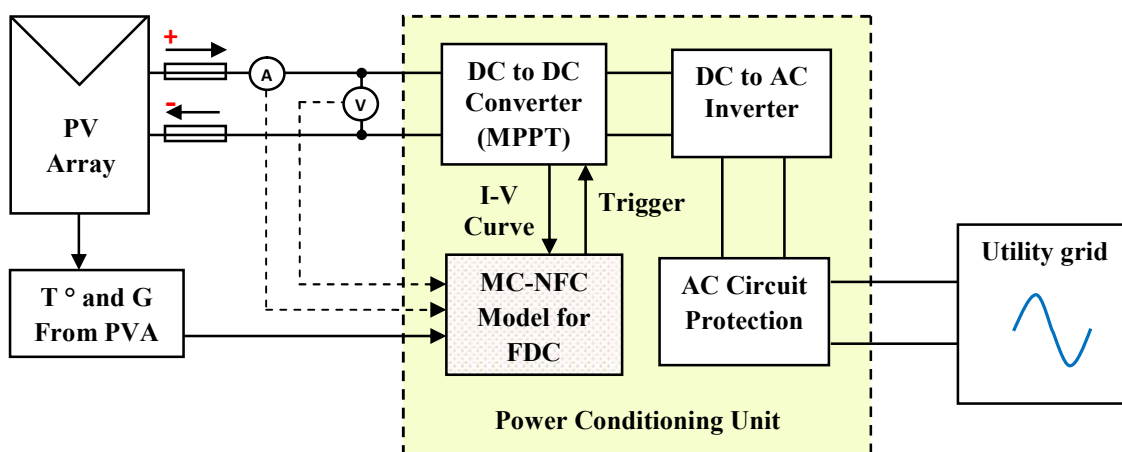

Figure .5.4: Schematic of the proposed FDC model for PVA.

MC-NFC classifier for FDC.

- ➢ A simplified grid connected PV system consists of a PV array that it connected to the grid via a suitable PV inverter, utility grid and protection devices as AC breakers and fuses. The PV inverter extracts as much as possible the power from the PV array using the optimization algorithms (MPPTs) at the specific voltage and frequency and then feeding it into the utility grid. Current-voltage (*I-V*) characteristics can provide useful information to use for the proposed MC-NFC classifier.

- ➢ The proposed MC-NFC classifier uses only available PV sensors. Therefore, the proposed method can take advantage of available PV sensors without additional costs. The MC-NFC classifier receives the instantaneous maximum current (I_{mpp}) and the maximum voltage (V_{mpp}) of the PV array from the inverter. When a fault is detected, a trigger (See Figure .5.4) will initiate *I-V* curve acquisition and then passing it into the MC-NFC classifier for fault classification.

- ➢ Power conditioning unit in Figure .5.4 does not rely on any particular additional power modules. One more advantages of the proposed MC-NFC classifier is that it can be integrated into PV inverters using only readily available data from existing sensors.

5.3 Multi-Class neuro-fuzzy Classifier (MC-NFC) Development

5.3.1 The Building blocks for MC-NFC Classifier

5.3.1.1 Fuzzy Classifier

Generally, fuzzy logic is used in designing controllers [5.22], but it can be used to design classifiers [5.23]. Fuzzy classifier (See Figure .5.5) is a universal approximator, which can approximate any function.

The use of fuzzy classifier is justified by:

1. Universal approximation: the exact match of classification boundaries. Many proofs demonstrate that exist a type of fuzzy if-then classifier, that can approximate any continuous function $R^n \rightarrow R$ on a compact domain to an arbitrary precision (universal approximation propriety)

2. Uncertainty and vagueness: real measurements and modeling uncertainty.

Designing a fuzzy classifier needs three steps, fuzzification, inference and then defuzzification.
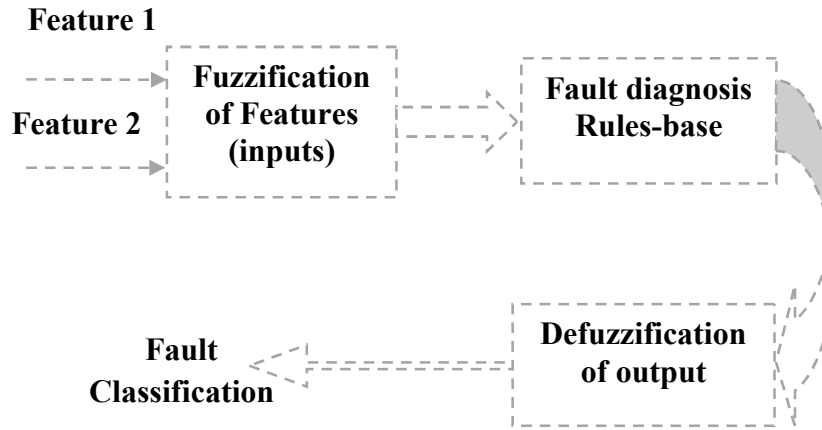
Figure .5.5: Fault Fuzzy classifier implementation concept.

A fuzzy classifier uses rule of the type:

$R_k: IF\ x_1 is\ A_{1,i(1,k)}\ AND\ ...\ AND\ x_n is\ A_{n,i(n,k)}$

$THEN\ g_{k,1} = z_{k,1} AND\ ...\ AND\ g_{k,c} = z_{k,c}$ (5.1)

Where $g_{k,i}$ is the discriminant function g_i associated with rule R_k. The subscript $i(j,\ k)$ is an *input* index function showing which linguistic label is used for feature x_j in the rule R_k. The values $z_{k,j} \in \Re$ can be interpreted as "support" for class w_j given by rule R_k if the antecedent part is completely satisfied.

The *TSK1* fuzzy classifier has the following characteristics [5.23]:

1) The rule-base is a general type of the if-then rules.
2) The conjunction (*AND* connective): A_t.

The *firing strength* of the rule is

$\tau_k(X)\ =\ A_t\{\mu_{1,i(1,k)}(x_1), ... , \mu_{n,i(n,k)}(x_n)\}.$ (5.2)

3) The computation of the consequents.

$K = 1,...,M$ is the index of the rules, $i = 1,...,c$ is the index for the classes, and $j\ = 1,...,n$ is the index for features.

- $z_{k,i} \in \{0,1\}, \sum_{i=1}^{c} z_{k,i} = 1$; (crisp labels)
- A_t is minimum;
- The *i*th *TSK1* output is

$g_i^{TSK1}(X) = \max_{k=1\ to\ M}\{z_{k,i}. \tau_k(X)\}$

$$= \max_{k=1 \, to \, M} \left\{ z_{k,i} \cdot \min_{j=1 \, to \, n} \left\{ \mu_{j,i(j,k)}(X_j) \right\} \right\} \tag{5.3}$$

5.3.1.2 Artificial Neural Network (ANN) Classifier

Artificial neural network (ANN) is inspired from a biological neural network; it is an intelligent method that processes information in the human brain manner. It can be used to create models for control and diagnosis purposes. ANN doesn't need detail mathematical formulas for describing the relationship between the input and the output of the system. Instead, it uses an architecture that is formed by an input layer, output layer, and one or more hidden layers. Each layer has a small number of parameters that are tuned by using some known algorithms like back propagation algorithm. ANN model development needs data sets for training, validation and testing.

Figure .5.6 shows the schematic of a multi-layered neural network. Each neuron input is a multiplication of the input of the previous neurons and its connection weights. At the output a linear or non-linear activation function is applied.
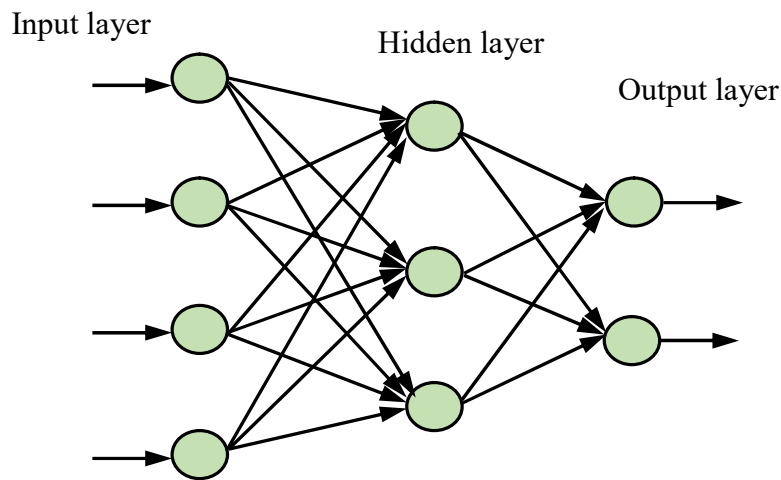

Figure .5.6: Multi-layer neural network concept.

More details about neural networks can be found in [5.24, 5.25, and 5.26].

The objective of the ANN-classifier is to detect and classify faults in the photovoltaic array using experimental data collected from the real time emulator (See chapter 3).

5.3.2 Detailed MC-NFC for FDC

5.3.2.1 Threshold Detection

To avoid false alarm and the problem of non-detection, a threshold should be chosen for all features, by taking into account measurement errors. For normal operation conditions, the features vector should be inside the hyperbox determined by the following threshold vector:

$$S_{th} = [S_{th1}, S_{th2}, ... S_{th12}] \qquad (5.4)$$

Each of the S_{th} vector components corresponds to one feature threshold.

Since the error of measurement is coming mainly from current and voltage sensors, one can compute the error just for these quantities. The remaining threshold components are derived from the current and voltage thresholds.

The IEC 61724-1998 standard [5.27] tolerates 1% for the current and voltage measurements. The errors for computation of $S_{th2}(I_{th})$ and $S_{th3}(V_{th})$ are the same as the tolerance previously mentioned. Accordingly, S_{th2} (I_{th}) and $S_{th3}(V_{th})$ are used for fault detection.

In the detection phase we focus only on the presence and the absence of the fault in PVA without looking for the type of the fault. In this section, a study of the detection accuracy in terms of precision and recall is conducted (this is a sort of binary classification, healthy or faulty PVA).

The following scheme is used to compute precision and recall percentages:
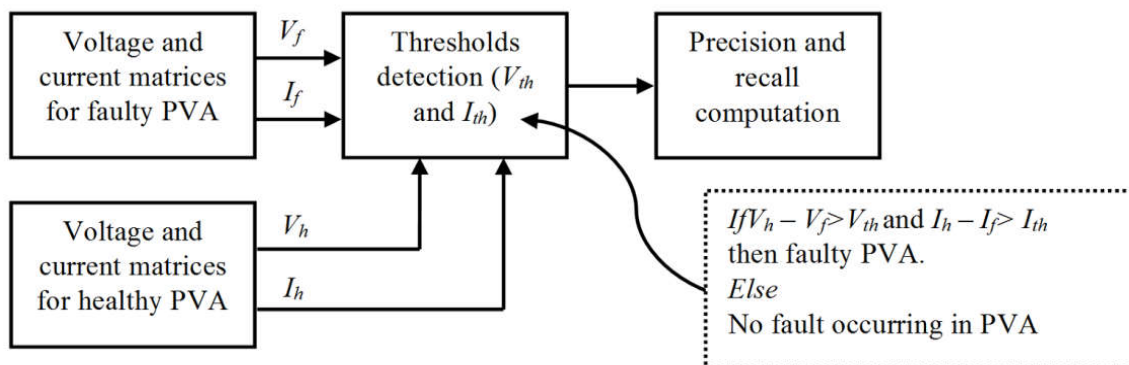
Figure .5.7: Scheme used for precision and recall computation in the detection phase.

Where V_h, V_f, I_h and V_f are the voltage and the current for the healthy and faulty cases. As reported in table 3.2 the number of instances for normal operation is 130 *I-V* curves, and for the faulty case, the number of instances is 2730 *I-V* curves. Using these data, the precision and recall percentages are given in the following:

The above scheme for recognizing faulty case in dataset identifies 2703 faulty instances in a dataset containing 2730 faulty instances. Of the 2703 faulty instances identified, 2680 actually are faulty (true positives), while the rest are healthy (false positives). Thus, the detection's precision is 99.15% (2680/2703) while its recall is 98.17 % (2680/2730).

5.3.2.2 Binary Adaptive Neuro-Fuzzy Classifier Concept

Fuzzy systems have the ability to handle uncertain and imprecise information, but cannot update and fine tune their parameters automatically. To overcome this drawback, some supervised learning algorithms were applied in [5.28], based on training data set. In this study, a well-known Sugeno Fuzzy Inference System (FIS) is used, where its consequent is a linear function, this FIS is known as "first-order Sugeno type" [5.29].

Before model development, we present a simple architecture that illustrates the procedure of the neuro-fuzzy. Assume we have two inputs; short-circuit current (S_2) and open-circuit voltage (S_3), and one output, increased series resistance. According to the first-order Sugeno type classifier and in the case where only two rules exist, the output R_s is computed by the summation of the following two functions (f_1, f_2):

➤ f_1: is computed by the rule:

If S_2 is A_1 and S_3 is B_1, then $f_1 = p_{11} \times S_2 + p_{12} \times S_3 + r_1$ (5.5)

➤ f_2 is computed by the rule:

If S_2 is A_2 and S_3 is B_2, then $f_2 = p_{21} \times S_2 + p_{22} \times S_3 + r_2$ (5.6)

Where p_{ij} and r_i ($i = j = 1, 2$), are the consequent parameters. Figure .5.8 shows a typical ANFIS architecture of such model. Note that in this architecture, squares represent adaptive nodes, whereas circles are fixed nodes.

The word 'adaptive' is specific to the neuro-fuzzy architecture itself. The adaptive-networks-based fuzzy inference system is a fuzzy inference system implemented in the structure of adaptive network. The output of an adaptive networks depends on the parameter

(not features) relevant to the adaptive nodes that is changed to minimize a given error measure using supervised learning procedure [29].
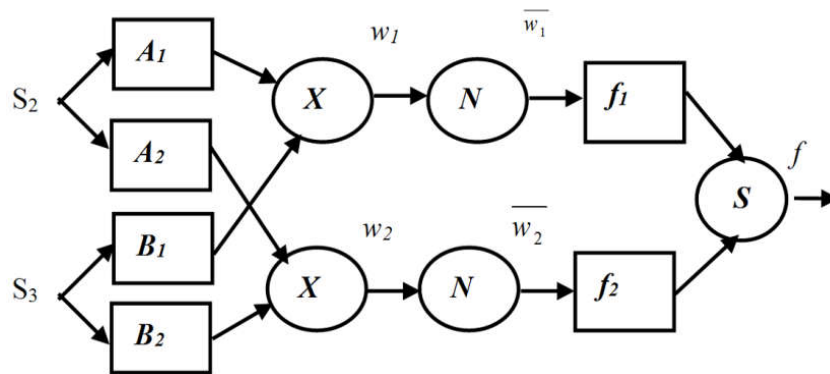

Figure .5.8: ANFIS architecture with two inputs, two membership functions and one output.

A brief description of the different layers is as follows:

a) Features layer

The output of the node i in this layer is calculated by eq.:

$$O_i^1 = \mu_{A1}(S_2) \text{for} \quad i = 1, 2;$$ (5.7)

Or

$$O_i^1 = \mu_{B-2}(S_3) \text{for} \quad i = 1, 2,$$ (5.8)

Where, S_2 and S_3 are the crisp features feeding the input of the node i. A_i and B_i are linguistic terms associated with their appropriate membership functions. Membership function for linguistic terms can be any suitable parameterized membership function. Trapezoidal membership function is one of the membership functions that will be used in this study.

$$\mu_{A_i} = \begin{cases} 0, & S_2 \leq a_i \\ \frac{S_2 - a_i}{b_i - a_i}, & a_i \leq S_2 \leq b_i \\ 1, & b_i \leq S_2 \leq c_i \\ \frac{d_i - S_2}{d_i - c_i}, & c_i \leq S_2 \leq d_i \\ 0, & d_i \leq S_2 \end{cases}$$ (5.9)

$$\mu_{B_i} = \begin{cases} 0, & S_3 \leq a_i \\ \frac{S_3 - a_i}{b_i - a_i}, & a_i \leq S_3 \leq b_i \\ 1, & b_i \leq S_3 \leq c_i \\ \frac{d_i - S_3}{d_i - c_i}, & c_i \leq S_3 \leq d_i \\ 0, & d_i \leq S_3 \end{cases} \tag{5.10}$$

Where a_i, b_i, c_i and d_i are the parameters to be changed by the training algorithm to deal with training data set. Hence, the trapezoidal function varies consequently.

b) Rules layer

The nodes in this layer provide what is known by firing strength O_i^2, and it is the product of all outputs coming from layer one. It can be seen that no parameter to be adjusted, so it is a fixed node.

$$O_i^2 = w_i = \mu_{A_i}(S_2)\mu_B(S_3), \quad i = 1, 2 \tag{5.11}$$

c) Normalization layer

The node i of this layer takes the ratio of the ith rule's firing strength to the sum of all rule's firing strengths. For that reason, outputs of this layer are called normalized firing strength.

$$O_i^3 = \overline{w_i} = \frac{w_i}{\sum_i w_i}, \quad i = 1, 2 \tag{5.12}$$

d) Consequent layer

The output of the node i of this layer is computed by the following node function:

$$O_i^4 = \overline{w_i} f_i \quad i = 1, 2 \tag{5.13}$$

Where, $\overline{w_i}$ is a normalized firing strength from the previous layer, and the formula that computes f_i is given in eq.5.4 and eq.5.5.

e) Output layer

The single fixed node in this layer computes the overall output by summing all coming signals from the previous layer. Consequently, the process of Defuzzification is achieved by getting a crisp overall output.

$$O_i^5 = ISR = \sum_i \overline{w_i} f_i = \frac{\sum_i w_i f_i}{\sum_i w_i}, \quad i = 1, 2 \tag{5.14}$$

(N.B: in figure 5.8, $f = ISR$).

We note that, the above described ANFIS classifier is just an example. In the following we will use more inputs. More rules will be also generated using learning algorithms. For more explanations on the ANFIS architecture the reader can refer to [5.29].

5.3.2.3 Extension to multiclass classification problem

For a multiclass problem, instead of using one binary classifier we can use a group of them [5.30]. We can then take their decision and compare it by using "winner-takes-all" rule. The diagram block of the MC-NFC concept is illustrated in Figure 5.9.
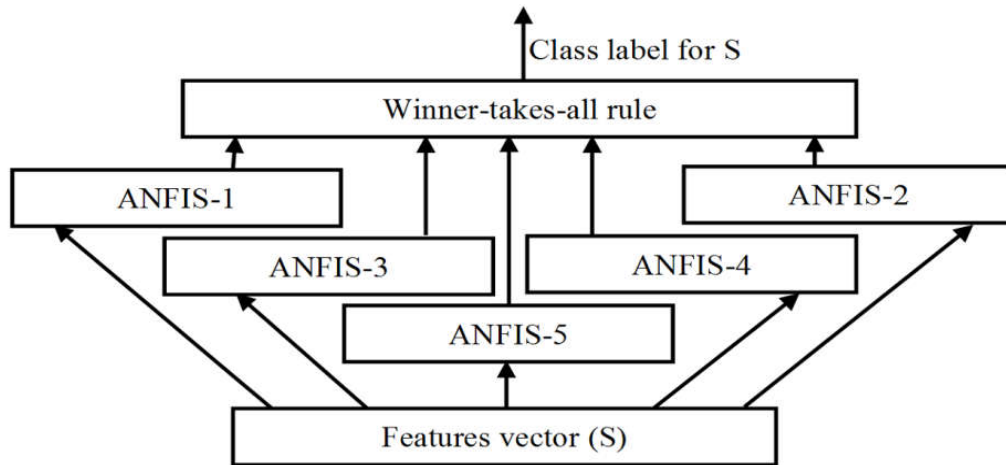

Figure .5.9: Diagram block of the MC-NFC concept [31, 32].

Each classifier feed this rule by a crisp class label which is assigned to *S*. The final class label of *S* is the one that have the biggest crisp value at the outputs of the classifiers pool. If the decision at the output of the classifier *i*, is d_i, then the label *L* at the output of the above mentioned rule is given by:

$$L = \max(d_i) \tag{5.15}$$

5.3.2.4 Classifier performance evaluation criterions

Any constructed classifier should be evaluated at the end of its design, and this allows us to compare it to other type of classifiers. Classifier performance will be evaluated by using some statistical criterions: sum squared error, correlation coefficient, mean percent relative error, root mean squared error and standard deviation.

➢ Sum squared error (SSE), that is given by the following expression:

$$SSE = \sum_{i=1}^{n} (m_i - p_i)^2$$

➢ Correlation coefficients (R^2), that is given by the following expression:

$$R^2 = 1 - \frac{SSE}{\sum_{i=1}^{n} p_i^2}$$

➢ Mean percent relative error ($MPRE$), that is given by the following expression:

$$MPRE = \frac{100\%}{n} \sum_{i=1}^{n} \frac{mi - pi}{p_i}$$

➢ Root mean squared error ($RMSE$), that is given by the following expression:

$$RMSE = \sqrt{\frac{\sum_{i=1}^{n} (m_i - p_i)^2}{n}}$$

➢ Standard deviation (STD), that is given by the following expression:

$$STD = \sqrt{\frac{\sum_{i=1}^{n} (m_i - p_i)^2}{n - 1}}$$

Where m_i is the actual value, p_i is the predicted output of the classifier, and n is the number of the input data.

5.4 FDC Experiments in PV Systems

5.4.1 Experimental Setup

A simple grid-connected PV system is built to collect data for both normal and faulty cases under real-working conditions (such as irradiance and temperature). As mentioned in section 3.2.1 the PV array consists of 6 PV modules in series forming one string.

The detailed parameters of the PVA are given in Table 3.1. Note that all the PV modules have the same electrical parameters and environmental conditions in case of normal working conditions. In the experiments, no filter is used to reduce the measurement noise.

Five types of faults have been created in the PV array: 1) Partial shading fault ($F1$): Nine different partial shading patterns have been considered. 25%, 50% and 75% of nine PV cell in one PV module, 25%, 50% and 75% of nine PV cell in two PV modules. Finally 25%, 50%

and 75% of nine PV cell in three PV modules; 2) Increased series resistance ($F2$): The Rs of one PV module is increased by 1 Ω, 5 Ω, 10 Ω, 15 Ω and 20 Ω. 3) By-pass diode short-circuited ($F3$): One by-pass diode in the whole PVA short-circuited. 4) By-pass diode impedance ($F4$): By-pass diode is assimilated to resistors with different values, 1 Ω, 5 Ω, 10 Ω, 15 Ω and 20 Ω. 5) PV module short-circuited ($F5$): The contribution of one PV module in the energy of PVA was eliminated by making it short-circuit. During the experiment, the solar irradiance is ranging between 100 *W/m2* and 1000 *W/m2*, and the solar cell temperature is changing between 0°*C* and 60°*C*.

The photograph of the experiment bench is given in Figure 3.2, and the flowchart of the MC-NFC model for FDC is given in Figure .5.10.

5.4.2 Experimental Results

5.4.2.1 Experiment 1: Feature selection for each neuro-fuzzy classifier

The importance of feature dimensionality reduction techniques and the advantage of MC-NFC over traditional ones will be shown. First, in the experiment 1, the proposed method for feature dimensionality reduction has been applied to five classifiers: Partial shading fault classifier (F_1 classifier), increased series resistance classifier (F_2 classifier), By-pass diode short-circuited classifier (F_3 classifier), By-pass diode impedance classifier (F_4 classifier), and PV module short-circuited classifier (F_5 classifier). Then, in the experiment 2, the proposed MC-NFC trained and tested with the reduced entire original feature space, which is defined by a vector of 12 features. Finally, in the experiment 3 the MC-NFC will be compared to an ANN classifier.

Finally classifier output decisions have been compared to decide which one is the biggest for final decision.
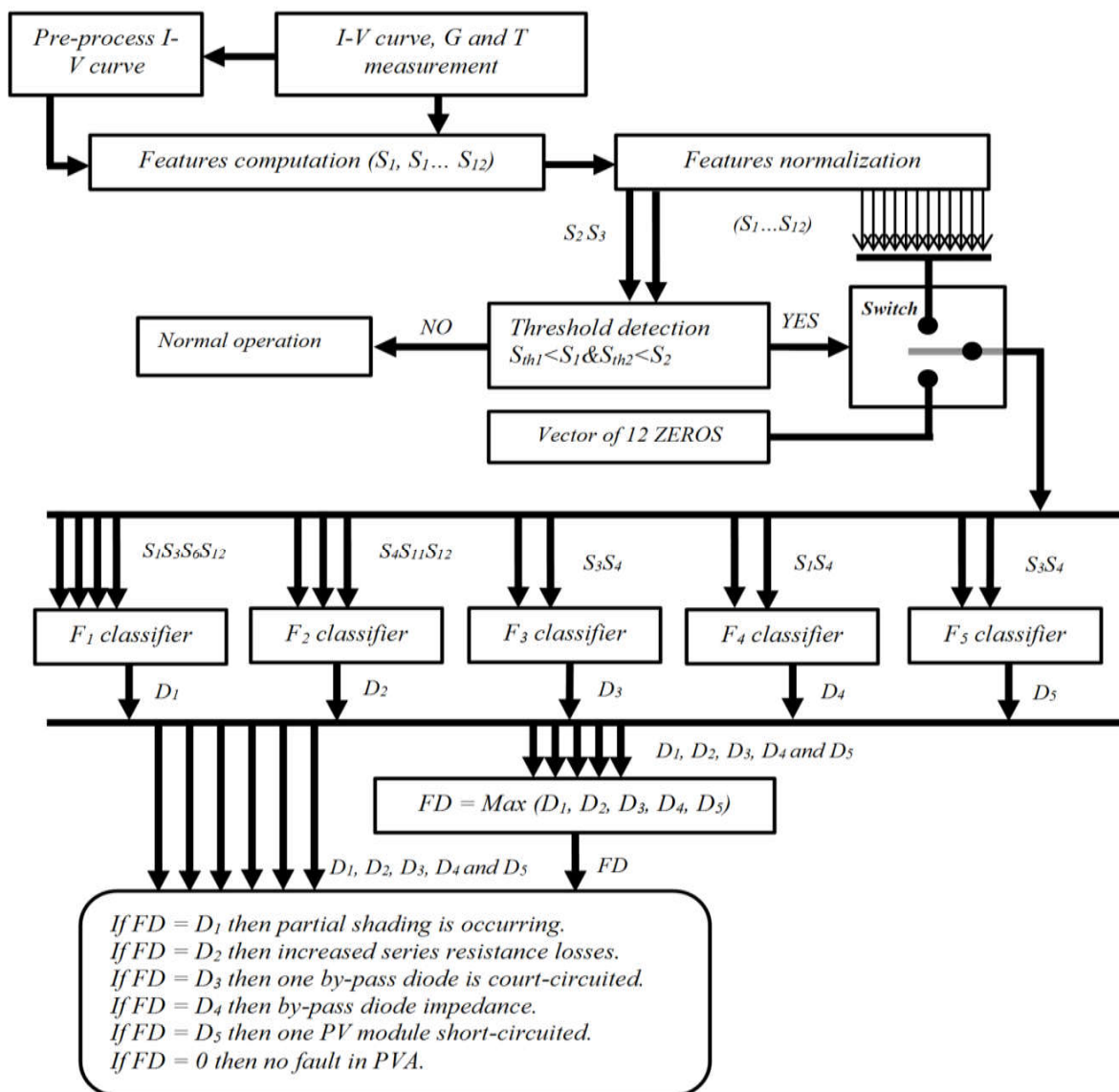
Figure .5.10: The structure of the fault detection and classification algorithm based on classifiers decision outputs fusion [31].

5.4.2.2 Experiment 2: MC-NFC building with reduced feature space

In this experiment, the MC-NFC will be trained and tested with the reduced entire original feature space, which is defined by a vector of 12 features. During the training phase, the ANFIS parameters have been tuned by a hybrid learning algorithm, which consists of a combination of the least-squares method and the back-propagation gradient descent method, and one versus all strategy was applied for all classifiers. The MC-NFC is based on considering the data of the fault to be discriminated as one set, and the remaining data of other

faults are forming the other set. Accordingly the problem of multiclass is reduced to a binary classification problem.

An efficient methodology has been adopted to find the best ANFIS model based on the idea of decreasing RMSE and increasing the accuracy of the designed architecture. The main parts of the MC-NFC that will be designed consists on the type of membership functions (Gaussian, triangular, pi-shaped curve, generalized bell-shaped, trapezoidal and differential of two sigmoidal), the number of MFs, output MFs types (constant, linear), the learning process that changes the parameters associated with the MFs and the number of epochs to avoid the problem of over fitting.

A grid partitioning method was applied to generate a rule base relationship between the input and the output of the classifier. The classifier output is a linear combination of its inputs (Sugeno fuzzy inference system).

During the optimization process different built-in membership functions (MFs) types has been involved to choose the most appropriate one for MC-NFC model development. Tables 5.1-5.5 demonstrate the errors of MFs during the optimization process. Moreover, the number of MF for each feature has been chosen according to the classifier output.

TABLE 5.1: Errors of F_1 classifier membership functions types during the optimization process

MF-MFN	Membership function type description	MPRE	RMSE	R^2
Gaussmf-2	Gaussian curve	-2.5478	0.16617	0.9724
Trimf-2	Triangular curve	-4.6026	0.18866	0.9644
Pimf-2	Pi-shaped curve	2.0421	0.16169	0.9738
Gbellmf-2	Generalized bell-shaped curve	-1.0257	0.17528	0.9693
Trapmf-2	Trapezoidal curve	2.3275	0.15921	0.9746
Dsigmf-2	difference of two sigmoidal membership functions	1.0529	**0.15022**	0.9774

TABLE 5.2: Errors of F_2 classifier membership functions types during the optimization process

MF-MFN	Membership function type description	MPRE	RMSE	R^2
Gaussmf-2	Gaussian curve	-5.1359	0.5406	0.7077
Trimf-2	Triangular curve	-8.4089	0.6119	0.6255
Pimf-2	Pi-shaped curve	-3.0729	0.5480	0.6997
Gbellmf-2	Generalized bell-shaped curve	-4.2902	0.5387	0.7098

Trapmf-2	Trapezoidal curve	-1.3245	0.5453	0.7027
Dsigmf-2	difference of two sigmoidal membership functions	-3.2864	**0.5378**	0.7107

TABLE 5.3: Errors of F_3 classifier membership functions types during the optimization process

MF-MFN	Membership function type description	MPRE	RMSE	R^2
Gaussmf-2	Gaussian curve	-0.2958	0.0093	0.9999
Trimf-2	Triangular curve	-0.1207	0.0073	0.9999
Pimf-2	Pi-shaped curve	0.0157	0.0020	0.9999
Gbellmf-2	Generalized bell-shaped curve	-0.5259	0.0112	0.9999
Trapmf-2	Trapezoidal curve	0.0054	**0.0018**	0.9999
Dsigmf-2	difference of two sigmoidal membership functions	-0.1370	0.0031	0.9999

TABLE 5.4: Errors of F_4 classifier membership functions types during the optimization process

MF-MFN	Membership function type description	MPRE	RMSE	R^2
Gaussmf-2	Gaussian curve	-0.6987	0.5272	0.7221
Trimf-2	Triangular curve	-4.6295	0.7077	0.4992
Pimf-2	Pi-shaped curve	-1.5422	0.5308	0.7183
Gbellmf-2	Generalized bell-shaped curve	-2.4022	**0.5256**	0.7237
Trapmf-2	Trapezoidal curve	-1.4081	0.5339	0.7150
Dsigmf-2	difference of two sigmoidal membership functions	-0.7887	0.5278	-0.7887

TABLE 5.5: Errors of F_5 classifier membership functions types during the optimization process.

MF-MFN	Membership function type description	MPRE	RMSE	R^2
Gaussmf-2	Gaussian curve	0.0021	0.00016	0.9999
Trimf-2	Triangular curve	-0.3748	0.00670	0.9999
Pimf-2	Pi-shaped curve	-0.0019	**0.00009**	0.9999
Gbellmf-2	Generalized bell-shaped curve	-0.0059	0.00018	0.9999
Trapmf-2	Trapezoidal curve	-0.0001	0.00003	0.9999
Dsigmf-2	difference of two sigmoidal membership functions	-0.0024	0.00010	0.9999

With reference to the above Tables (5.1-5.5), it can be summarized that the best membership functions for each classifier is as follows:

About F_1 classifier the best membership function is the differential of two sigmoidal membership function (dsigmf). For F_2 classifier the best membership function is also the differential of two sigmoidal membership function (dsigmf).Concerning F_3 classifier the best membership function is the trapezoidal membership function (trapmf). The best membership function is the generalized bell-shaped membership function (gbellmf) in the case of F_4 classifier. About the F_5 classifier the best membership function is the pi-shaped membership function (pimf).

TABLE 5.6: Errors of all classifiers membership functions number during the optimization process

| | *F1*-dsigmf | | *F2*-dsigmf | | *F3*-trapmf | | *F4*-gbellmf | | *F5*-pimf | |
	RMSE	R^2	RMSE	R^2	RMSE	R^2	RMSE	R^2	RMSE	R^2
2 MFs	**0.235**	**0.945**	0.737	0.456	**0.000**	**1.000**	0.526	0.724	**0.000**	**1.000**
3 MFs	0.248	0.938	0.626	0.607	0.000	1.000	**0.514**	**0.736**	0.000	1.000
4 MFs	0.244	0.940	**0.592**	**0.648**	0.000	1.000	0.515	0.734	0.000	1.000
5 MFs	0.30	0.91	0.61	0.63	0.00	1.00	0.52	0.73	0.00	1.00

With respect to Table 5.6, it can be reported that the best number of membership function for each classifier is as follows:

- F_1 classifier: the number of differential of two sigmoidal membership functions is ***two***.
- F_2 classifier: the number of differential of two sigmoidal membership functions is ***four***.
- F_3 classifier: the number of trapezoidal membership functions is ***two***.
- F_4 classifier: the number of generalized bell-shaped membership function is ***three***.
- And finally, F_5 classifier the number of pi-shaped membership function is ***two***.

Input membership functions for each classifier (classifier 1, 2, 3, 4, and 5) before and after training process is as follows:
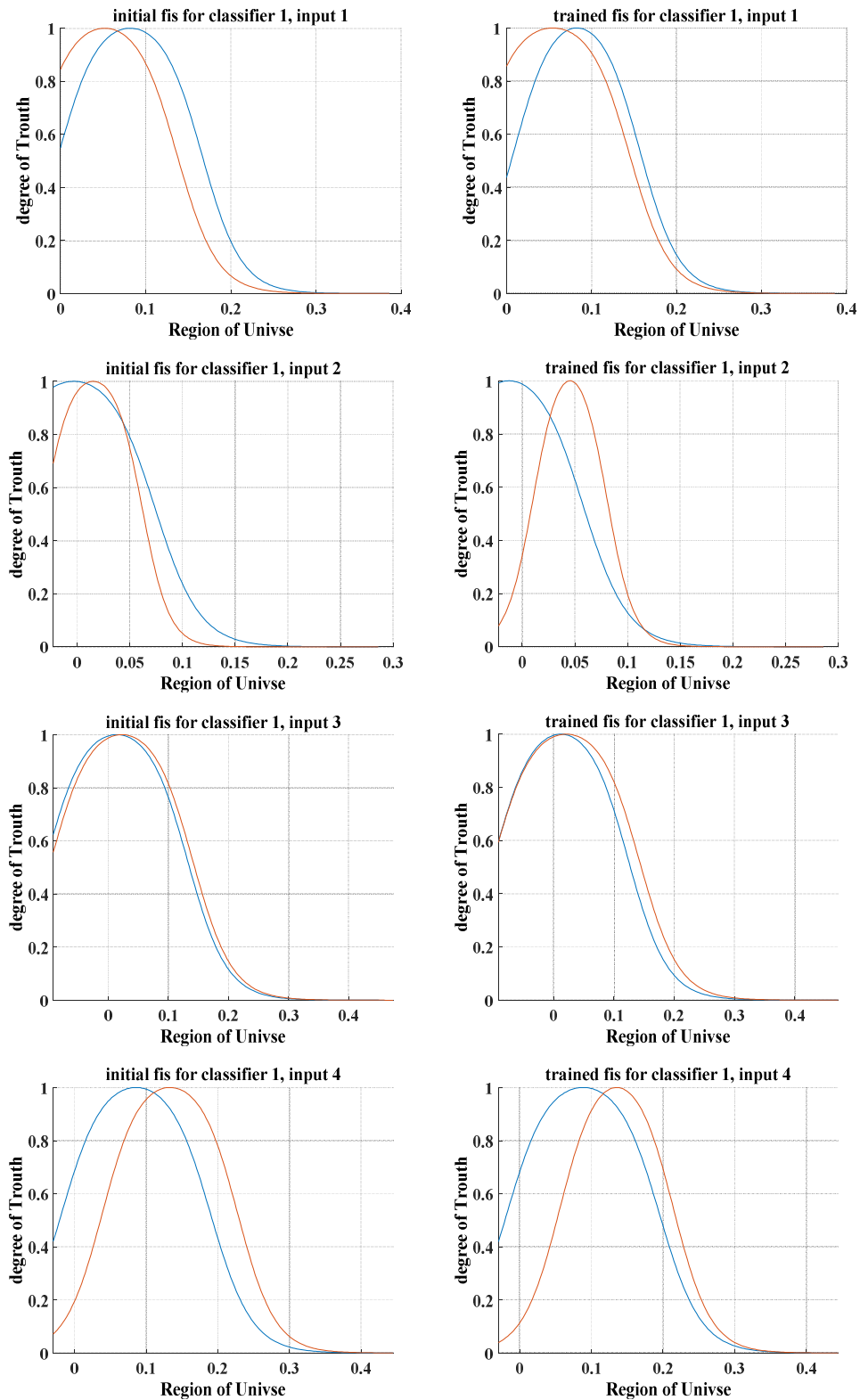
Figure .5.11: FIS Membership functions for initial and trained classifier (classifier's 1 Inputs).
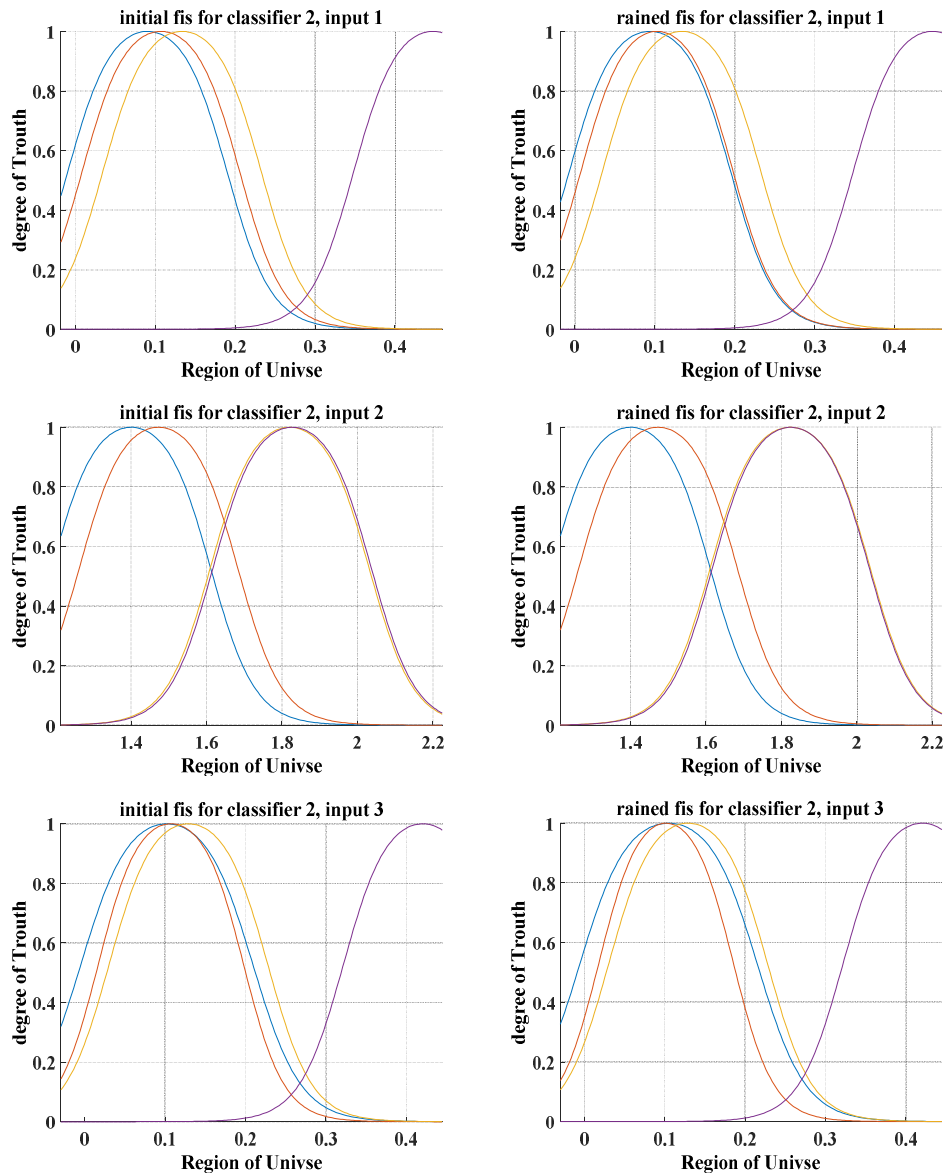
Figure .5.12: FIS Membership functions for initial and trained classifier (classifier's 2 Inputs).
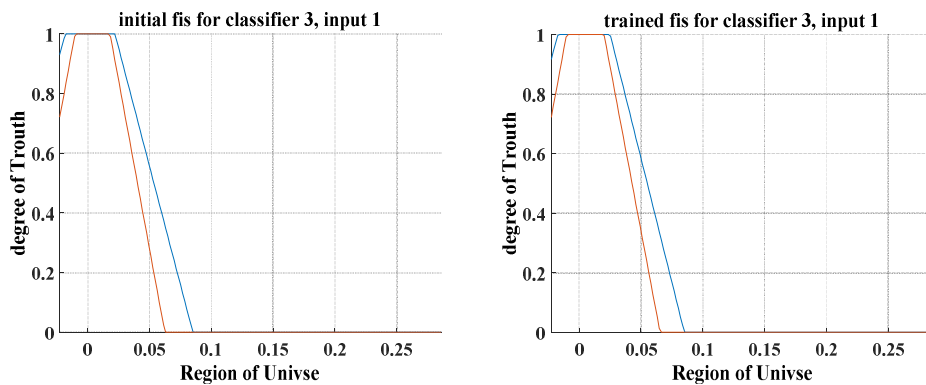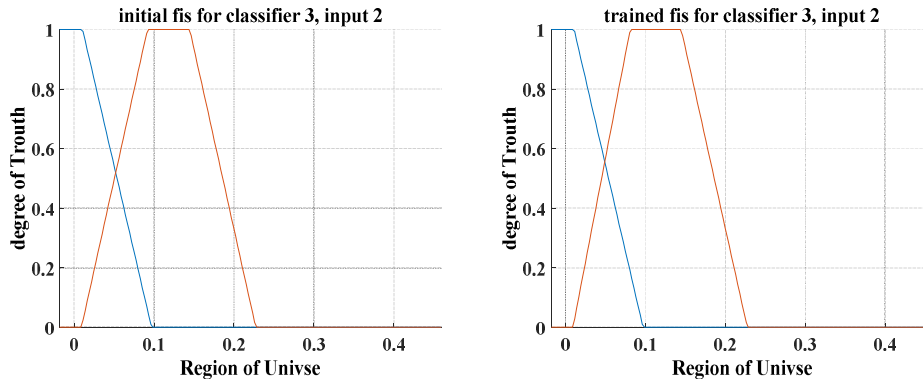
**Figure .5.13:** FIS Membership functions for initial and trained classifier (classifier's 3 Inputs).
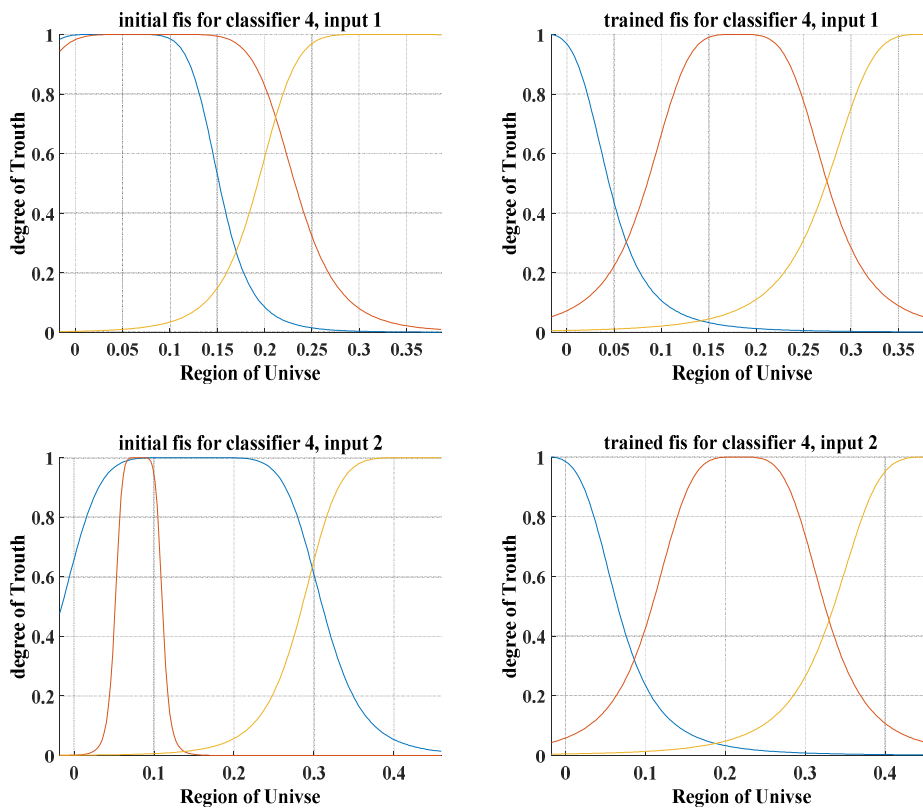
Figure .5.14: FIS Membership functions for initial and trained classifier (classifier's 4 Inputs).
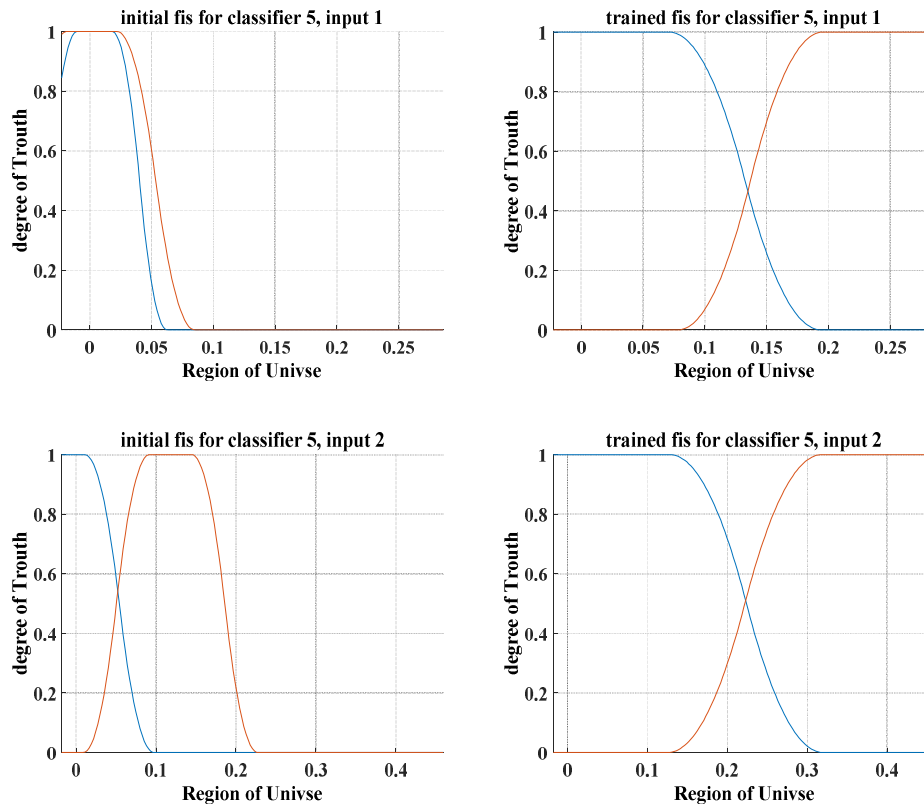
Figure .5.15: FIS Membership functions for initial and trained classifier (classifier's 5 Inputs).

TABLE 5.7: Summary of the ANFIS models structures and optimal parameters.

	Classifier F_1	Classifier F_2	Classifier F_3	Classifier F_4	Classifier F_5
Type	T-S	T-S	T-S	T-S	T-S
Number of inputs	4	3	2	2	2
Number of outputs	1	1	1	1	1
Number of fuzzy rules	2	4	4	9	4
Input membership function type	dsigmf	dsigmf	trapmf	gbellmf	pimf
Output membership function type	Linear	Linear	Linear	Linear	Linear
Number of epochs	100	100	100	100	100
Total number of data pairs	2860	2860	2860	2860	2860
Number of input/output membership function	2-2	4-4	2-4	3-9	2-4

The MC-NFC models are now available. The optimal parameters allowing the reproduction of these models are given in Table 5.7. We can see clearly that the models are very light in terms of structure parameters. In fact, we have tasted them and the results in

terms of fault classification rapidity were very satisfactory. N.B: For fault detection phase, we need just to know thresholds of the second and third features (maximum current and maximum voltage at the MPP). Thus, fault detection was very quick and avoiding fire hazards in PV systems.

5.4.2.3 Experiment 3: Classification with artificial neural network (ANN) classifier

For comparisons purpose, the designed MC-NFC has been compared to ANN classifier (See Table 5.7). This later is a multilayer feed-forward perceptron (MLP) with one hidden layer. For fast optimization of the network, a Levenberg-Marquardt (LM) back-propagation algorithm has been applied.

TABLE 5.8: Comparison between MC-NFC and ANN-classifier

	F1		*F2*		*F3*		*F4*		*F5*	
	MC-NFC	ANN	MC-NFC	ANN	MC-NFC	ANN	MC-NFC	ANN	MC-NFC	ANN
RMSE	0.23	0.55	0.59	0.65	0.00	0.31	0.51	0.58	0.00	0.00
R^2	0.95	0.56	0.65	0.66	1.00	0.91	0.74	0.66	1.00	1.00

This experiment shows clearly the superiority of the MC-NFC [31] over traditional ANN-classifier with respect to the reduced feature space dimensionality. Moreover, the proposed MC-NFC can be used to further improve these important results.

5.4.3 Discussion

A Multiclass Adaptive Neuro-Fuzzy Classifier (MC-NFC) for fault detection and classification in photovoltaic (PV) array has been developed. Firstly, Fuzzy Logic (FL) classifiers have been built based on experimental datasets to show the generalization capability in the automatic faults classification of a PV array (PVA). Subsequently, a novel classification system based on Adaptive Neuro-fuzzy Inference System (ANFIS) has been proposed to improve the generalization performance of the FL classifiers. The experiments have been conducted on the basis of collected data from a PV array (PVA) to classify five kinds of faults in the PVA, and the normal operation. Results showed the advantages of using the fuzzy approach with reduced features over using the entire original chosen features. The designed MC-NFC has been compared with an Artificial Neural Networks (ANN) classifier.

Results demonstrated the superiority of the MC-NFC over the ANN-classifier and suggest that further improvements in terms of classification accuracy can be achieved by the proposed classification algorithm; furthermore faults can be also considered for discrimination.

5.5 Conclusion

In this chapter, a MC-NFC has been developed for fault detection and classification in photovoltaic arrays. From the conducted experiments, it can be strongly recommended the use of the MC-NFC classifier.

The selection of the architecture of the MC-NFC has an important role, input membership function type, number of membership function for each input leads to an optimized model.

The built MC-NFC can discriminate between five types of fault occurring in a PV array. Furthermore, the developed algorithm is implemented in a DS1104 platform to show its ability to detect and classify PV array faults in real time applications. Classifiers have been built based on the best combination of the original feature space for each case. Then, the constructed MC-NFC was compared to an ANN classifier, and the results show the importance of using the MC-NFC over the traditional ones.

REFERENCES

[5.1] Belaout, A., Krim, F., & Mellit, A. (2016). Neuro-fuzzy classifier for fault detection and classification in photovoltaic module. *8th international Conference on Modelling, Identification and Control (ICMIC), Algiers*, 144-149.

[5.2] Chine, W., Mellit, A., Lughi, V., Malek, A., Sulligoi, G., & Massi Pavan. A. (2016). A novel fault diagnosis technique for photovoltaic systems based on artificial neural networks. *Renewable Energy*, 90, 501-512.

[5.3] Kim, I. S. (2016). On-line fault detection algorithm of a photovoltaic system using wavelet transform. *Solar Energy*, 126, 137-145.

[5.4] Spataru, S., Sera, D., Kerekes, T., & Teodorescu, R. (2015). Diagnostic method for photovoltaic systems based on light I–V measurements. *Solar Energy*, 119, 29-44.

[5.5] Zhao, Y., Ball, R., Mosesian, J., de Palma, J. F., & Lehman., B. (2015). Graph-based semi-supervised learning for fault detection and classification in solar photovoltaic arrays. *IEEE Transactions on Power Electronics*, 30.5, 2848-2858.

[5.6] Dhimish, M., Holmes, V., & Dales. M. (2017). Parallel fault detection algorithm for grid-connected photovoltaic plants. *Renewable Energy*, 113, 94-111.

[5.7] Grichting, B., Goette, J., & Jacomet. M. (2015). Cascaded fuzzy logic based arc fault detection in photovoltaic applications. *Clean Electrical Power (ICCEP), 2015 International Conference on: IEEE*, 178-183.

[5.8] Mekki, H., Mellit, A., & Salhi. H. (2016). Artificial neural network-based modelling and fault detection of partial shaded photovoltaic modules. *Simulation Modelling Practice and Theory*. 67, 1-13.

[5.9] Madeti, S.R., & Singh., S.N. (2017). Online fault detection and the economic analysis of grid-connected photovoltaic systems. *Energy*, 134, 121-135.

[5.10] Zhicong, C., Wu, L., Cheng, S., Lin, P., Wu, Y., & Lin., W. (2017). Intelligent fault diagnosis of photovoltaic arrays based on optimized kernel extreme learning machine and I-V characteristics. *Applied Energy*, 204, 912-931.

[5.11] Cai, B., Liu, Y., Ma, Y., Huang, L., & Liu., Z. (2015). A framework for the reliability evaluation of grid-connected photovoltaic systems in the presence of intermittent faults. *Energy*, 93, 1308-1320.

[5.12] Daliento, S., Chouder, A., Guerriero, P., Pavan, M., Mellit, A., Moeini, R., & Tricoli, P. (2017). Monitoring, diagnosis, and power forecasting for photovoltaic fields: a review. *International Journal of Photoenergy*.

[5.13] Massi Pavan, A., Mellit, A., De Pieri, D., & Kalogirou, S.A. (2013.) A comparison between BNN and regression polynomial methods for the evaluation of the effect of soiling in large scale photovoltaic plants. *Applied Energy*. 108, 392-401.

[5.14] Tsanakas, J. A., Ha, L. D., & Al Shakarchi, F. (2017). Advanced inspection of photovoltaic installations by aerial triangulation and terrestrial georeferencing of thermal/visual imagery. *Renewable Energy*. 102, 224-33.

[5.15] Hsu, C.W., & Lin, C. J. (2002). A comparison of methods for multiclass support vector machines. *IEEE transactions on Neural Networks*, 13.2, 415-425.

[5.16] Hachana, O., Tina, G. M., & Hemsas, K. E. (2016). PV array fault Diagnostic Technique for BIPV systems. *Energy and Buildings*, 126, 263-274

[5.17] Ovid and Martin, C. (2004). Metamorphoses. *W.W. Norton*. 1.

[5.18] Sparkes, B. (1996). The Red and the Black: Studies in Greek Pottery. *Routledge*.

[5.19] Tandy, D. W. (1997). Works and Days: A Translation and Commentary for the Social Sciences. *University of California Press.*

[5.20] Menabrea, Federico, L., & Lovelace, A. (1842). Sketch of the analytical engine invented by Charles Babbage.

[5.21] Goodfellow, I., Bengio, Y., Courville, A., & Bengio, Y. (2016). Deep learning. *(Vol. 1). Cambridge: MIT press*.

[5.22] Pipe, G., & Carse, B. (2003). Further experiments in Fuzzy Classifier Systems for mobile robot control. *Intelligent Control. 2003 IEEE International Symposium on IEEE conference publications*, 805-810.

[5.23] Kuncheva, L.I. (2000). How good are fuzzy if-then classifiers?. *IEEE Transactions on Systems, Man, and Cybernetics, Part B (Cybernetics)* 30.4, 501-509.

[5.24] Kalogirou, S.A., Mathioulakis, E., & Belessiotis, V. (2014). Artificial neural networks for the performance prediction of large solar systems. *Renewable Energy, 63,* 90–97.

[5.25] Haykin S. (1999). Neural Networks: A Comprehensive Foundation. *2nd Edition, Prentice-Hall, New Jersey.*

[5.26] Fausett, L.V. (1994). Fundamentals of Neural Networks: Architectures, Algorithms, and Applications. *Prentice-Hall, Englewood Cliffs, New Jersey.*

[5.27] IEC, (1998). Photovoltaic System Performance Monitoring—Guidelines for Measurement. *Data Exchange and Analysis, in International Standard IEC 61724*, ed.

[5.28] Møller, M. F. (1993). A scaled conjugate gradient algorithm for fast supervised learning. *Neural networks*, 6.4, 525-533.

[5.29] Jang, J. S. R. (1993). ANFIS: adaptive-network-based fuzzy inference system. *In IEEE Transactions on Systems, Man, and Cybernetics*, 23.3, 665-685.

[5.30] Belaout, A., Krim, F., Sahli, A., & Mellit, A. (2017). Multi-class neuro-fuzzy classifier for photovoltaic array faults diagnosis. *In 5th International Conference on Electrical Engineering-Boumerdes (ICEE-B), Boumerdes, Algeria,* 1-4.

[5.31] Belaout, A., Krim, F., Mellit, A., Talbi, B., & Arabi, A. (2018). Multiclass adaptive neuro-fuzzy classifier and feature selection techniques for photovoltaic array fault detection and classification. *Renewable Energy*, 127, 548-558.

[5.32] Belaout, A., Krim, F., Sahli, A., & Mellit, A. (2017). Multi-class neuro-fuzzy classifier for photovoltaic array faults diagnosis. *In Electrical Engineering-Boumerdes (ICEE-B), 2017 5th International Conference on*, 1-4.

CHAPTER 6

Conclusions and Future Work

The research presented in this thesis has presented the existing fault detection and protection methods and their limitations, discovered the shortcomings in conventional protection devices in PV systems, and developed new fault detection and classification method to eliminate the fault gap of the existing methods. The major contributions are presented below as well as the suggestion for forthcoming work.

6.1 Conclusions

The accomplished results and major research contributions of this thesis consist of:

> **In Chapter 3, real time emulator for PV Arrays is constructed, and data for classifier building is collected.**

This chapter focuses on real time emulator development and data collection for classifier building. The implemented model in ds1104 platform can be manipulated easily, Setting the exact couple (temperature, irradiance), implementation of any PV module technology, characteristics and parameters, choosing any type of configuration, series, parallel, series-parallel modules to get the desired output current, voltage and power. And finally, create different fault scenarios inside PV arrays.

The real time emulator consists basically of two parts:

> A software part: Matlab/Simulink and ControlDesk.

➢ A hardware part: the DS1104 platform which is connected to the PC via PCI slot, and to the APS-1102A programmable DC/AC power source via PLC1104 module.

Current sensor is used to provide a feedback signal to the implemented SPVA model. The control voltage in the external input of the programmable power comes from the controller board. Duty cycle changes regularly from 0 to 1 with a constant slope, then controlling the I-V plotter switch. A resistive load of 5 (ohms) /8 (A) is used.

As a real time emulator has been used, and the data collection period was accelerated by implementing a loop that changed the type of the fault and its severity by considering all possible combinations of solar irradiance and module temperature. The whole dataset was collected within about 6 hours divided into two days. In fact, the whole dataset cannot be stored at once, because of memory limitation in our system.

➢ **In Chapter 4, features reduction technique is proposed in solar PV Arrays diagnosis leading to optimized classifier's architectures.**

In this chapter, the importance of feature dimensionality reduction techniques has been shown. First, Feature is constructed using raw data which is a couple of current-voltage characteristics by making a map from raw data to the classifier input. The aim of this latter is to build more efficient features for fault detection and classification task. The obtained values for all features are normalized by using Eq (16), and the final product is a matrix of dimension (2860x12). This latter has been used for MC-NFC model construction. Then, the proposed method for feature dimensionality reduction has been applied to five classifiers: Partial shading fault classifier (F_1 classifier), increased series resistance classifier (F_2 classifier), By-pass diode short-circuited classifier (F_3 classifier), By-pass diode impedance classifier (F_4 classifier), and PV module short-circuited classifier (F_5 classifier).

➢ **In Chapter 5, multiclass neuro-fuzzy classifier (MC-NFC) is proposed for fault detection and classification in solar PV arrays.**

In addition to fault detection, this thesis proposes fault classification which main objective is to indicate the fault type and further help eliminate fault effectively and quickly.

Chapter 3 has shown that the *I-V* output characteristics of a PV array can widely change as temperature and solar irradiance vary. As a result, it is possible that the faulted PV array has similar and even overlapping operating points as the normal PV array, making fault detection difficult. To solve this issue, new parameters are firstly introduced, and then normalized. Taking weather information into consideration, the new parameters tend to remain constant for each condition. That is PV data with same condition tend to cluster together.

For the first time, MC-NFC is proposed for fault detection and classification (FDC) in solar PV arrays. The proposed MC-NFC is a supervised learning algorithm, which exhibits ability to learn from data. By spreading the information from measured data to the classifier output, fault classification can be achieved. Also, the proposed method is utilizing readily available PV measurements in PV systems (i.e., MPPT voltage and current, and weather information) so that it saves the hardware upgrades and related labor costs.
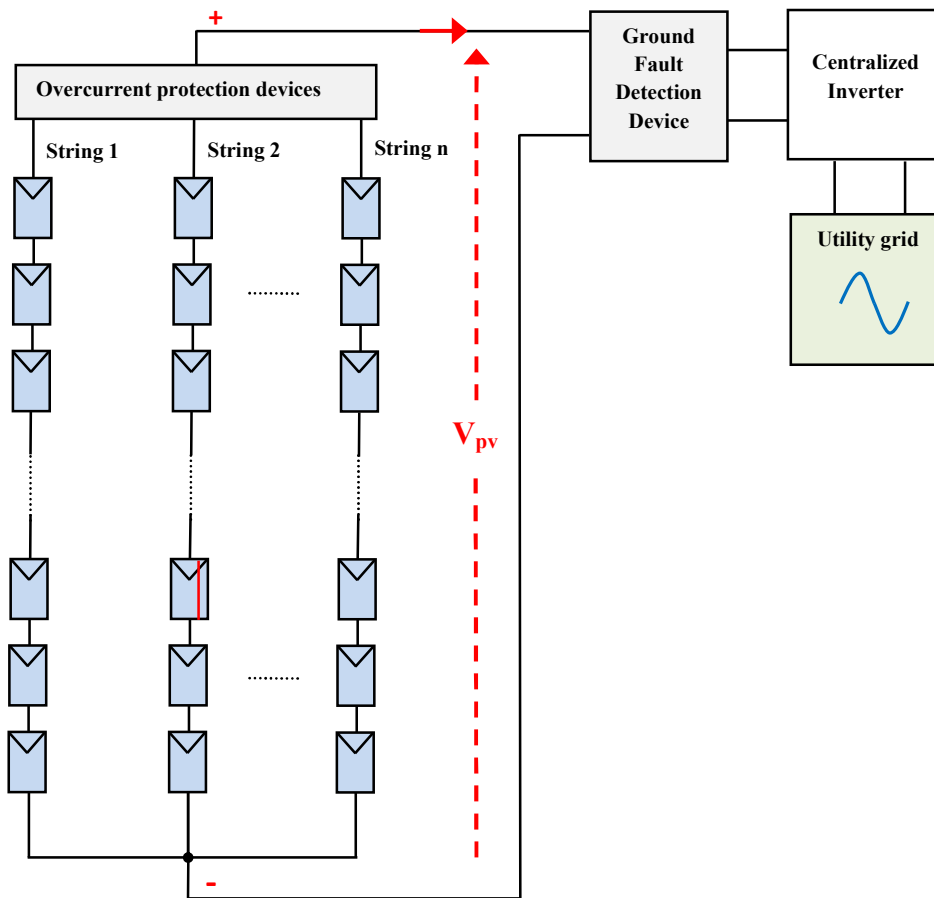
Figure 6.1: Schematic diagram of a typical grid-connected PV system, including conventional protection devices.

The proposed MC-NFC can discriminate between five types of fault occurring in a PV array. Furthermore, the developed algorithm is implemented in a DS1104 platform to show its ability to detect and classify PV array faults in real time applications. First, the original space features was reduced according to their effect on the classifier output. Second, classifiers have been built based on the best combination of the original feature space for each case. Finally, the constructed MC-NFC was compared to an ANN classifier, and the results show the importance of using the MC-NFC over the traditional ones.

6.2 Future Work

As shown in Fig. 6.1, conventional fault detection and protection methods use overcurrent protection devices (OCPD) and ground fault detection interrupters (GFDI) in solar PV arrays. However, this thesis has shown that OCPD may fail in fault protection when the fault current is not high enough. This is caused by the irradiance-dependent and current-limit feature of PV arrays. Since OCPD (e.g., fuses or circuit breakers) are passive components that can only be blown or tripped at certain current/energy level, their limitations can be found in the solar PV arrays, leaving faults undetected and not eliminated.

In this thesis, we have proposed a new decision-making algorithm to detect and classify faults using artificial intelligence techniques, such fuzzy classifier, neural network classifier and finally a multiclass neuro-fuzzy classifier. Their performance has been validated in experimental platform, making it a promising choice for fault detection and classification. To continue this research, future work may explore new active fault protection solutions, such as how to clear the fault actively, responsively and safely. Based on the tripping signal generated from the proposed methods, the active fault protection solution should increase the system efficiency, reliability, safety and fault immunity. Therefore, an integration of active fault protection approaches with the proposed methods would be a nice future research topic.

As the PV penetration level becomes more widespread, PV inverters take more and more responsibilities, not only in power conversions and maximum power point tracking, but also in fault detection and protection. As the most intelligent component in the PV system, PV inverters have the potential to provide more safety features. For example, recent PV inverters are featured with several different fault detection solutions, such as ground fault detection, dc arc fault detection, insulation detection in ungrounded PV arrays, and residual current detection. However, the existing fault detection solutions of PV inverters are usually based on

signal-processing, merely relying on the instantaneous measurement. For this reason, fault classification is still not available for PV inverters. To make good use of readily available historical data, future research may be focused on how to integrate the proposed fault classification methods to the PV inverters. This would provide better fault detection features and potentially increase the PV system reliability and safety.

Scientific production

The following list includes all the papers published by the author during his graduate studies. Papers designated by "*" are directly related with research results presented in this thesis.

Journal Papers

[J1].   Arabi, A., Bourouba, N., Ayad, M., & **Belaout, A.** (2018). An Accurate Classifier Based on Adaptive Neuro-Fuzzy Classifier and Features Selection Techniques for Fault Classification in Analog Circuits. *Integration the VLSI Journal. In Press, corrected Proof.*

[J2].   * **Belaout, A.**, Krim, F., Mellit, A., Talbi, B., & Arabi, A. (2018). Multiclass adaptive neuro-fuzzy classifier and feature selection techniques for photovoltaic array fault detection and classification. *Renewable Energy*, 127, 548-558.

[J3].   Talbi, B., Krim, F., Rekioua, T., Mekhilef, S., Laib, A., & **A. Belaout** (2018). A high performance control scheme for photovoltaic pumping system under sudden irradiance and load changes. *Solar Energy*, 159, 353-368.

[J4].   Feroura, H., Krim, F., Talbi, B., Laib, A., & **Belaout, A.** (2018). Sensorless field oriented control of current source inverter fed induction motor drive. *Revue roumaine des sciences techniques-serie electrotechnique et energetique*, 63(1), 100-105.

[J5].   Feroura, H., Krim, F., Talbi, B., Laib, A., & **Belaout, A.** (2017). Finite-Set Model Predictive Direct Power Control of Grid Connected Current Source Inverter. *Elektronika ir Elektrotechnika*, 23(5), 36-40.

Conference Papers

[C1].   Sahli, A., Krim, F., & **Belaout A.** (2017). Energy Management and Power Quality Improvement in Grid Connected Photovoltaic Systems. *In International Renewable and Sustainable Energy Conference (IRSEC'17).*

[C2].   * **Belaout**, **A.,** Krim, F., Sahli, A., Mellit A. (2017). Multi-class neuro-fuzzy classifier for photovoltaic array faults diagnosis. *In Electrical Engineering-Boumerdes (ICEE-B), 2017 5th International Conference on*, 1-4.

[C3].   * **Belaout**, **A.,** Krim, F., Talbi, B., Feroura, H., Laib, A., Bouyahia, S., & Arabi, A. (2017). Development of real time emulator for control and diagnosis purpose of Photovoltaic Generator. *In Systems and Control (ICSC), 2017 6th International Conference on*,139-144.

[C4].   * **Belaout**, **A.,** Krim, F., & Mellit, A. (2016). Neuro-fuzzy classifier for fault detection and classification in photovoltaic module. *In Modelling, Identification and Control (ICMIC), 2016 8th International Conference on*, 144-149.

[C5].   * **Belaout**, **A.,** Krim, F., Arabi, A., & Ayad, M. Comparaison entre les Modèles à une seule Diode et de Bishop de la Cellule Solaire. *In 1st National Conference on Electronics and Electrical Engineering (NCEEE'2016).*

[C6].   Arabi, A., Bourouba, N., **Belaout**, **A.,** Ayad, M. Single Parametric Fault Detection of Analog Circuit Using Monte-Carlo Analysis. *In 1st National Conference on Electronics and Electrical Engineering (NCEEE'2016).*

[C7].   * **Belaout**, **A.,** Krim, F., & Mellit, A. (2016). Fuzzy Classifier for Fault Detection and Classification in Photovoltaic Module. *In International Conference on Technological Advances in Electrical Engineering.*

[C8].   Bouyahia, S., Semcheddine, S., & **Belaout**, **A.** (2016). Takagi-Sugino Fuzzy Model of the Anaerobic Digestion of Organic Wastes. *In the 9th international conference on electrical engineering and first workshop on robotics and controls.*

[C9].   Arabi, A., Bourouba, N., Ayad, M., & **Belaout**, **A.** (2015). Catastrophic Faults Detection of Analog Circuits. *In Modelling, Identification and Control (ICMIC-2015), 2015 7th International Conference on*. 144-149.

Appendix

These figures represent I-V curves for normal and faulty cases.
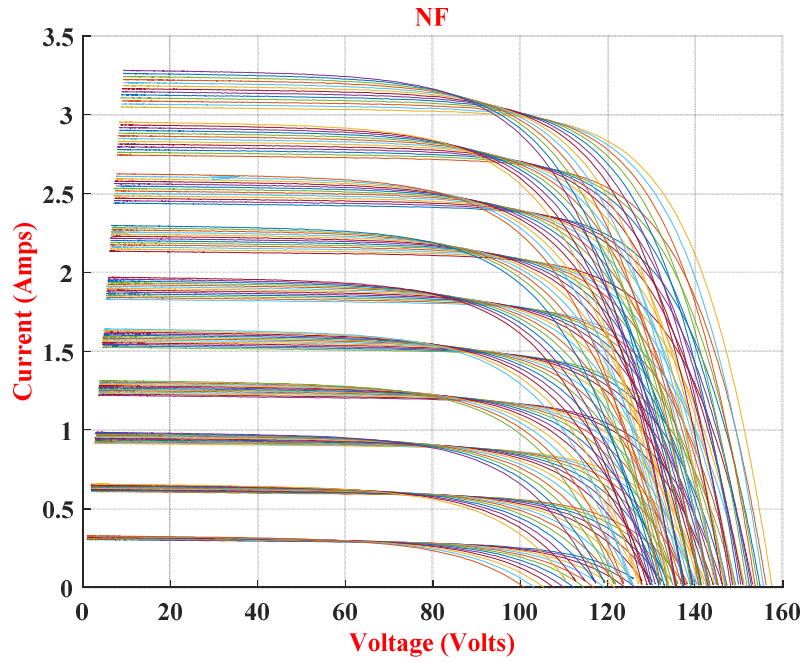
Figure 1: *I-V* curves for normal operation
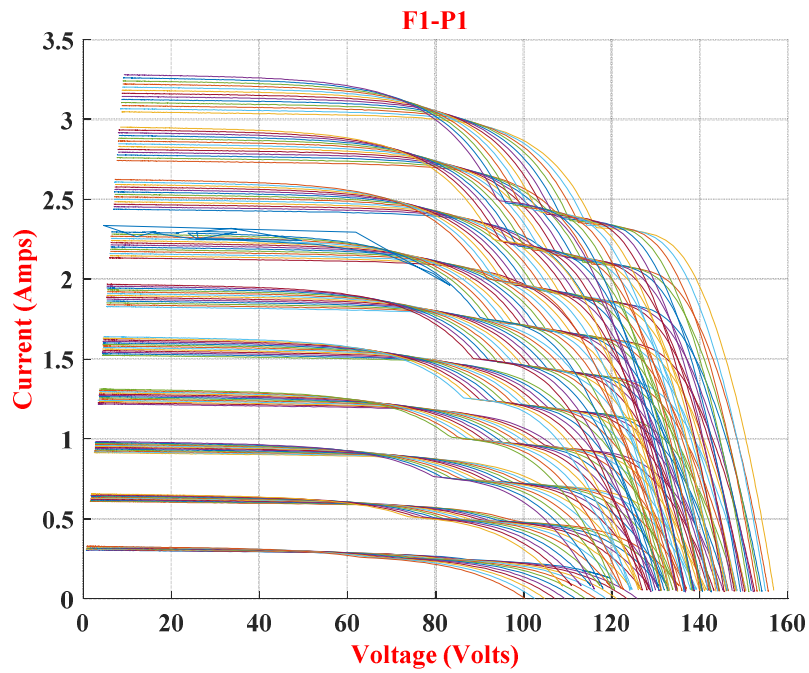
Figure 2: *I-V* curves for shading *pattern-1* (25% of nine PV cell in one PV module)
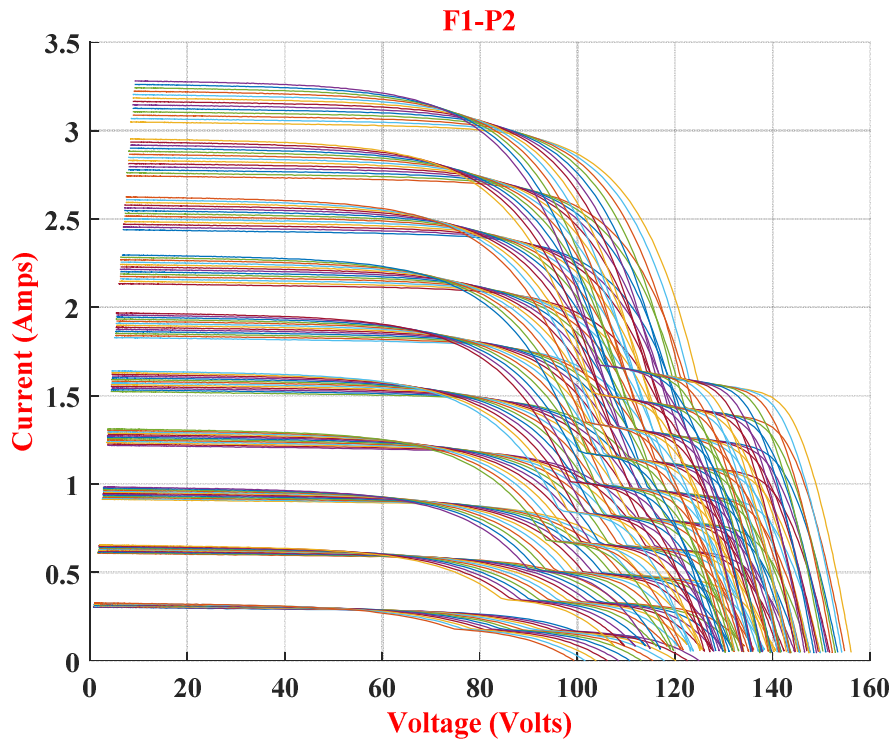
Figure 3: *I-V* curves for shading *pattern-2* (50% of nine PV cell in one PV module)
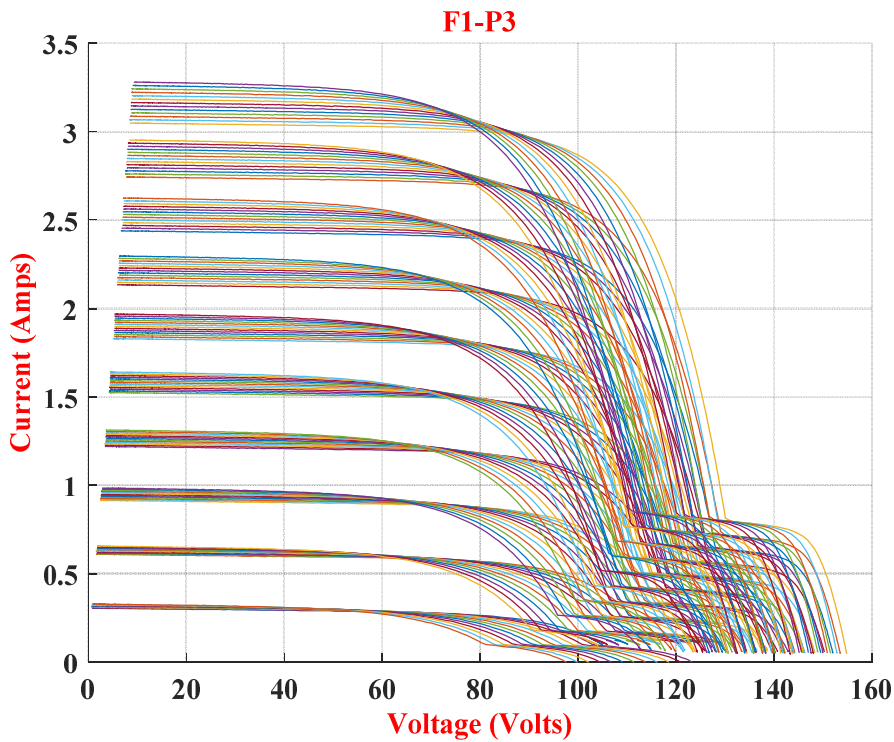

**Figure 4:** *I-V* curves for shading *pattern-3* (75% of nine PV cell in one PV module)
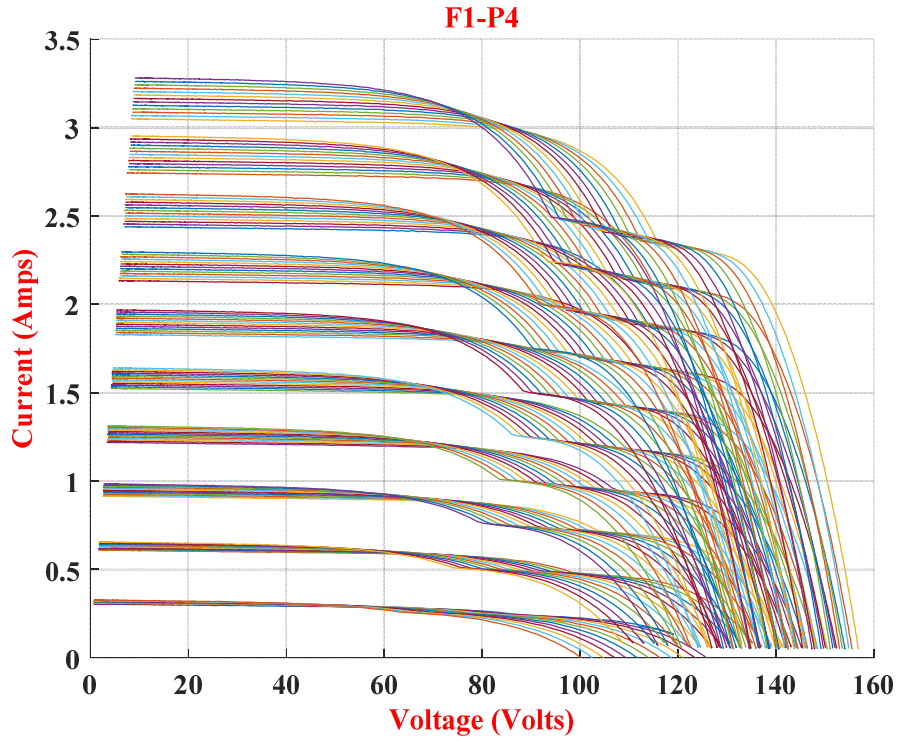
Figure 5: *I-V* curves for shading *pattern-4* (25% of nine PV cell in two PV modules)
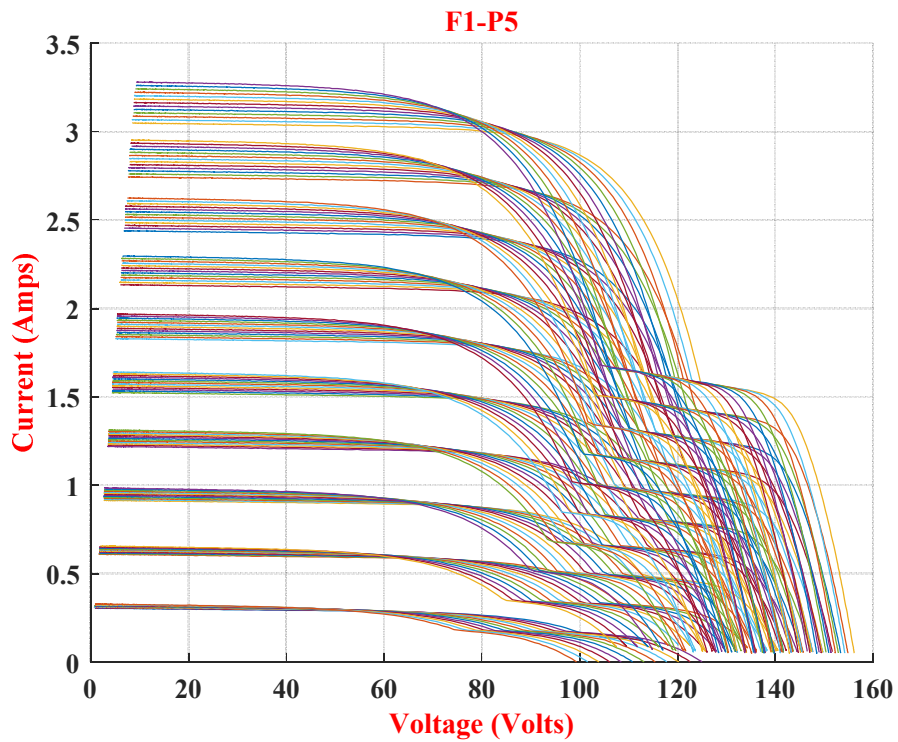
Figure 6: *I-V* curves for shading *pattern-5* (50% of nine PV cell in two PV modules).
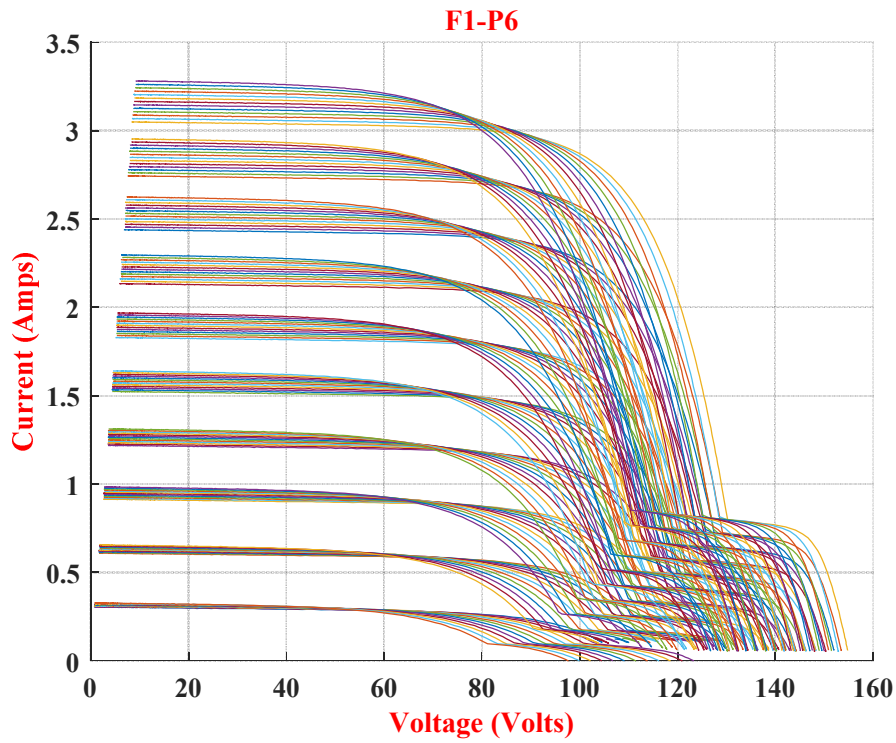
Figure 7: *I-V* curves for shading *pattern-6* (75% of nine PV cell in two PV modules).
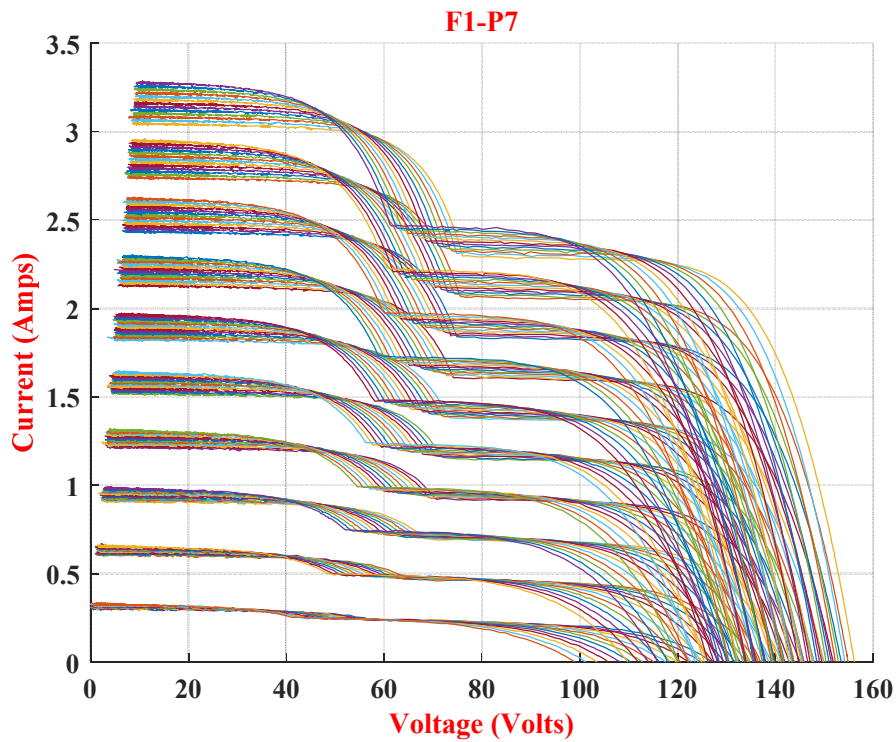
Figure 8: *I-V* curves for shading *pattern-7* (25% of nine PV cell in three PV modules)
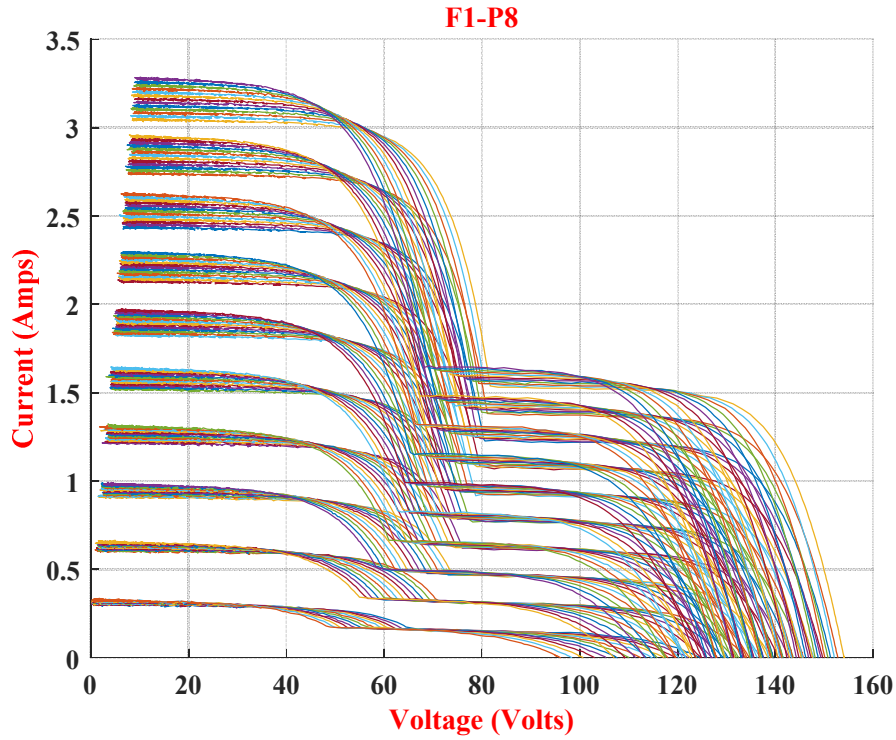
Figure 9.h: *I-V* curves for shading *pattern-8* (50% of nine PV cell in three PV modules)
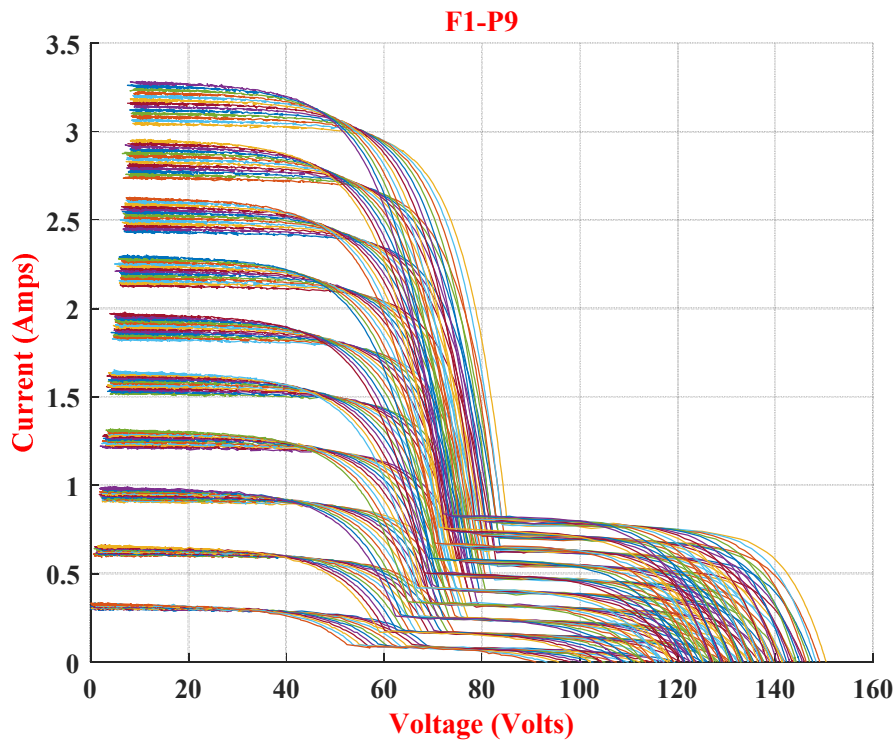
Figure 10: *I-V* curves for shading *pattern-9* (75% of nine PV cell in three PV modules)
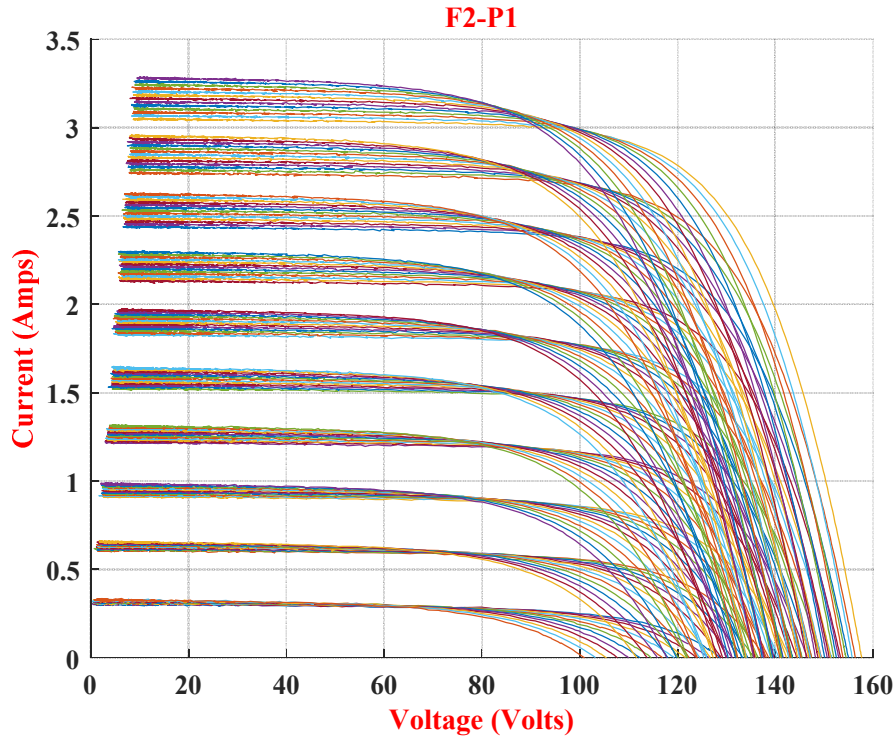
Figure 11: ISR *pattern-1* (the series resistance of one module is increased by 1 Ω).
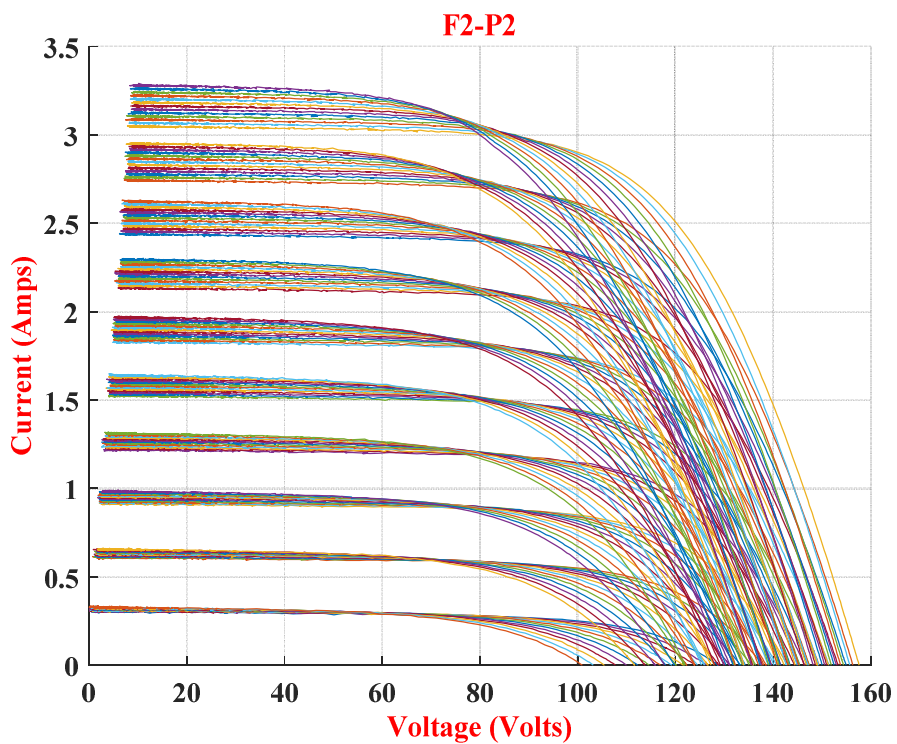
Figure 12: ISR *pattern-2* (the series resistance of one module is increased by 5 Ω).
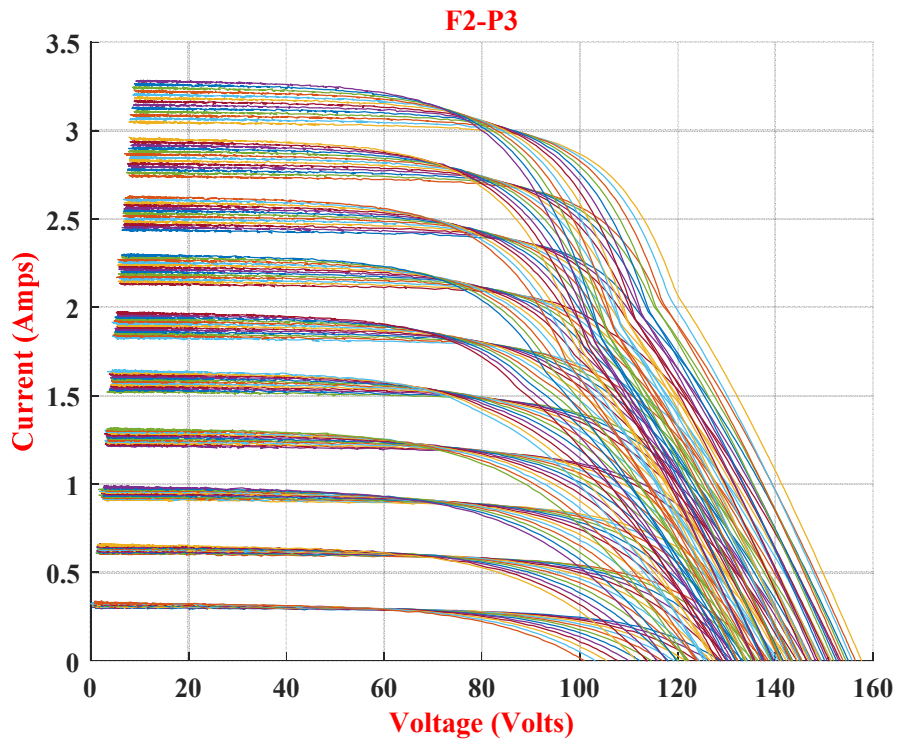
Figure 13: ISR *pattern-3* (the series resistance of one module is increased by 10 Ω).
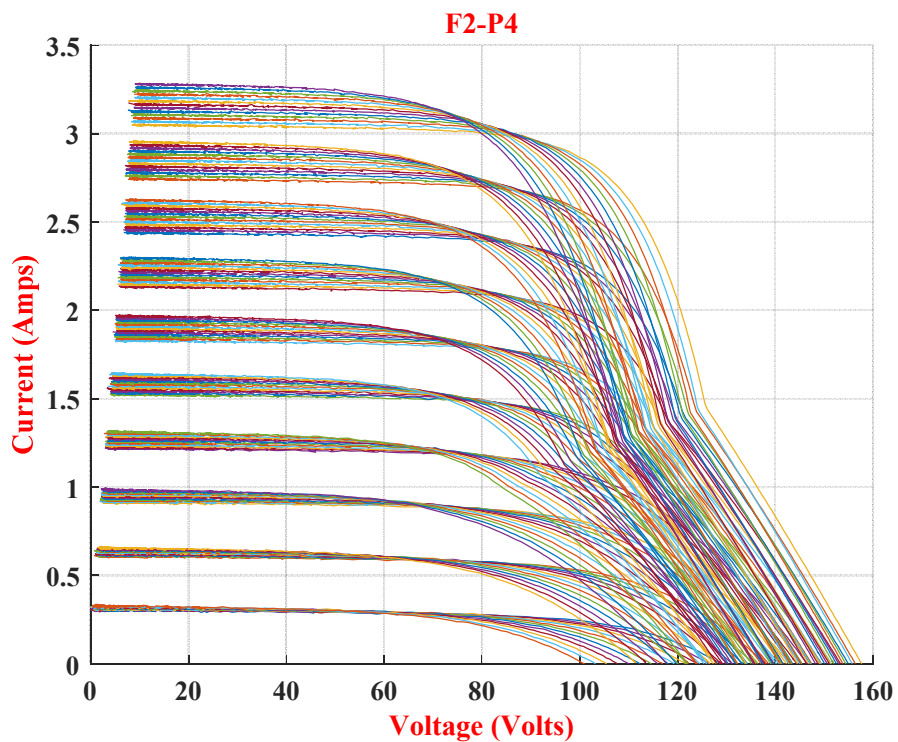
Figure 14: ISR *pattern-4* (the series resistance of one module is increased by 15 Ω).
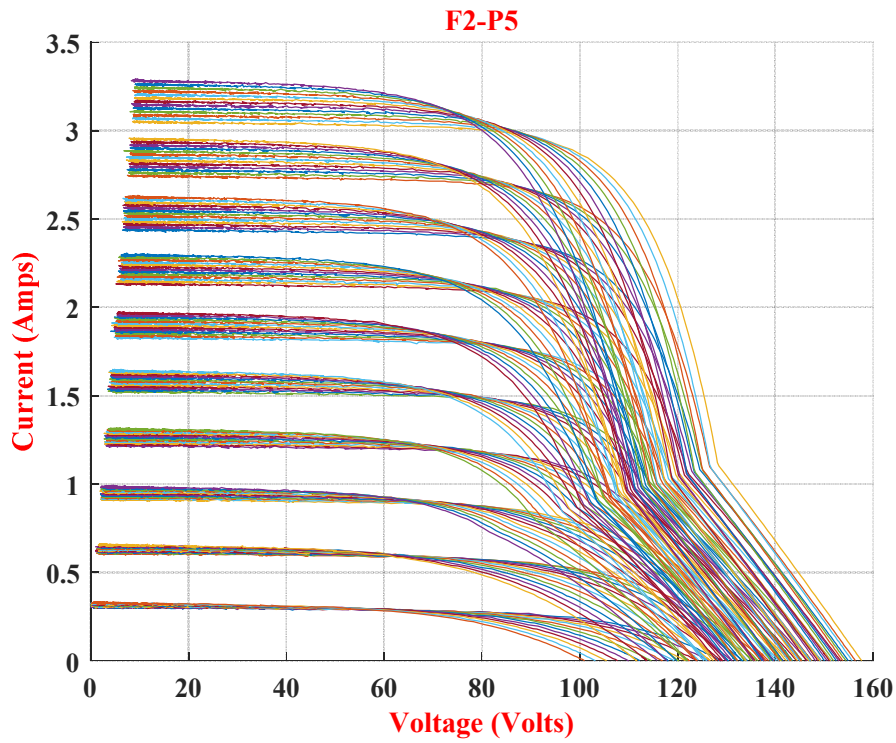
Figure 15: ISR *pattern-5* (the series resistance of one module is increased by 20 Ω).
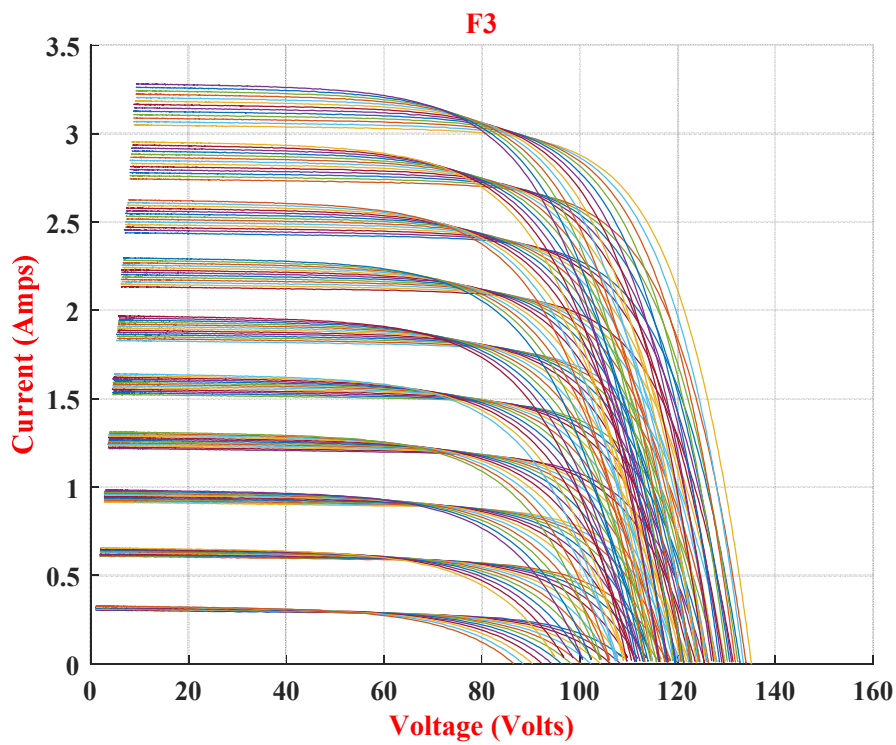
Figure 16: By-pass diode short-circuited (1 BPD in the whole PVA short-circuited).
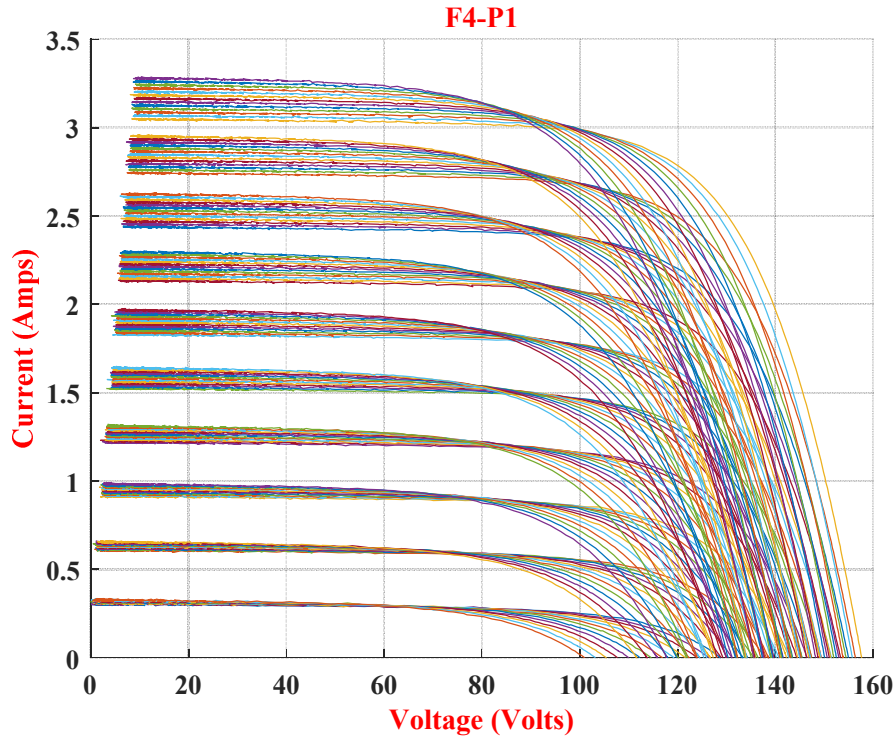
Figure 17: By-pass diode impedance (BPD is assimilated to a resistor of 1 Ω).
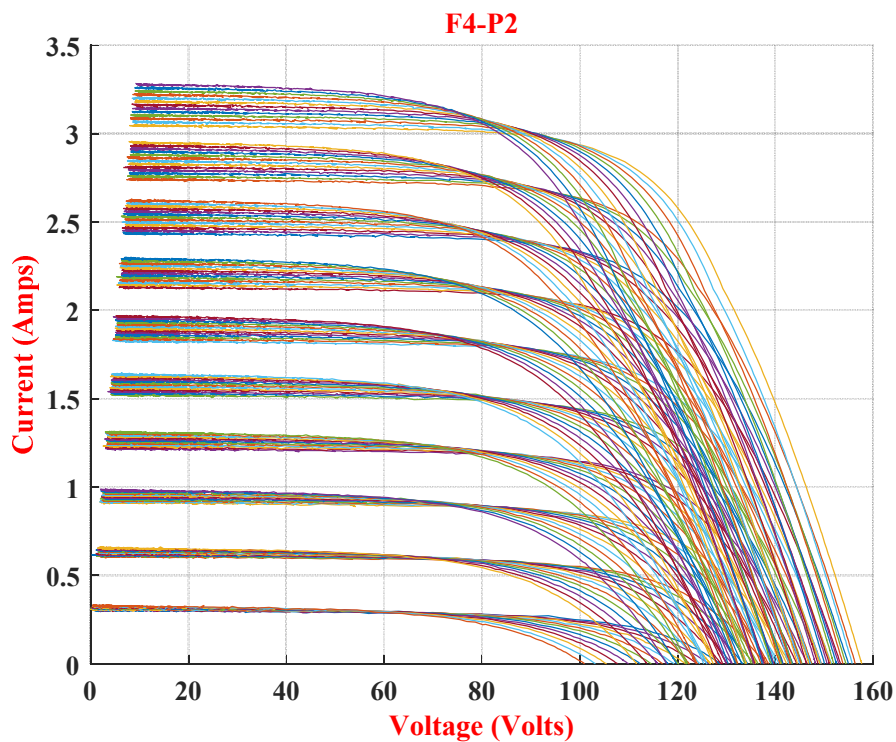
Figure 18: By-pass diode impedance (BPD is assimilated to a resistor of 5 Ω).
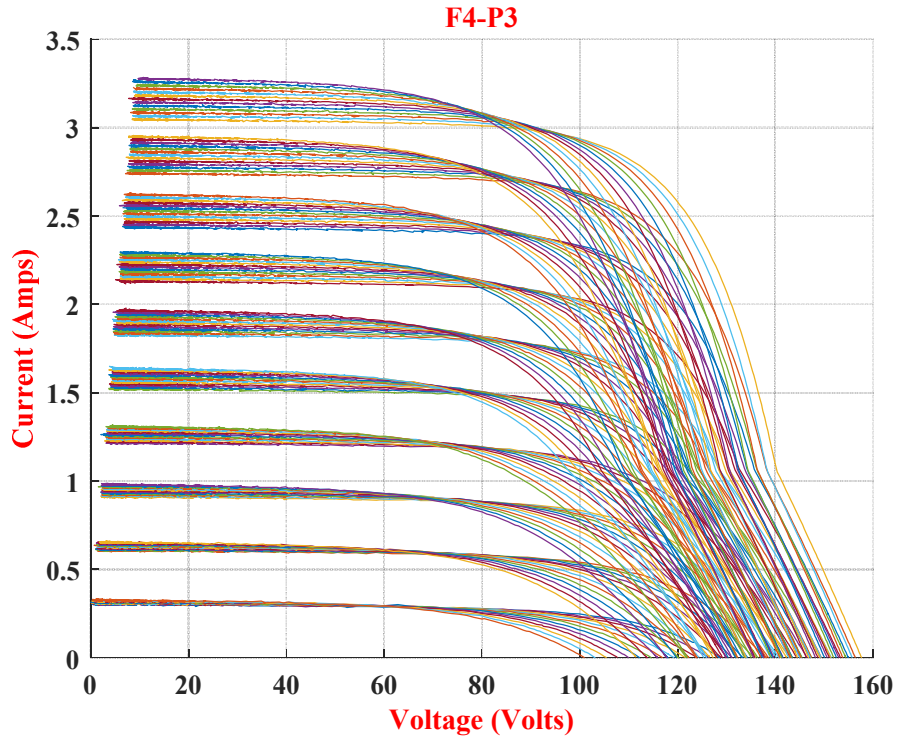
**Figure 19:** By-pass diode impedance (BPD is assimilated to a resistor of 10 Ω).
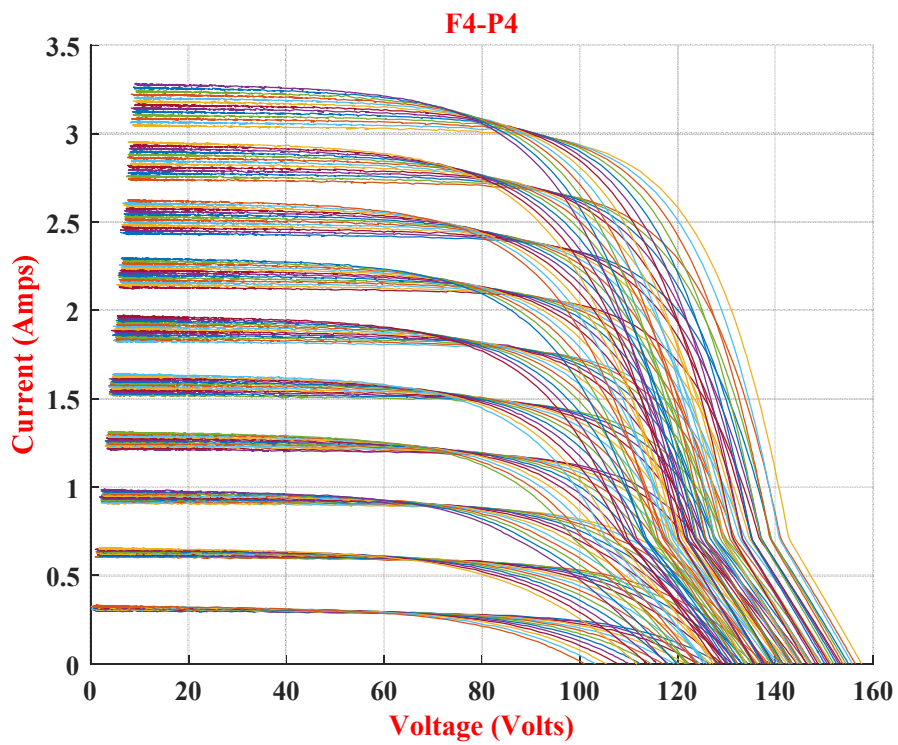
**Figure 20:** By-pass diode impedance (BPD is assimilated to a resistor of 15 Ω).
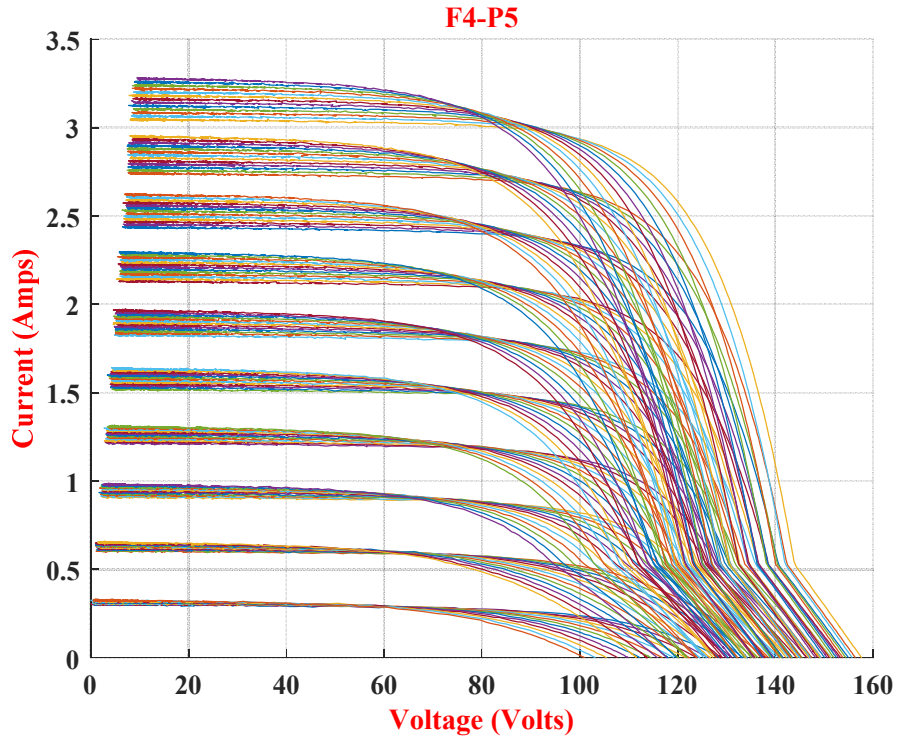
Figure 21: By-pass diode impedance (BPD is assimilated to a resistor of 20 Ω).
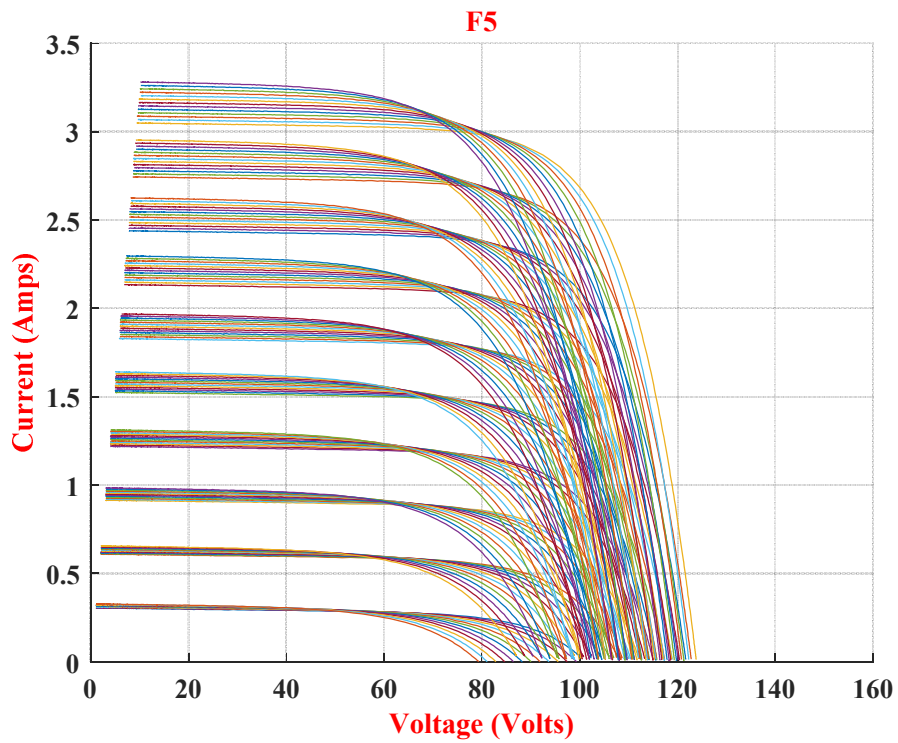

Figure 22: One PV module is short-circuited.

Artificial Intelligence Techniques Application in Photovoltaic Systems for Faults Diagnosis

Abstract:

This thesis deals with the application of artificial intelligence techniques for the diagnosis, detection and classification of defects in photovoltaic systems. These latter like all electrical and electronic systems, can break down and degrade during the operating period. This requires a diagnostic whose main objective is to provide an automatic tool that can early detect defects to protect the persons and installations, and in addition can classify this defects. At the end of 2016, 303 GW of photovoltaic energy was installed around the world. About 75 GW installed only in the year of 2016, and this comes from the fact that new solutions have encouraged government to rely more and more on this kind of energy. For the development of fault classification algorithms in photovoltaic systems, at the beginning, a database is collected using real time emulator. Then, classifiers based on artificial intelligence were built, such as the fuzzy classifier, neuronal and the neuro-fuzzy classifier. Finally, the diagnostic task was sophisticated with the introduction of a new classifier "multi-class neuro-fuzzy classifier (MC-NFC)". This latter has been implemented on a DSPACE platform "DS1104" to demonstrate its ability to detect and classify faults in real time.

Keywords: Artificial Intelligence; neuro-fuzzy classifier; diagnostic; faults classification; photovoltaic systems; real time simulation.

Application des Techniques d'Intelligence Artificielle dans les Systèmes Photovoltaïques en vue de Diagnostic des Défauts

Résumé:

Cette thèse porte sur l'application des techniques d'intelligence artificielle au diagnostic, la détection et la classification des défauts dans les systèmes photovoltaïques. Ces derniers comme tous les systèmes électriques et électroniques, peuvent tomber en panne et se dégradent pendant la durée de fonctionnement. Ce qui nécessite un diagnostic dont l'objectif principal est de fournir un outil automatique qui permet la détection précoce des défauts pour protéger l'installation et les personnes, et de classifier le défaut en plus. A la fin de l'année 2016, 303 GW d'énergie photovoltaïque ont été installés mondialement. Plus de 75 GW ont été installés durant seulement l'année 2016, et ceci est due à des nouvelles solutions qui ont encouragé les gouvernements à faire de plus en plus confiance à ce type d'énergie. Pour le développement des algorithmes de classification de défauts dans les systèmes photovoltaïques, au début, une base de données est collectée en utilisant un émulateur temps réel. Ensuite, des classificateurs à base d'intelligence artificielle ont été construits, tels que les classificateurs flou, neuronal et neuro-flou. Finalement, le diagnostic a été amélioré par l'introduction d'un nouveau classificateur "classificateur neuro-flou multi-classe (MC-NFC) ". Ce dernier a été implémenté sur une plateforme DSPACE " DS1104 " pour montrer sa capacité à détecter et classifier les défauts en temps réel.

Mots clés : Intelligence Artificielle ; classificateur neuro-flou ; diagnostic ; classification des défauts ; systèmes photovoltaïques ; simulation temps réel.

تطبيق تقنيات الذكاء الاصطناعي لتشخيص الأعطال في الأنظمة الكهروضوئية

ملخص:

هذه الأطروحة تتفق مع تطبيق تقنيات الذكاء الاصطناعي لتشخيص, اكتشاف وتصنيف الأعطال في الأنظمة الكهروضوئية. هذه الأخيرة مثلها مثل الأنظمة الكهربائية والإلكترونية الأخرى, يمكنها أن تتعطل وتتلف خلال مدة عملها. الأمر الذي يتطلب التشخيص, الذي يرمي أساساً إلى توفير الوسيلة الآلية التي تسمح بالاكتشاف المبكر للأعطال لحماية الأشخاص و العتاد. وزيادة على ذلك تصنيف هذه الأعطال. في نهاية سنة 2016, 303 جيقاواط من الطاقة الكهروضوئية قد تم تركيبها في جميع أنحاء المعمورة. في سنة 2016 وحدها تم تركية ما يزيد عن 75 جيقاواط, وهذا راجع إلى حلول جديدة شجعت الحكومات على الثقة أكثر فأكثر في هذا النوع من الطاقة. لتطوير خوارزميات تصنيف الأعطال في الأنظمة الكهروضوئية, في البداية, يتم جمع قاعدة بيانية باستعمال محاكاة هذا الأخير في الزمن الحقيقي. بعد ذلك، تم بناء المصنّفات المبنية على الذكاء الاصطناعي، مثل المصنف الغامض، والعصبي، والمصنف العصبي الغامض. و أخيرًا، كانت مهمة التشخيص متطورة مع إدخال مصنف جديد "مصنف عصبي غامض متعدد الطبقات (MC-NFC)". وقد تم تنفيذ هذا الأخير على منصة "DSPACE DS1104" لإثبات قدرته على اكتشاف وتصنيف الأعطال في الوقت الحقيقي.

الكلمات المفتاحية : الذكاء الاصطناعي؛ المصنف العصبي الغامض؛ التشخيص؛ تصنيف الأعطال؛ الأنظمة الكهروضوئية؛ المحاكاة في الزمن الحقيقي.